LINKING BENTHIC ALGAE TO SEDIMENT OXIDATION-REDUCTION DYNAMICS: IMPLICATIONS FOR SEDIMENT-WATER INTERFACE NUTRIENT CYCLING

A DISSERTATION SUBMITTED TO THE GRADUATE DIVISION OF THE UNIVERSITY OF HAWAIʻI AT MĀNOA IN PARTIAL FULFILLMENT OF THE REQUIREMENTS FOR THE DEGREE OF
DOCTOR OF PHILOSOPHY IN OCEANOGRAPHY

AUGUST 2012

By: Jennifer Lynn Murphy

Dissertation Committee:
Dr. Brian Glazer (Chairperson), Dr. Margaret McManus, Dr. Kathleen Ruttenberg, Dr. Celia Smith, Dr. Florence Thomas

Keywords: invasive algae, biogeochemistry, oxidation reduction chemistry, redox, sediments

Dedication

In loving memory of my grandma,

Bernice McFarland.

Acknowledgements

I am thankful for everyone who volunteered their time, knowledge and support to help me complete this project. My husband Ryan Murphy, offered unending support throughout this process, including during multiple 24-hour field days, and without him I never would have completed this work. Many friends and colleagues volunteered hours of field assistance, and it is thanks to the efforts of Kyle Aveni Deforge, Rebecca Baltes, Rebecca Briggs, In Chieh Chen, Heather Mills, Kristen Fogaren, Danielle Hull, Kahoalii Keahi, Francesca Koethe, Sherril Leon Soon, Kathryn MacDonald, Michael Matzinger, and Mari Okahara, for the hours of field assistance they volunteered, without whom the data presented here would not have been collected. Òscar Roig wrote the MATLAB codes used to analyze the ADV data and assisted with interpretation of the data, and I am especially grateful for his expertise. I also truly appreciate the guidance I received from my committee. Dr. Chris Measures provided me the opportunity to teach OCN 201, an experience on which I hope to base my career upon. My family supported me throughout this project, especially my sister, Julie, who offered all of her words of encouragement. Finally, I thank you to my son, Kelvin, for providing me with the motivation to complete my writing.

This project was funded in part by the University of Hawai‘i, Department of Oceanography. This paper is funded in part by a grant/cooperative agreement from the National Oceanic and Atmospheric Administration, Project R/AQ-84, which is sponsored by the University of Hawaii Sea Grant College Program, SOEST, under Institutional Grant No. NA09OAR4171060 from NOAA Office of Sea Grant, Department of Commerce. The views expressed herein are those of the author(s) and do not necessarily reflect the views of NOAA or any of its subagencies. UNIHI-SEAGRANT-XD-09-03. and the University of Hawai‘i Sea Grant College Program. This research was partially supported by U.S. NSF grants OCE-0536616 and OCE-1031947. I am also grateful for the field assistance, boat use and site access provided by Paepae O He‘eia.

Abstract

Invasive macroalgae threaten the diversity and function of ecosystems and have the potential to alter environmental biogeochemistry. In Hawai‘i two red macroalgae, *Acanthophora spicifera* and *Gracilaria salicornia,* are successful invasive species. Morphologically these species are different, *A. spicifera* is more flexible and forms less dense canopies than the dense mats created by *G. salicornia.* This dissertation examined the influence of *A. spicifera* on diel variations in water column nutrient concentrations and sediment oxidation-reduction (redox) chemistry and the effect of *G. salicornia* on water flow and redox chemistry. Diel changes were evident through changes in the concentration of water column oxygen and sediment Mn^{2+} and ammonium concentrations, especially in sites colonized by *A. spicifera.* Additionally, sites with *A. spicifera* had higher sediment ammonium concentrations and ammonium flux to the water column. *In situ* electrochemical profiles revealed that hydrogen sulfide was present in the water column within *A. spicifera* canopies. The detection of Mn^{2+} and dissolved iron, both in surface waters and at the sediment water interface, provide evidence that colloidal Fe^{3+} and manganese oxides may be sorbing phosphate, contributing to the low dissolved phosphate concentrations observed throughout the study. Despite the difference in sediment redox chemistry and sediment nutrient concentrations between sites with and without the invasive macroalga, no difference in water column nutrients was found. Similar nutrient concentrations between areas with *A. spicifera* and devoid of the alga are likely due to interception and uptake of nutrients at the SWI by the macroalga. *Gracilaria salicornia* was found to reduce water velocity (xRMS), turbulent kinetic energy and turbulent xRMS compared to adjacent macroalgae free regions. Thin, (less than 1 cm) vertically isolated suboxic zones occurred within the otherwise oxic water column of algal mats, which corresponded to regions within the mat where turbulent xRMS of the dominant flow direction dropped to speeds near 0.001 m/s. These suboxic microniches provide environmental conditions suitable for redox sensitive nutrient transformations, such as reductive solubilization of phosphate bound to iron oxides, to take place. Invasive algae are altering sediment and water column redox conditions which may provide an ecological advantage to the algae.

Table of Contents

List of Tables

List of Figures

Chapter 1

Chapter 2

Chapter 3

Chapter 4

Chapter 5

Chapter 1

Introduction

Nutrient cycling in coastal regions is an essential component of near shore ecosystem function. Riverine input is a well-studied source of nutrients to the coastal ocean, and sediments serve as vast reservoirs of biologically important elements. In shallow coastal environments, benthic remineralization products can be mixed into the water column and made available for use by primary producers. Sediments in coastal regions are a unique component of nutrient cycling dynamics. Sediments can act as sources or sinks for different nutrients depending upon local oxidation-reduction (redox) conditions, as well as physical processes, such as mixing, and biological processes, such as bioturbation.

The bioavailabilities of nutrients are controlled by a variety of factors, including ambient oxygen concentration. For example, in oxygenated sediments phosphorus is adsorbed to ferric-oxyhydroxides ($Fe(OH)_3$), rendering phosphorus biologically unavailable (Chambers and Odum 1990, Blomqvist and Elmgren 2004). Under anoxic conditions, $Fe(OH)_3$ undergoes reductive dissolution, causing phosphorus release and diffusion into the surrounding water (Krom and Berner 1980, Jensen et al. 1995, Rozan et al.2002, Hupfer and Lewandowski 2008). Nitrogen cycling is also dependent upon redox state. Sediment oxygen penetration influences biotic nitrogen cycling pathways and nitrogen availability upon release from sediments (e.g. Seitzinger 1988, Rysgaard et al. 1996). The biotic and abiotic processes occurring in sediments influence the burial and release of biologically important elements, including phosphorus, nitrogen, iron and other trace elements, and are influenced by redox conditions in sediments.

The dependence of nutrient bioavailability on local redox conditions highlights the importance of the distribution of redox-reactive chemical species in sediments. Perturbations of the depth oxygen penetrates in sediments, such as through increased organic matter (OM) deposition and subsequent increases in benthic respiration rates, will alter redox cycling and nutrient release to the water column (Rysgaard et al.1996, Rozan et al. 2002, Corzo et al. 2009). Additionally, local physical conditions, including wind speed and bottom shear stress, can influence the concentrations of nutrients available in the water column (Oldham and Lavery 1999). The perturbation of local redox and flow conditions can have ecosystem-wide effects because changes in water column nutrients are known to alter the community composition of primary producers (e.g. Hecky and Kilham 1988, and sources therein, Burkepile and Hay 2006).

Microbial Biogeochemistry

One of the simplest classification schemes for life is based on metabolism, which in its most fundamental form is a series of oxidation-reduction (redox) reactions. Autotrophic organisms fix carbon, while heterotrophs rely on previously fixed carbon compounds. Photosynthetic autotrophs reduce CO_2 and oxidize H_2O to form sugars and O_2 (Falkowski 2008), as described in Equations 1.1 through 1.3.

Oxidation: $2H_2O \rightarrow O_2+4H^+ + 4e^-$ (loss of e^-) (1.1)

Reduction: $CO_2+4H^+ +4e^- \rightarrow CH_2O+H_2O$ (gain of e^-) (1.2)

Full reaction: $H_2O+CO_2 \rightarrow CH_2O + 2O_2$ (1.3)

Respiration redox reactions performed by heterotrophs are the reverse of the photosynthetic process, where carbon-based sugars are oxidized and O_2 is reduced, creating water and carbon dioxide. The metabolic pathways of heterotrophic microorganisms, however, are not limited to the use of oxygen (Figure 1.1).

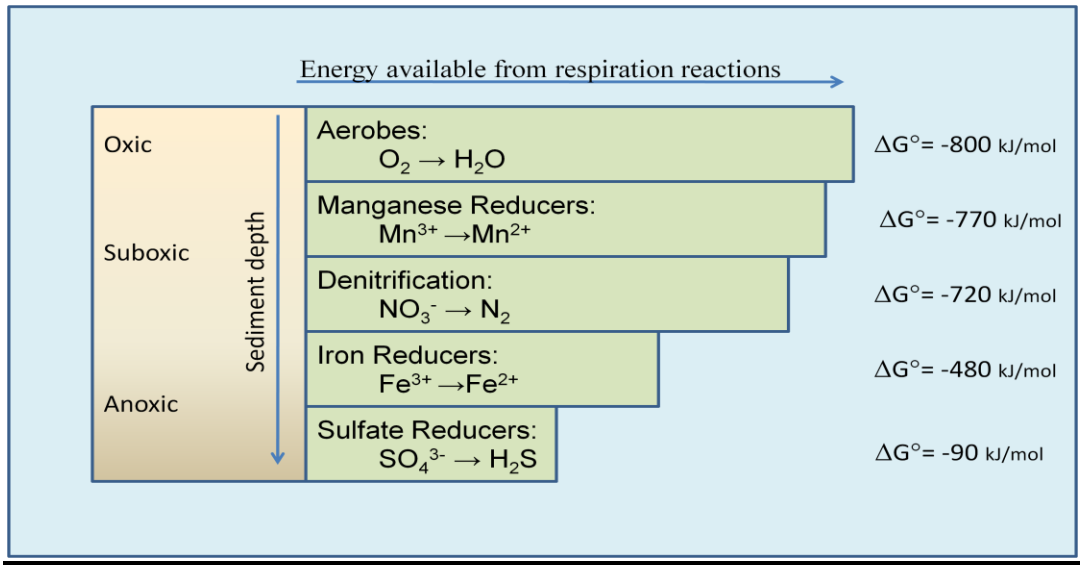

Figure 1.1: Metabolic pathways for organic matter oxidation with the most energetically favorable oxidant (O_2) at the top, and the least (SO_4^{3-}) at the bottom. Gibbs free energy* is given on the right side for the oxidation of one mole of acetate using the stated oxidant (Canfield et al. 2005). The far left side lists the terms commonly used to describe the different sediment zones where the given microbial processes take place.

*The Gibbs free energy ($\Delta G°$) for an equation determines whether a reaction is spontaneous, with more negative $\Delta G°$ values indicating a more thermodynamically favorable reaction.

Numerous oxidants can be utilized by microbes, including nitrate (Payne 1973), MnO_2 (Nealson and Saffarini 1994), FeOOH (Nealson and Saffarini 1994), and sulfate (Jørgensen 1982). It is the free energy of the redox reactions that determines the order in which they occur. Denitrification, for example, yields more energy than sulfate

reduction, and therefore microbial populations will exploit the higher energy reaction first. Once the most energetically favorable oxidant is no longer available, the next in the series is used, creating layers in sediments as the higher energy yielding chemical species are used first leaving the less favorable ones to oxidize OM in deeper regions. These shifts in microbial metabolism can be seen in pore water as dissolved species appear and disappear depending upon the redox reaction occurring. For example, increasing concentrations of Mn^{2+} in pore water indicates that the majority of the more energetically favorable oxygen has been reduced.

The biological reduction of sulfate accounts for a large portion of the total organic carbon respiration in near shore marine environments (Jørgensen 1982, Capone and Kiene 1988, Koretsky et al 2003), and is very important over geologic timescales (Falkowski et al. 2008). Sulfate reduction occurs in these areas because of the availability of organic carbon and the high concentration of sulfate in sea water. Sulfide concentrations increase in marine sediments after all of the more energetically favorable oxidants have been utilized, because sulfate reduction has the lowest energy yield (Figure 1.1). Therefore, by measuring changes in the concentrations of redox species, and knowing the abiotic rates of those transformations, one can determine the rates of microbial metabolic reactions in sediments.

Redox-reactive Nitrogen Cycling

Despite comprising 78% of the atmosphere, nitrogen is a biologically limiting nutrient in marine ecosystems because the dominant gaseous form of nitrogen in the atmosphere is dinitrogen (N_2) which is not biologically available to the majority of

eukaryotic primary producers (Sprent et al. 1987). Dinitrogen must first be converted into either ammonia (NH_3) or nitrate (NO_3^-) before the nitrogen is available for biological uptake. Lightening and nitrogen fixing prokaryotes (diazotrophs) are the only known natural pathways for nitrogen fixation, and the majority of diazotrophs can only fix nitrogen under anoxic conditions (Paerl and Pinckney 1996, and sources there in). Redox chemistry influences rates of nitrogen fixation because of the specific environmental conditions required by diazotrophs. Specifically, other than through nitrogen fixation, nitrogen becomes biologically available to primary producers through the remineralization of OM. Under oxidizing conditions, ammonium (NH_4^+) is transformed into nitrite (NO_2^-) and NO_3^- by nitrifying bacteria. Available nitrogen can also be further transformed and lost from the system through denitrification (Equation 1.4).

$$NO_3^- \rightarrow NO_2^- \rightarrow N_2O \rightarrow N_2 \qquad (1.4)$$

A major source of nitrate for denitrification is from the remineralization of OM in sediments (Seitzinger 1988). Denitrification can occur under oxic and anoxic conditions depending upon the nitrate reducing prokaryotes present (Payne 1973), and serves as an important mechanism for nitrogen loss from marine sediments (Capone and Kiene 1988).

The microbial community composition in sediments not only determines rates of nitrogen fixation and denitrification, but can also alter the concentrations of bioavailable forms of nitrogen. For example, Straub et al. (1996) and Muehe et al. (2009) show nitrate-reducing bacteria oxidize Fe^{2+} (Equation 1.5).

$$10\ FeCO_3 + 2\ NO_3^- + 24\ H_2O \rightarrow 10\ Fe(OH)_3 + N_2 + 10\ HCO_3^- + 8\ H^+ \quad (1.5)$$

This process not only removes available nitrogen from the system but also produces insoluble $Fe(OH)_3$, which removes phosphorus from pore water. Thus, the microbial community alters nutrient availability through redox reactions that directly and indirectly influence nutrient concentrations.

Nitrogen transforming prokaryotes must also compete with photoautotrophs, such as benthic microalgae, which require nitrate or ammonium for OM production. Dalsgaard (2003) and Sundback et al. (2004) demonstrated that benthic microalgae decrease rates of denitrification by limiting available nitrogen sources for nitrifying bacteria. Thus, nitrogen cycling is controlled not only by redox reactions, but also by the biological community composition of autotrophs and heterotrophs competing for available nitrogen.

Redox-reactive Phosphorus Cycling

Redox chemistry influences the solubility of phosphorus through interactions with the iron and sulfur cycles. Phosphate becomes biologically unavailable when it adsorbs onto $Fe(OH)_3$. The abiotic reduction of $Fe(OH)_3$ in sediments releases adsorbed phosphate, increasing its pore water concentration (Krom and Berner 1980). The rate of dissolved inorganic phosphorus (DIP) solubilization is influenced by phosphate-particle interactions. Adsorption and desorption of phosphate from particle surfaces is a

kinetically fast reaction, occurring at a rate of minutes to hours, while its diffusion after absorption by particles is much slower (days to months) (Froelich 1988). Phosphate pore water concentrations are also affected by the movement of phosphate from the pore water to the overlying water (Sundby et al. 1992). Additionally, phosphate solubility is influenced by sediment composition, as there are adsorption-desorption differences between carbonate and iron rich sediments (Jensen et al. 1995).

Dissolved phosphate concentrations are indirectly influenced by additional processes in benthic environments. Sediment oxygen concentrations and rates of organic matter deposition influence iron speciation and, as stated above, DIP concentrations (McManus et al. 1997, Colman and Holland 2000). Sulfur cycling also impacts DIP due to its interaction with iron. The abiotic reductive dissolution of amorphous iron and subsequent FeS and pyrite (FeS_2) formation decreases the phosphate retention capacity of sediments (Anschutz et al. 1998). The formation of FeS and pyrite also removes toxic HS^- from the pore water.

Seasonal cycling is another important factor to consider regarding sediment phosphorus cycling. Seasonal changes in sediment redox conditions, due to deposition of OM from seasonal biological production, alter pore water concentrations of iron, sulfur, and phosphate and the flux of those species into the overlying water column (Rozan et al. 2002), as increased OM deposition to sediments increases microbial respiration which decreases O_2 availability. The depletion of O_2 favors the use of less energy-yielding microbial respiration pathways to oxidize OM. Oxygen availability, iron speciation, and

microbial respiration all influence redox cycling in sediments, which then controls the release or burial of phosphate.

Impact of Benthic Photosynthesis on Sediment Chemistry

Communities of benthic photosynthesizers affect sediment nutrient flux and redox chemistry through both physical and chemical alteration of the environment. Morphological differences between macroalgae and microalgae cause macroalgae to alter flow conditions at the sediment-water interface (SWI), while physiological differences influence nutrient uptake rates and oxygen production. Thus, the alteration of benthic algal community composition can impact sediment redox chemistry and the concentrations of nutrients and oxygen released to the water column. Water flow and turbulent energy affect sediment deposition and nutrient transport.

Within dense macroalgal canopies, water flow can be reduced to less than 10% of that above the canopy (Escartin and Aubrey 1995). Reduced flow within canopies can result in the deposition of smaller particles and higher accumulation of OM (Kleeberg et al. 2010) relative to areas without canopies. Flow rates can also influence whether sediments or the water column act as the major nutrient supplier to benthic algae (Larned and Atkinson 1997). Additionally, in seagrass communities, the type of flow influences ammonium uptake, with oscillatory flow corresponding to greater uptake rates than unidirectional flow (Thomas and Cornelisen 2003). Thus, flow dynamics affect the availability of nutrients for primary producers.

Benthic photosynthesizers can influence the release of nutrients from sediments as well. Some species of benthic primary producers intercept NH_4^+ diffusing from underlying sediments to the water column (McGlathery et al. 1997, Dalsgaard 2003). Other species of algae have been shown to elevate rates of denitrification (An and Joye 2001) and deplete sediments of available nitrogen (Boyle et al. 2004). Additionally, those species with rhizoids, such as sea grasses, increase sediment oxygen concentrations. Macroalgae can also increase sediment OM pools, microbial activity and sulfide concentrations (Holmer et al. 2009). As noted above, sulfide reacts abiotically with iron, forming pyrite and FeS. The concentration and availability of iron in sediments is therefore an important component in regions inhabited by macrophytes and algae, serving as a sink for toxic sulfide and disrupting phosphate sequestration by iron-oxides (Chambers et al. 2001, Marba et al. 2008, Ruiz-Halpern et al. 2008).

The availability of light is also important for photoautotrophs, and affects local redox chemistry and nutrient concentrations as well. The presence of light on sediments colonized by benthic microalgae has been shown to significantly decrease the nitrate flux from sediments (Sundback et al. 2004) and the macroalgae *Gracilaria* spp. is known to increase photosynthetic rates in response to high levels of irradiance, increasing the release of oxygen to the water column (Phooprong et al. 2007). Thus, light is important both for influencing the rate of oxygen production by photosynthesis, and decreasing nitrate release from sediments.

In summary, sediment redox conditions can be altered by the morphological and physiological characteristics of benthic algae. Flow rates and light levels at the sediment-

water interface (SWI) are important factors influencing the availability of oxygen and nutrients at the SWI. Therefore changes to the benthic photosynthetic community structure which alter flow conditions or light availability can impact sediment redox chemistry and the availability of nutrients at the SWI.

Study Objectives

The cycling of iron, sulfur, nitrogen and phosphorus are all interlinked through the biotic and abiotic reactions taking place in sediments and at the SWI. We propose that the type of dominant benthic photosynthesizer influences sediment redox chemistry, affecting nutrient flux across the SWI (Figure 1.2). The work presented in this dissertation focuses on the influence of two invasive macroalgae, *Acanthophora spicifera* and *Gracilaria salicornia*, on sediment redox chemistry and pore water nutrient dynamics. The major objectives of this work include: (i) quantifying the effect of invasive macroalgae on ammonium, nitrate and phosphate release from and retention by sediments (Chapters 2 and 3), (ii) contrasting sediment redox zonation between microalgal- and macroalgal-dominated benthic substrates (Chapters 2, 3 and 4) and (iii) quantifying vertical oscillations of redox transition zones and changes in concentrations of dissolved chemical species in sites with and without macroalgae under varying flow conditions (Chapter 4). Chapter 5 represents work completed during my time as the Head TA for the Oceanography Department undergraduate course, OCN 201- Science of the Sea, in conjunction with Dr. Chris Measures. We developed a simplified, hands-on,

laboratory exercise to teach students the relationship between burning fossil fuels (CO_2 release to the atmosphere) and ocean acidification.

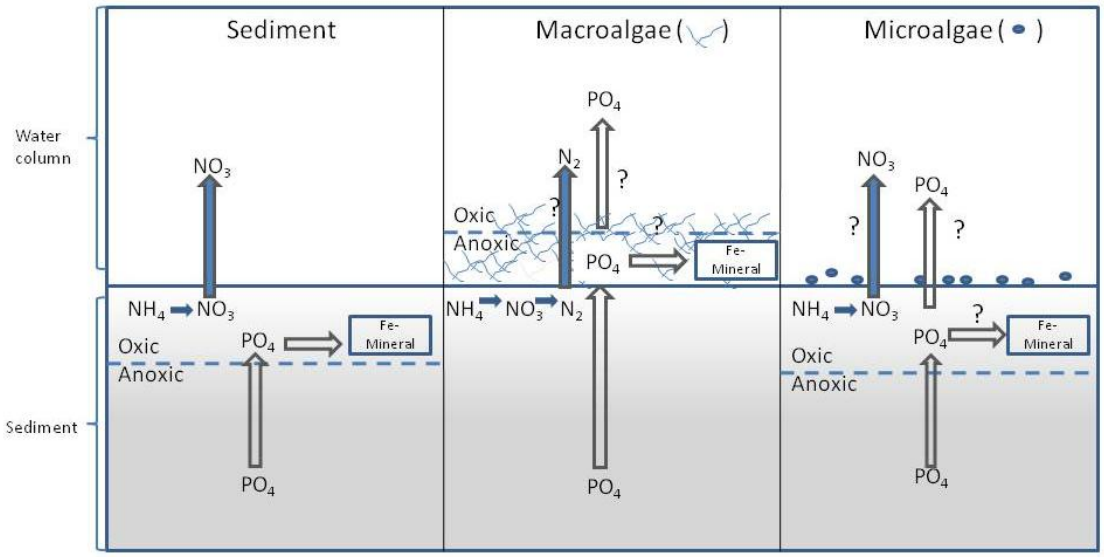

Figure 1.2: Schematic of nutrient release as a consequence of presence/absence of benthic algal types. Changes in oxygen penetration depth impact the bioavailability of nutrients. Formation of an oxic surface layer promotes nitrification, and also phosphate sequestration with Fe minerals. An anoxic surface layer provides an environment favorable of nitrogen loss via denitrification, and enhances phosphate bioavailability as iron-minerals reductively dissolve and release phosphate.

Chapter 2

Effects of benthic macroalgae on sediment-water interface redox oscillations and nutrient cycling

(He‘eia 2010)

Abstract

Invasive algae are known to displace native algal communities and have the potential to alter environmental biogeochemistry. This study examined the influence of an invasive red alga, *Acanthophora spicifera,* on water column nutrients and oxidation-reduction (redox) chemistry over a diel cycle within sandy and muddy sediments in He‘eia Fishpond, O‘ahu, Hawai‘i. Water column oxygen concentrations ranged between 40 and 300 µM over the diel cycle above muddy sediment, and from 100 and 340 µM above sandy sediment, with lowest concentrations in both sediment types occurring before dawn at the sediment water interface in the presence of *A. spicifera*. Diel redox oscillations were observed within sandy sites, especially in regions hosting abundant *A. spicifera*, where pore water Mn^{2+} concentrations were at a maximum before dawn (23 µM), dropping to the lowest concentration in the afternoon (5 µM). Ammonium concentrations and fluxes from the sediment into the overlying water column were higher in the sites containing *A. spicifera* for both sandy and muddy sediment types. Despite the presence of reducing conditions in sediments at all sites, pore water phosphate levels remained at 1 µM or less throughout the entire diel cycle. In He‘eia Fishpond, the presence of *A. spicifera* canopies causes decreased oxygen concentrations at the sediment-water interface and in the water column and the invasive alga increases the concentration of reduced species, including Mn^{2+} and ammonium, in the sediment.

Introduction

Nutrient cycling in coastal regions is an essential component of near shore ecosystem function. Rivers are a well known source of nutrients to coastal environments (Eppley and Peterson 1979) and sediments serve as vast reservoirs of nutrients (Fisher et al. 1982). In shallow coastal environments, benthic remineralization products can diffuse into the water column and are then made available for use by primary producers (Rozan et al. 2002). Sediments are a unique component of nutrient cycling dynamics because they can act as sources or sinks for different nutrient species depending upon local oxidation-reduction (redox) conditions (Mortimer 1941, 1942; Klump and Martens 1987).

The sequence with which microbially-mediated redox reactions occur is dependent upon the lability of organic matter (OM) and availability of oxidants, such that a succession of thermodynamically favorable reactions occurs within sediments (Figure 2.1). The most energetically favorable reactions typically occur in surface sediments and less favorable ones occur at deeper depths. Exceptions to this simplistic paradigm of vertically-stratified redox zones include locations where there are pockets of high organic matter content and in regions of bioturbation (Canfield et al. 1993, Aller 1994). The most favorable oxidant, oxygen, is used first as it provides the greatest energy yield. Nitrate (Payne 1973), iron and manganese oxides (Nealson and Saffarini 1994), and sulfate (Jørgensen 1982) are also important oxidants in marine systems. The presence or absence of oxidized or reduced chemical species in sediments and pore waters can indicate the depth at which different microbial processes are occurring.

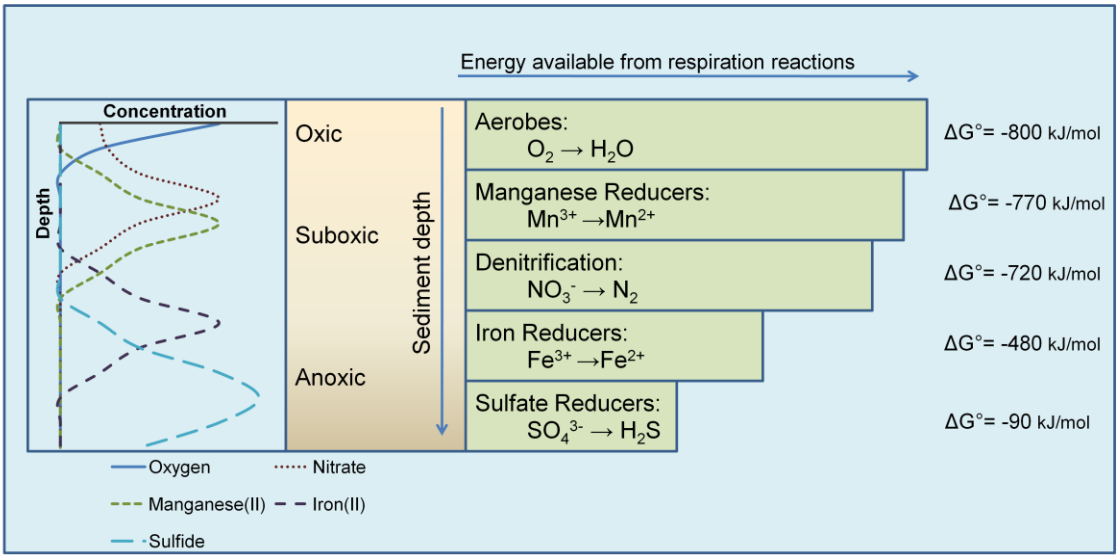

Figure 2.1: Idealized pore water distribution of commonly measured redox species with depth (left panel) are juxtaposed with the metabolic pathways for OM oxidation (right panel), with the most energetically favorable oxidant (O_2) at the top, and the least (SO_4^{3-}) at the bottom. Gibbs free energy for the oxidation of one mole of acetate using the stated oxidant (Canfield et al. 2005) is given on the right side. The terms commonly used to describe the different sediment zones where the given microbial processes take place are shown in the middle panel. (The Gibbs free energy ($\Delta G°$) for an equation determines whether a reaction is spontaneous, with more negative $\Delta G°$ values indicating a more thermodynamically favorable reaction.)

Redox controls on nutrients

Microbial nitrogen cycling in sediments is influenced by sediment redox conditions because of the numerous stable oxidation states of nitrogen. Oxygen availability and benthic microbes influence the speciation of nitrogen and set the depths at which different nitrogen transformations occur. Remineralization of OM in sediments occurs under aerobic and anaerobic conditions, and is a major source of ammonium in benthic regions (Herbert 1999). Nitrifying bacteria are obligate aerobes, and are therefore restricted by the depth of oxygen penetration in sediments. Nitrifiers oxidize

ammonium via a two step nitrification process, to form nitrate (Henricksen and Kemp 1988). Anaerobic ammonium oxidation (anammox), in contrast, results in the removal of nitrogen from the environment through the oxidation of ammonium using nitrite. Nitrate can also be removed from sediments as dinitrogen gas (N_2) through denitrification. In coastal regions, sediment nitrate production is a major source of the nitrogen used for denitrification (Seitzinger 1988). Nitrate is also removed from sediments through uptake by microphytobenthos, which are known to compete with denitrifying bacteria for nitrate (Dalsgaard 2003).

Redox chemistry influences the solubility of phosphorus through interactions with the iron and sulfur cycles. Under oxic conditions, phosphate (PO_4^{3-}) becomes biologically unavailable when it adsorbs to iron oxyhydroxides, while reducing conditions can cause the reduction of oxyhydroxides and subsequent release of adsorbed phosphate into pore waters (e.g. Krom and Berner 1980, Sundby et al. 1986, Jensen et al. 1995, Slomp et al. 1996a and b, Blomqvist and Elmgren 2004). Sulfide indirectly influences phosphate availability through the reductive dissolution of amorphous iron and subsequent FeS and pyrite formation, decreasing the phosphate retention capacity of sediments (Anschutz et al. 1998). Ultimately, the bioavailability of phosphate in pore water is influenced by the redox state of sediments due to the reactivity of phosphate with iron oxyhydroxides, and iron-sulfide interactions.

Manganese and iron as active participants and indicators

Iron and manganese speciation play a role in OM remineralization and the movement of dissolved nutrients from sediments to the overlying water (Canfield et al.

1993). Sediment microbes are capable of using manganese oxides (Myers and Nealson 1988, Nealson and Saffarini 1994) and iron oxides (Nealson and Saffarini 1994) as electron acceptors in the oxidation of OM. The stratification of redox reactions in sediments can be observed in the vertical stratification of reduced species, such as Fe^{2+} and Mn^{2+}, in sediment pore waters (Sørensen and Jørgensen 1987) (Figure 2.1). Abiotic processes also influence the speciation of manganese and iron in sediments. Sulfide rapidly reduces iron (Canfield and Berner 1987, Nealson and Saffarini 1994) and manganese oxides (Burdige and Nealson 1986) forming numerous chemical species, including Fe^{2+}, FeS and Mn^{2+}. Manganese oxides can also be reduced by Fe^{2+} to form iron oxyhydroxides and Mn^{2+}. Therefore the presence of Mn^{2+} and Fe^{2+} in pore waters indicates the depth at which biotic and abiotic redox reactions are occurring in sediments.

In addition to determining the depth of different redox transformations, manganese and iron reduction are important to nutrient cycling. As mentioned above, PO_4^{3-} adsorbs onto iron oxyhydroxides under oxic conditions and is released to pore water when iron is reductively solubilized. Therefore the quantity and oxidation state of iron and manganese influence the amount of phosphate in sediment pore waters. These metals are especially important in Hawai‘i because of the iron and manganese rich basalt that comprises the islands. Seasonal cycling of iron and manganese has been found in coastal sediments (Rozan et al. 2002, Thamdrup et al. 1994), where the deposition of OM leads to anoxic conditions and the shoaling of manganese and iron redox transition zones. Rozan et al. (2002) observed that the shoaling of the iron reduction zone in anoxic sediments was accompanied by a release of phosphate, and actually stimulated a

secondary benthic algal bloom, highlighting the importance of sediment redox conditions on water column nutrients and ecology.

Benthic Macroalgae and Microalgae

The dependence of nutrient availability on OM remineralization and on local redox conditions highlights the importance of water column oxygen concentrations on sediment chemistry. Therefore, processes that alter ambient oxygen at the sediment water interface (SWI) have the potential to affect OM remineralization and release or burial in sediments. Anoxic water column conditions that occur after a large die off of phytoplankton or macroalgae, for example, are driven by the remineralization of labile OM. Such episodes have been observed on monthly (Sundback et al. 1990) and seasonal time scales to alter water column nutrient concentrations (Jørgensen 1983, Lavery and McComb 1991, Rozan et al. 2002, Corzo et al. 2009). The type of benthic primary producer, whether microalgae, macroalgae, or macrophyte, also influences sediment nutrient cycling. For example, oxygen is increased through benthic photosynthesis and the oxidizing rhizosphere of macrophytes and sea grasses (Ottosen et al. 1999), while oxygen is decreased when aquatic vegetation reduces water flow (Forster et al. 1996) and during night time respiration by primary producers. Therefore a change in the dominant type of benthic primary producer, especially from microalgae to macroalgae, can impact sediment redox conditions and influence nutrient cycling.

Project Objectives

The purpose of this study was to examine the effect of benthic macroalgal canopies on SWI nutrient exchange over diel cycles. We contrasted SWI nutrient concentrations and redox chemistry of sediments dominated by microphytobenthos to those colonized by an invasive benthic red algae, *Acanthophora spicifera*, in two sediment types. One set of study sites was characterized by a coarse, sandy, carbonate facies while the second set of sites was located in a fine-grained, muddy facies. Major objectives of the project were: (i) to quantify extent of vertical oscillations of redox transition zones within the sediment column and coincident changes in the concentration of dissolved chemical species over a diel cycle, (ii) to contrast sediment manganese, iron and nutrient cycling between microalgae and *A. spicifera* dominated benthic substrates, and (iii) to examine the effect of *A. spicifera* on sediment nitrogen and phosphorus release and retention. We considered the site without the invasive macroalgae to be the control, approximating what benthic conditions would look like in the absence of the invasive species. We hypothesized that there would be reduced oxygen concentrations at night within the thick *A. spicifera* canopies, relative to the control site, as a consequence of increased microbial respiration due to a higher concentration of organic matter, and decreased water transport, resulting in greater vertical oscillations in redox zones and an alteration of sediment redox chemistry that favors phosphate and ammonium release from sediments.

Methods

Site description

He‘eia Fishpond is located adjacent to Kāne‘ohe Bay on the northeast side of the island of O‘ahu, Hawai‘i. An 88-acre ancient Hawaiian aquaculture pond, the fishpond is situated at the land-ocean boundary and separated from the ocean by a rock wall. Historically He‘eia Fishpond was used as a source of fish for local Hawaiians and is currently being restored by repair of the two meter wide wall and removal of predators from the pond through the work of the non-profit group Paepae O He‘eia. Six gates in the wall of the pond allow freshwater and saltwater to flow into and out of He‘eia Fishpond. Sediment type varies in a systematic way across the pond, with a fine-grained, muddy facies located near the stream inputs, and a coarse-grained, sandy, carbonate facies found closer to the ocean. The average depth of the pond is less than one meter, with tidal fluctuations of less than 0.5 m during neap tidal cycles (Young 2011).

The pond and adjacent Kāne‘ohe Bay have been colonized by the invasive benthic macroalgae, *A. spicifera*, introduced to O‘ahu in the early 1950s via barge fouling (Doty 1961). This algae forms dense canopies in the pond and is one of the most common non-indigenous algal species found in Hawaiian waters (Smith et al. 2002). *Acanthophora spicifera* canopies are variable in size, but the patches studied here were 2-3 m across and 0.1 to 0.3 m tall.

Experimental Design

Within each sediment facies, we identified adjacent plots, one dominated by the macroalgae *A. spicifera,* the other devoid of macroalgae and dominated by microalgae. A total of four experimental sites were selected for data collection over the diurnal, two within each facies. At each site, sediment and water column samples were collected between 12-3 a.m. (midnight), 4-7 a.m. (dawn), 7-10 a.m. (morning) and 3-6 p.m. (afternoon) on August 25 and 27, 2010. Sampling was conducted during neap tide to minimize potential tidal effects.

Water column parameters

At each sampling time point, water was collected from three depths: 0.1 m below the air-water interface (surface), just inside the *A. spicifera* canopy (canopy), and at the sediment water interface (SWI), using Teflon© tubing and a 60-cc syringe. This design allowed for minimal disturbance to the macroalgal canopy during water collection. For the corresponding microalgae sites, where no canopy was present, water was collected at the same corresponding depths above the SWI. Immediately after collection samples were filtered through 0.2 µm Whatman polycarbonate filters, and subsamples were stored in acid clean HDPE bottles. Samples for phosphate analysis were placed into bottles with 12 N HCl to achieve a final pH of 1, and samples for ammonium and nitrate analyses were stored in a second, unacidified bottle, and frozen until analyzed. In addition to water collection, the water column was profiled for temperature and dissolved oxygen (AADI optode) and pH (Sensorex submersible pH probe coupled with an Orion 5-star meter).

Sediment coring and sectioning

For each time point, a 10 cm deep sediment core, 9.5 cm in diameter, was collected, sealed, and transferred via boat to the shore for immediate sectioning. The core was sectioned in a glove bag purged with ultra high purity nitrogen at 0.25 cm resolution for the top 2 cm and in 0.5 cm intervals from 2 cm to a minimum depth of 6 cm. Overlying water from the core was also collected while the core was in the glove bag, and was treated as described below for sediment pore water samples. After sectioning, the sediment was transferred to Whatman VectaSpin 20® 50 mL centrifuge tubes for pore water extraction (Briggs 2011). After centrifugation, the tubes were transferred to a clean, nitrogen purged glove bag where pore water was filtered through 0.2 µm Whatman polycarbonate filters and stored for later analysis. Samples for dissolved phosphate analysis were placed into pre-acidified vials, as described above for water column samples. All samples were stored on ice until transported back to the laboratory, where acidified samples were stored at 4 °C and those for ammonium and nitrate analysis were stored at -20 °C.

Pore Water Analyses

The reactive nature of manganese, iron and ammonium warranted timely analysis. Within six hours of collection, pore water samples were transported to the laboratory for colorimetric analysis of manganese (Mn^{2+}) (Tebo 2007) and total dissolved iron (Stookey 1970). Ammonium colorimetric analysis was completed within 12 hours of sample thawing (Koroleff 1979). Nitrate + nitrite analysis was conducted by first reducing all nitrate to nitrite using the nitrate reductase enzymatic reaction (Campbell et al. 2006),

followed by standard nitrite colorimetric determination (Grasshoff et al. 1983). Nitrate + nitrite will be referred to as nitrate in subsequent discussion. Dissolved inorganic phosphate (DIP) was analyzed using the molybdate blue method (Grasshoff et al. 1983). Total dissolved phosphate (TDP) was determined by drying 1.0 mL of water with 40 µL of $Mg(NO_3)_2$ and combusting at 550 °C. The TDP samples were then shaken with 400 µL of 1 N HCl for 24 hours to hydrolyze and solubilize sediment phosphorus (Monaghan and Ruttenberg 1999) and, after adjusting the pH of each sample to 1.0, colorimetrically analyzed using the molybdate blue method (Grasshoff et al. 1983). All colorimetric analyses were conducted on a Synergy HT BioTek Multi-Mode Microplate Reader using Thermo Scientific Nuc 96-well Optical Bottom Microplates©.

Flux

The flux of nutrients, ammonium, nitrate, and phosphate, based on pore water concentrations from each sediment core was calculated using on Fick's first law of diffusion (Equation 3.1).

$$J = (ø)(D_{sed})(dC/dz) \qquad (3.1)$$

$$D_{sed} = D_{sw}/\Theta^2 \qquad (3.2)$$

For each profile, a least squares regression line was fit to the concentration profile of each species to determine the change in concentration with depth (dC/dz). The sediment diffusivity (D_{sed}) of nitrogen, ammonium and phosphate was calculated using the diffusivity of each species in seawater (D_{sw}) (Boudreau 1997) and tortuosity (Equation 3.2). Tortuosity (Θ^2) was determined based on the sediment porosity (ø) from values in

Boudreau (1997). Briggs (2011) determined the porosity of the sediment in the muddy facies to be 0.61 and 0.51 in the sandy facies.

Results

Water column parameters - Sandy Facies

Water column oxygen concentrations at sites within the sandy facies ranged between 100 and 340 µM over the course of the 24 hour (diel) period (Table 2.1). Minimum oxygen concentrations were observed at the SWI at midnight and highs occurred in the canopy and at the SWI during the day (Figure 2.2 a and b). Temperatures ranged from 23.5°C (dawn) to 25.4°C (afternoon). Low temperatures occurred at the water surface and highs at the SWI. In surface waters, pH ranged from 8.4 to 8.6, and at the SWI it ranged from 8.3 to 8.9 (Table 2.1). The highest pH (8.9) was measured in the microalgal site, 20 cm above the SWI, before dawn.

Differences in oxygen concentration between sites occurred during the midnight and afternoon samplings (Figure 2.2 a and b). At midnight, the dissolved oxygen concentration in the *A. spicifera* site dropped from 250 µM at the water surface to 200 µM in the canopy (Figure 2.2b), while in the microalgal site the dissolved oxygen concentration remained at 260 µM (Figure 2.2a). At midnight, dissolved oxygen concentrations were similar between sites at the SWI. At dawn the SWI oxygen concentration was 50 µM lower in the *A. spicifera* site (130 µM) than the microalgal site

(180 µM), while below the air-water interface and at the depth of the canopy, similar concentrations were present (Figure 2.2). These oxygen variations correlated with temperature differences. At midnight the canopy was 0.9 °C warmer in the *A. spicifera* site that the microalgal site, and by dawn the *A. spicifera* SWI was 4.4 °C warmer than the microalgal one (Table 2.1). Between sites at dawn, pH at the SWI was 0.5 pH units lower in the *A. spicifera* site than the microalgal site (Table 2.1).

At each site, water column nutrient data collected from three locations at each sampling time. As a consequence of the lack of variability in concentration across the diel, it seemed reasonable to pool the concentration across all sampling time points for each depth (Figures 2.3a and 2.4a). This approach allowed simplification of data presentation without loss of information. Nitrate and DIP concentrations were below the detection limit (BDL) of 0.5 µM for all water column sampling points. Ammonium concentrations ranged from BDL to 0.6 µM (Figure 2.3a). The *A. spicifera* site had detectable ammonium levels for most sampling points; while the microalgal site had no detectable ammonium. TDP values ranged from below detection limit to 0.9 µM (Figure 2.4a). The *A. spicifera* site had higher TDP values for all three locations.

Table 2.1: Water column parameters for sites located in muddy and sandy facies. Times are defined as follows: 12-3 a.m. (midnight), 4-7 a.m. (dawn), 7-10 a.m. (morning), and 3-6 p.m. (afternoon). Location refers to depth within the water column: surface is below the air-sea interface, canopy is the depth where the top of the macroalgal canopy occurred, and SWI is above the surface of the sediment. Data from sites with *A. spicifera* are presented in the Macro columns, while sites without the macroalgae, the microalgal sites, are listed in the Micro columns.

	Muddy Facies					Sandy Facies			
Oxygen (µM)	**Time**	**Location**	**Micro**	**Macro**	Oxygen (µM)	**Time**	**Location**	**Micro**	**Macro**
	dawn	surface	210	180		midnight	surface	260	250
		canopy	200	130			canopy	260	200
		SWI	70	40			SWI	110	100
	morning	surface	210	190		dawn	surface	210	210
		canopy	210	220			canopy	190	170
		SWI	270	50			SWI	180	130
	afternoon	surface	270	290		afternoon	surface	250	250
		canopy	300	300			canopy	300	310
		SWI	210	240			SWI	340	330
pH	**Time**	**Location**	**Micro**	**Macro**	pH	**Time**	**Location**	**Micro**	**Macro**
	dawn	surface	8.30	8.10		midnight	surface	8.58	8.51
		canopy	8.29	8.29			canopy	8.54	8.45
		SWI	8.23	8.13			SWI	8.27	8.44
	morning	surface	8.14	8.06		dawn	surface	8.46	8.44
		canopy	8.13	8.40			canopy	8.88	8.40
		SWI	8.50	8.31			SWI	8.81	8.34
	afternoon	surface	8.43	8.28		afternoon	surface	8.40	8.40
		canopy	8.66	8.65			canopy	8.53	8.63
		SWI	8.54	8.57			SWI	8.67	8.70
Temperature (°C)	**Time**	**Location**	**Micro**	**Macro**	Temperature (°C)	**Time**	**Location**	**Micro**	**Macro**
	dawn	surface	29.2	25.6		midnight	surface	24.4	24.6
		canopy	25.6	26.6			canopy	24.7	25.6
		SWI	26.6	27.0			SWI	25.7	25.9
	morning	surface	25.4	25.2		dawn	surface	24.0	23.4
		canopy	25.5	25.6			canopy	28.2	28.6
		SWI	26.1	26.2			SWI	24.5	28.9
	afternoon	surface	26.7	26.6		afternoon	surface	25.4	25.4
		canopy	27.2	27.6			canopy	26.2	26.4
		SWI	28.1	27.8			SWI	27.0	27.3

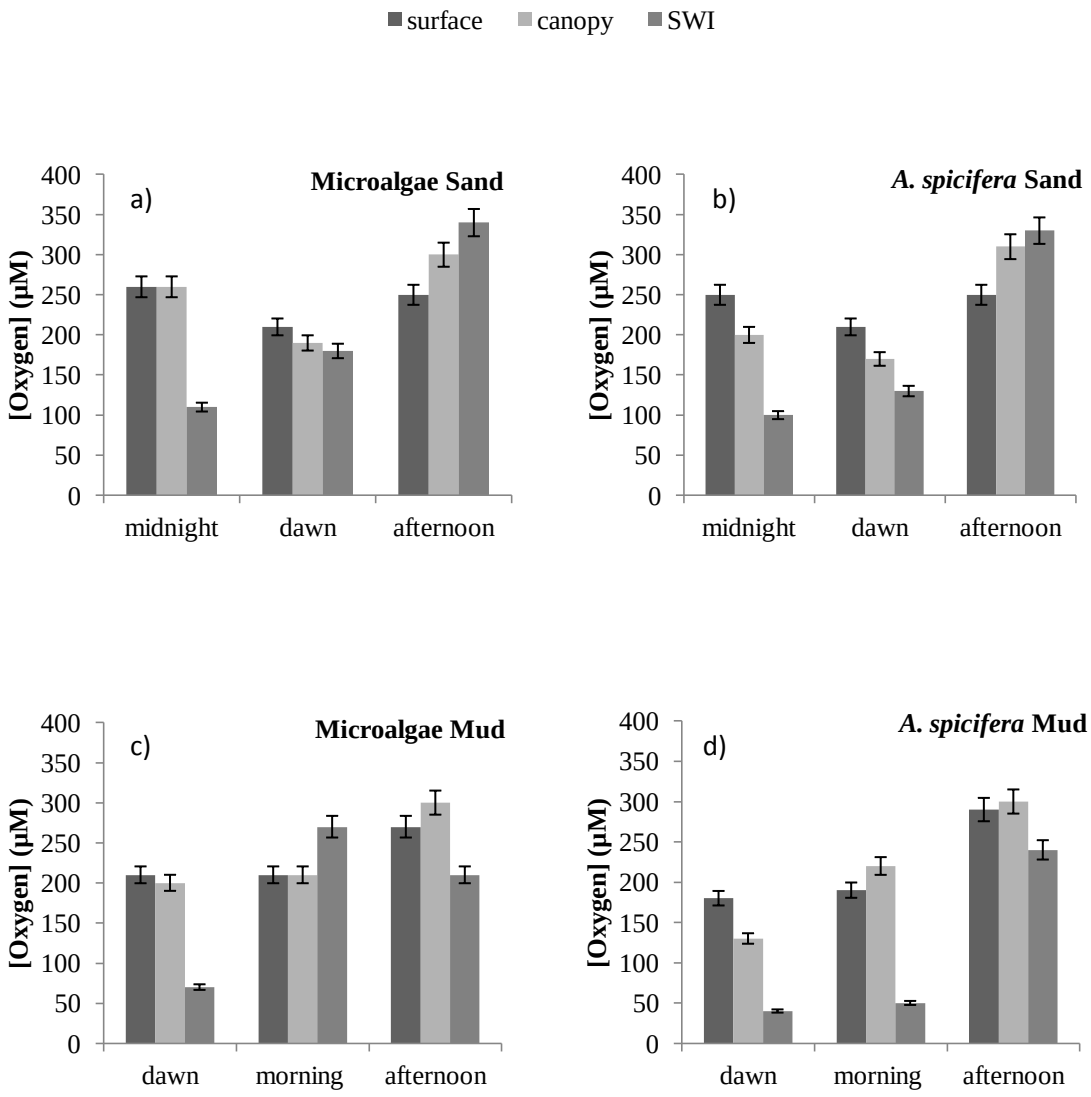

Figure 2.2: Water column oxygen concentrations over the course of the diel cycle for each of the four study sites. The top row shows the muddy facies and the bottom row shows the sandy facies. The column on the left has microalgae only sites and the one on the right is for sites dominated by the invasive macroalgae. Each bar represents a water column location, and error bars are ± 5%, the error of the optode.

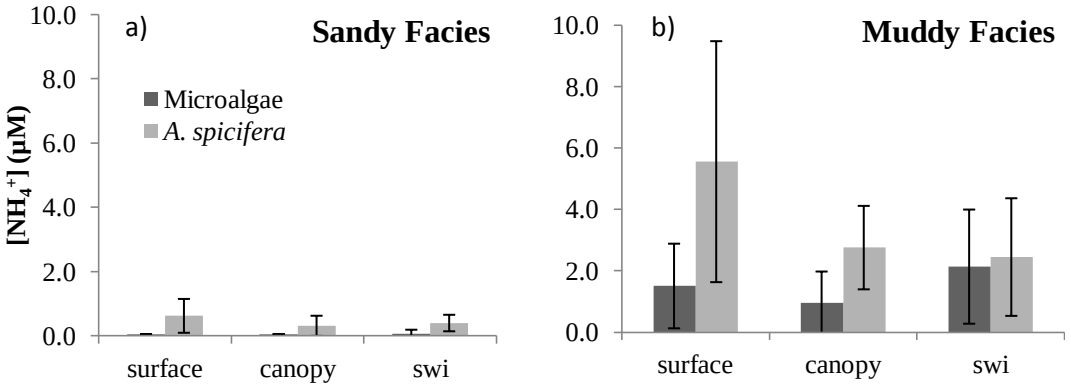

Figure 2.3: Water column ammonium concentrations for the (a) sandy and (b) muddy facies from the surface, canopy and sediment-water interface (SWI) locations. Water collected at each of the three time points (see Table 2.1) was pooled within each site, due to similarity between most readings. Areas where data appears to be missing are from samples where the reading was below the detection limit. Error bars represent ±1 SD (n=3 samples).

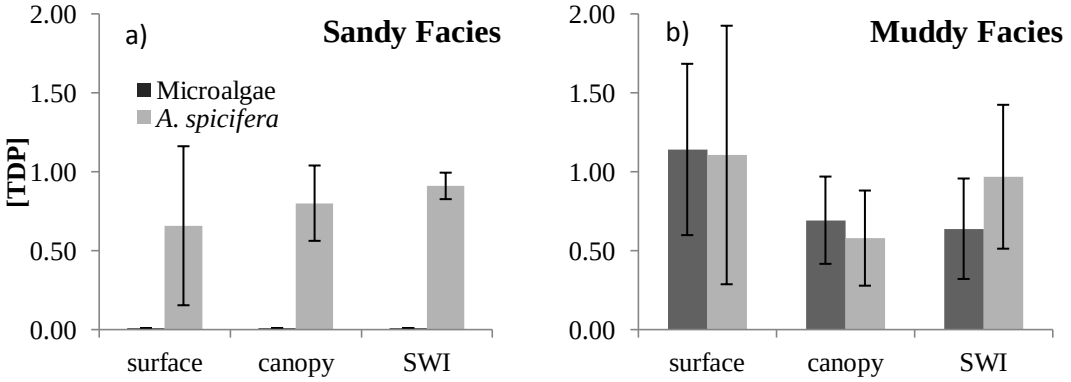

Figure 2.4: Water column total dissolved phosphorus concentrations for the (a) sandy and (b) muddy facies from the surface, canopy and sediment-water interface (SWI) locations. Water collected at each of the three time points (see Table 2.1) was pooled within each site, due to similarity between most readings. Areas where data appears to be missing are from samples where the reading was below the detection limit. Error bars represent ±1 SD (n=3 samples).

Water column parameters - Muddy Facies

Oxygen concentrations varied between 40 and 300 µM in the muddy facies (Figure 2.2b), with highest values occurring in the afternoon and lowest at the SWI before dawn (Table 2.1). Temperatures ranged from 25 to 28 °C, with coolest values at the surface in the morning and warmest at the SWI in the afternoon. The pH varied between 8.1 and 8.4 in surface waters and 8.1 to 8.7 at the SWI; the highest pH (8.7) was measured in the canopy during the afternoon. For five of the six water column profiles in the muddy sites, pH was lower at the SWI than at the canopy depth (Table 2.1).

Dissolved oxygen concentrations varied between the *A. spicifera* and microalgal sites. At both the dawn and morning samplings, the microalgal site had higher surface and SWI oxygen concentrations than the *A. spicifera* site (Figure 2.2c and d). The reverse occurred in the afternoon, where the *A. spicifera* site had higher surface and SWI oxygen concentrations. The largest difference between sites occurred at the SWI in the morning, when the oxygen concentration in the microalgal site was 220 µM higher than in the *A. spicifera* site. During this sampling the largest pH difference between sites also occurred. The pH of the *A. spicifera* site was 0.3 lower at the canopy depth and 0.2 lower at the SWI than the corresponding microalgal pH values (Table 2.1). During the dawn sampling, at the canopy depth, oxygen in the microalgal site was 70 µM higher and 1.0 °C cooler than at the corresponding *A. spicifera* location.

At each site, water column nutrient data was collected from three locations at each sampling time. As with the sandy facies, concentrations were pooled across all sampling time points at each depth because of a lack of variability in concentration across the diel.

Similar to the sandy sites, no detectable nitrate or DIP was found in the water column at either site. Ammonium concentrations ranged from 1 to 6 µM (Figure 2.3b), and TDP values ranged from 0.58 to 1.1 µM (Figure 2.4b). As indicated by the overlap of the error bars, no significant difference in ammonium or TDP concentrations were found between sites.

Pore water- Sandy Facies

Nutrients

In the sandy facies, nutrient depth profiles varied over the diel cycle. Nitrate was detected in the water overlying the sediment in cores taken at the dawn and afternoon time points (Table 2.2). When nitrate was at detectable levels, peak concentrations ranged from 2 to 5 µM. The maximum nitrate concentration varied over the diel cycle; nitrate was BDL at midnight and 5 µM in the afternoon. The depth of the maximum nitrate concentration ranged from -1.0 cm in the dawn core to -0.75 cm in the afternoon and midnight cores. The highest peak nitrate concentration (5 µM) occurred at -0.75 cm, in the afternoon sampling.

Ammonium concentrations ranged from 2.4 to 37 µM in the water overlying the core (Table 2.2). In the sediment, maximum pore water ammonium concentrations ranged from 46 to 140 µM between depths of -0.25 and -2.5 cm. Highest peak concentrations were found in the dawn sampling. DIP concentration was low to undetectable in the cores, ranging from BDL to 1 µM. DIP was only measurable in the water overlying the core at dawn at the microalgal site (0.7 µM).

Considerable variability in pore water nutrient concentrations was also observed between the two sandy sites. Nitrate concentrations were 2 to 3 µM higher in the microalgal cores than those hosting *A. spicifera*, though concentration maxima occurred at the same depth. The *A. spicifera* site had the same maximum nitrate concentration, 2 µM, at all sampling times. At the microalgal site, the maximum nitrate concentration was more variable, with the highest concentration occurring in the afternoon (5 µM). Unlike nitrate, ammonium maxima did not occur at the same depths between sites. At each sampling, the depth of the maximum ammonium concentration was distinct for the *A. spicifera* and microalgal sites, with a maximum depth discrepancy of 1.5 cm for the afternoon sampling. While the depth at which the peak ammonium concentrations occurred was different between sites, in both sites the maximum concentrations occurred at the dawn sampling.

When detectable, maximum DIP concentrations occurred at shallower depths in the microalgal core relative to the core colonized by *A. spicifera*. Except for the midnight sampling, higher DIP levels were observed in the microalgal cores. Over the course of the study higher nitrate and DIP concentrations were observed at the microalgal site, while the *A. spicifera* site was characterized by higher ammonium concentrations.

Metals

In the water overlying the cores, Mn^{2+} concentrations ranged between BDL and 1.5 µM (Table 2.2). The highest Mn^{2+} concentrations occurred during the dawn sampling, while the lowest were recorded in the afternoon (Figure 2.5 a and b). Measurable dissolved iron was only present in the overlying water once (9 µM, dawn

microalgal site) (Table 2.2). Maximum pore water dissolved iron concentrations were lowest at the dawn sampling for both sites and highest at the midnight sampling for the microalgae and in the afternoon for the *A. spicifera* site (Figure 2.6 a and b).

Mn^{2+} maxima at both sites occurred at a shallower depth at the dawn sampling than during the afternoon. At dawn, higher Mn^{2+} concentrations occurred in the *A. spicifera* site (23 µM) than the microalgal site (13 µM), however Mn^{2+} concentrations were similar between sites at the afternoon and midnight time points (Figure 2.5 a and b). Unlike Mn^{2+}, the highest iron concentration did not occur at the dawn sampling. Instead, the maximum iron concentration occurred at midnight in the microalgal site (36 µM) and in the afternoon for the *A. spicifera* site (25 µM) (Figure 2.6 a and b). Depths at which maximum iron concentrations occurred also varied between sites. At the *A. spicifera* site, maxima occurred at the same depth for midnight and afternoon samplings, however in the microalgal site the maximum iron concentration occurred at the same depth during the midnight and dawn samplings.

Table 2.2: Pore water data from the sandy facies. The top row for each site gives the concentration in the water overlying the core The second line for each site gives the maximum (peak) pore water concentration and depth (cm) at which the concentration maximum occurs.

Sandy Facies			midnight		dawn		afternoon	
			depth (cm)	*Conc. (µM)*	*depth (cm)*	*Conc. (µM)*	*depth (cm)*	*Conc. (µM)*
Nitrate	***A. spicifera***	overlying water		BDL		0.7		2
		sediment	-0.75	2	-1	2	-0.75	2
	Microalgae	overlying water		BDL		4		4
		sediment	--	BDL	-1	4	-0.75	5
Ammonium	***A. spicifera***	overlying water		27		13		37
		sediment	-1	100	-0.25	140	-1	100
	Microalgae	overlying water		13		23		2.4
		sediment	-1.5	57	-1.75	120	-2.5	46
DIP	***A. spicifera***	overlying water		BDL		BDL		BDL
		sediment	-3.5	0.8	-1.5	0.5	--	BDL
	Microalgae	overlying water		BDL		0.7		BDL
		sediment	-1.25	0.6	-1.25	1	-2.5	1
Mn^{2+}	***A. spicifera***	overlying water		1.2		BDL		0.7
		sediment	-0.25	13	-0.25	23	-1.25	5
	Microalgae	overlying water		1.5		1.5		BDL
		sediment	-0.25	11	-0.25	13	-0.5	6
Fe(TD)	***A. spicifera***	overlying water		BDL		BDL		BDL
		sediment	-1.25	15	-0.75	8	-1.25	25
	Microalgae	overlying water		BDL		9		BDL
		sediment	-0.25	36	-0.25	9	-1	21

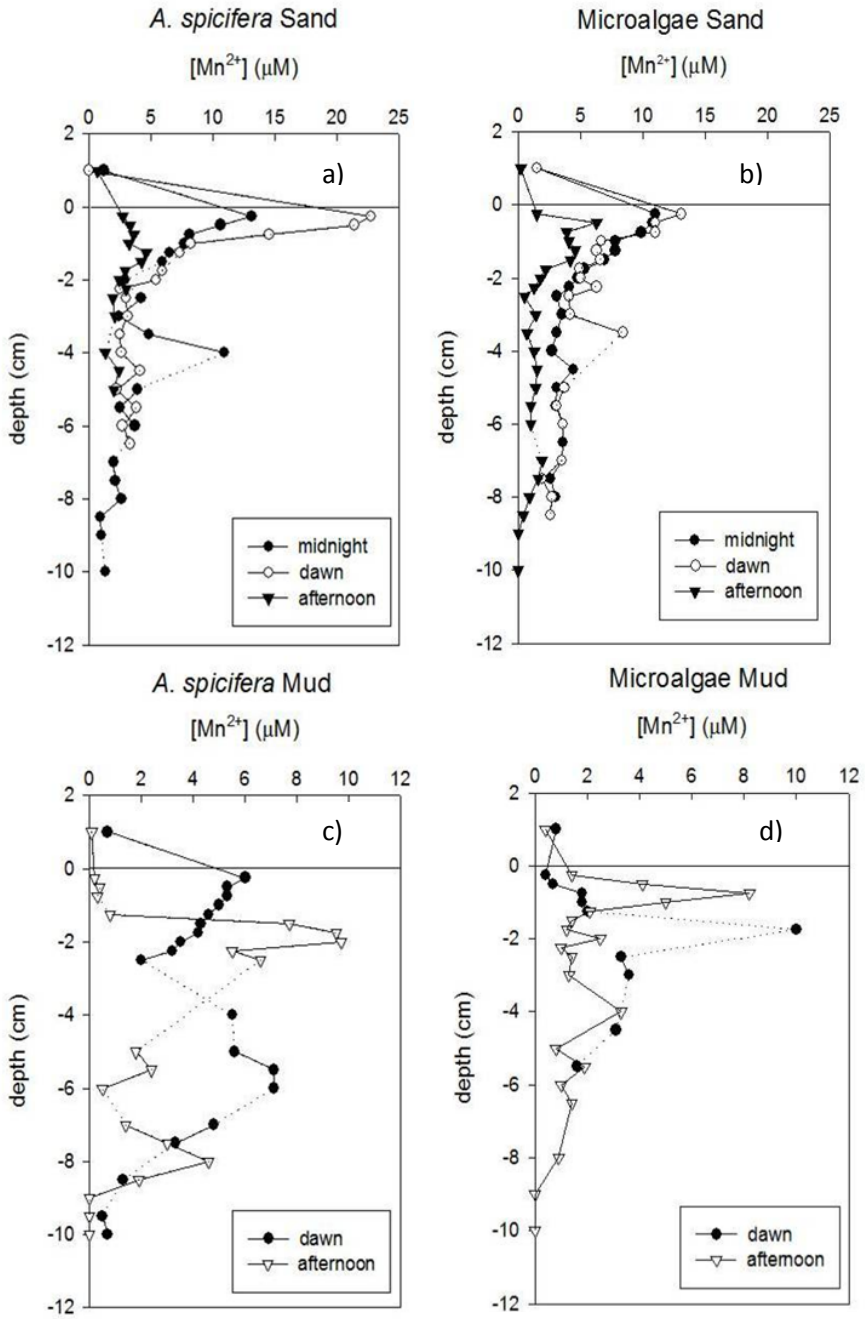

Figure 2.5: Pore water Mn^{2+} concentration in µM. Points located at 1 are values obtained from the water overlying the core. The horizontal line indicates the location of the sediment-water interface, and dotted lines connect data where points are missing.

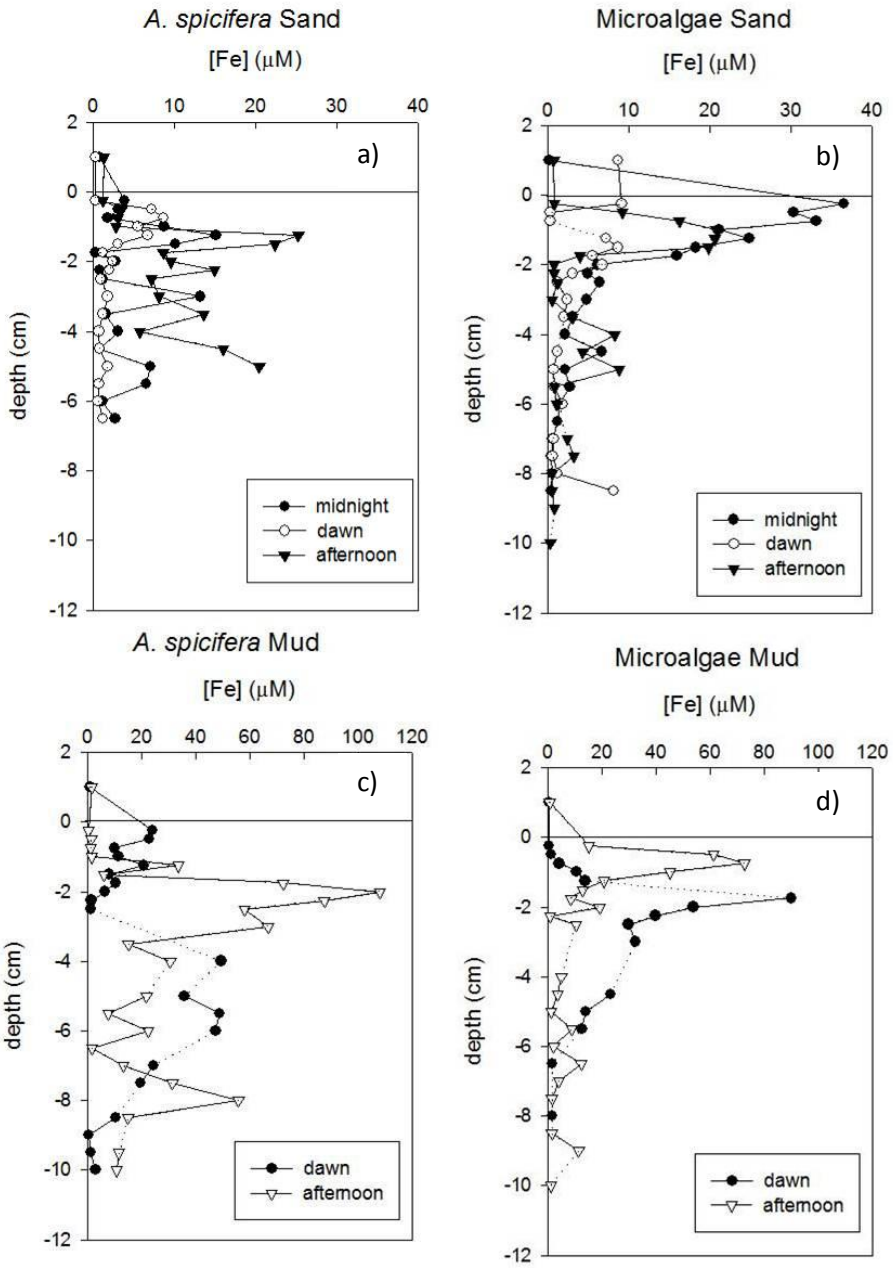

Figure 2.6: Pore water total dissolved iron concentration in μM. Points located at 1 are values obtained from the overlying core water. The horizontal line indicates the location of the sediment-water interface, and dotted lines connect data where points are missing.

Pore water- Muddy Facies

Nutrients

Nutrient concentrations over the diel cycle were similar in cores taken from sites within the muddy facies (Table 2.3). No nitrate was detected in the water overlying the cores at either site. Pore water nitrate concentration maxima of between 5 and 7 µM occurred at depths ranging between -0.25 to -1.25 cm. Ammonium was present in the water overlying the core for all cores, and ranged from 11 to 26 µM. Pore water ammonium concentrations did not display a distinct maximum peak, but remained relatively constant over the top few cm of the core. Therefore, rather than reporting a maximum peak concentration, ammonium concentrations were averaged from -0.25 to -2.0 cm for each core. Over that depth interval, average ammonium concentrations ranged between 22 and 42 µM. DIP concentrations were low, ranging from BDL to 0.9 µM; no DIP was detectable in the water overlying the cores.

Maximum pore water nutrient concentrations observed at the two sites from within the muddy facies were similar. At the dawn and afternoon time points, the maximum nitrate concentration at the microalgal site occurred at -0.5 cm, while in the *A. spicifera* site the maximum shifted from -0.25 cm at dawn to -1.25 cm in the afternoon (Table 2.3). The pore water ammonium concentration was near 40 µM for the *A. spicifera* site but only 25 µM for the microalgal site. At dawn, the ammonium in the water overlying the core from the microalgal site (26 µM) was more than double that at the *A. spicifera* site (11 µM), however in the afternoon both sites had similar ammonium concentrations (20 µM) in the water overlying the core. In the dawn core, DIP was BDL

at all depths in the *A. spicifera* core, however it was detectable in the microalgal core (-1.75 cm, 0.6 µM). In the afternoon, DIP peaks occurred at the same depth in cores from both sites, but at a higher concentration in the *A. spicifera* core (0.9 µM) than in the microalgal core (0.6 µM). The major difference in nutrients between sites was observed in pore water ammonium concentrations: the *A. spicifera* site had nearly double the ammonium concentration of the microalgal site.

Metals

In the muddy facies, variability in the iron and manganese concentrations exceeded that observed in the nutrient data (Table 2.3). Mn^{2+} was only detected in the water overlying the core once, during the dawn *A. spicifera* sampling (0.7 µM) (Figure 2.5c). Maximum Mn^{2+} pore water concentrations ranged between 6 and 10 µM, and occurred in the top 2 cm of the sediment. Dissolved iron concentrations in the overlying water of the *A. spicifera* site ranged between 0.5 and 1.5 µM (Figure 2.6c). Maximum pore water dissolved iron concentrations ranged between 24 and 110 µM, and concentrations were higher when the peak occurred deeper in the sediment (Figure 2.6 c and d).

Between sites, large variations were observed in the depth of manganese maxima and the concentration and depth of iron maxima; however within each core the manganese and iron peaks occurred at the same depth. Mn^{2+} concentrations varied minimally between sites and sampling points, however peak depths varied by 1.5 cm between sites (Figure 2.5 c and d). In *A. spicifera* cores the Mn^{2+} concentration peaked at a shallower depth at night (-0.25 cm, 6 µM) compared to the day (-2 cm, 10 µM) (Figure

2.5c), unlike the microalgal site where Mn^{2+} peaked at a deeper depth during the night (-1.75 cm, 7 µM) than during the day (-0.75 cm, 7 µM) (Figure 2.5d). In the *A. spicifera* cores, dissolved iron peaked at a shallower depth at night (-0.25 cm, 24 µM) than during the day (-2.0 cm 110 µM) (Figure 2.6c), and for the microalgal cores it peaked at a deeper depth at night (-1.75 cm, 90 µM) than during the day (-0.75 cm, 75 µM) (Figure 2.6d).

Table 2.3: Pore water data from muddy facies. Top row for each site lists the concentration of the water overlying the core. The second line for each site gives the maximum pore water concentration and depth (cm) at which the concentration maximum occurred.

Muddy Facies			dawn		afternoon	
			Depth (cm)	*Conc. (µM)*	*Depth (cm)*	*Conc. (µM)*
Nitrate	***A. spicifera***	overlying water		BDL		BDL
		sediment	-0.25	7	1.25	5
	Microalgae	overlying water		BDL		BDL
		sediment	-0.5	7	-0.5	7
Ammonium	***A. spicifera***	overlying water		11		20
		sediment	*	41	*	42
	Microalgae	overlying water		26		22
		sediment	*	25	*	22
DIP	***A. spicifera***	overlying water		BDL		BDL
		sediment	--	BDL	-2	0.9
	Microalgae	overlying water		BDL		BDL
		sediment	-1.75	0.6	-2	0.6
Mn^{2+}	***A. spicifera***	overlying water		0.7		BDL
		sediment	-0.25	6	-2	10
	Microalgae	overlying water		0.8		BDL
		sediment	-1.75	7	-0.75	7
Fe(TD)	***A. spicifera***	overlying water		1		1.5
		sediment	-0.25	24	-2	110
	Microalgae	overlying water		0.5		0.7
		sediment	-1.75	90	-0.75	75

*Ammonium profile did not display a distinct peak, and therefore the mean over the top 2 cm is reported.

Flux

Muddy Facies

The flux of nitrate from the sediment to the water column in the muddy microalgal site occurred at a similar rate both at dawn and in afternoon (Figure 2.7a). The macroalgal site had a higher nitrate flux at dawn than in the afternoon. Ammonium flux in the *A. spicifera* site was highest at dawn, while the microalgal site had a higher ammonium flux in the afternoon (Figure 2.8a). The microalgal site had a higher phosphate flux at dawn, and the *A. spicifera* site had a higher flux in the afternoon (Figure 2.9a).

Sandy Facies

In the sandy facies, nitrate flux was similar between the microalgal and *A. spicifera* sites at dawn, while the flux of nitrate to the water column was higher in the microalgal site in the afternoon and higher in the *A. spicifera* site at midnight (Figure 2.7b). The flux of ammonium to the water column was highest in the *A. spicifera* site at all time points, especially in the afternoon (Figure 2.8b). Phosphate flux was higher in the microalgal site than the adjacent *A. spicifera* site at midnight and dawn, and no flux of phosphate occurred from either site in the afternoon (Figure 2.9b).

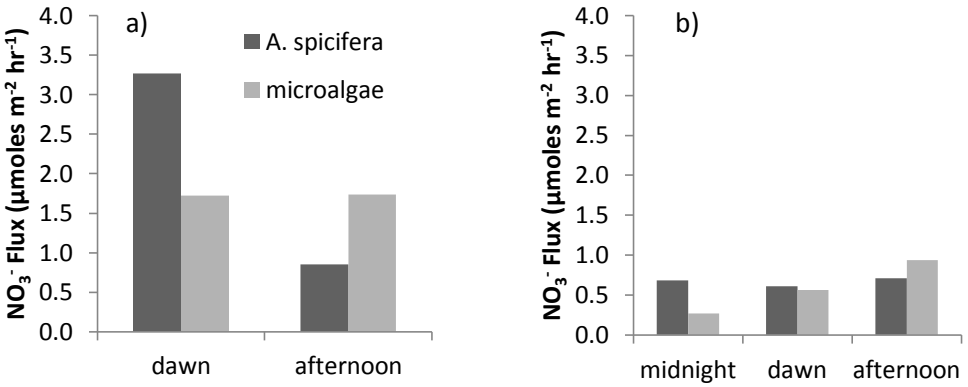

Figure 2.7: Flux of nitrate from the sediment into the water column for a) the muddy facies and b) the sandy facies.

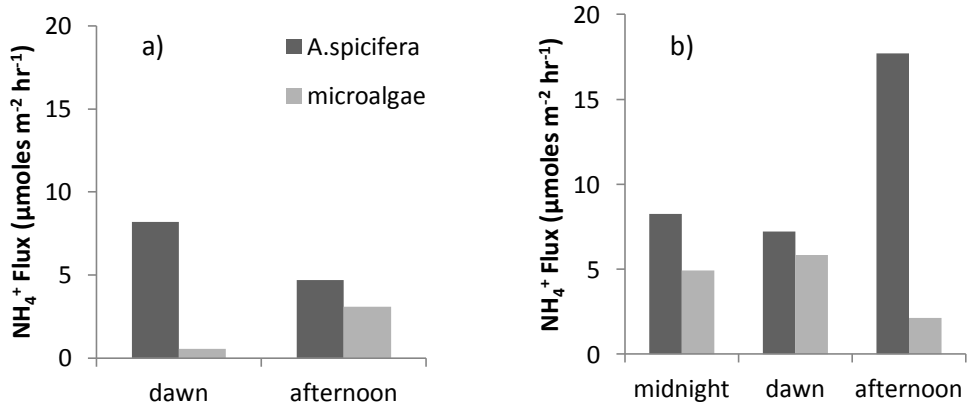

Figure 2.8: Flux of ammonium from the sediment into the water column for a) the muddy facies and b) the sandy facies.

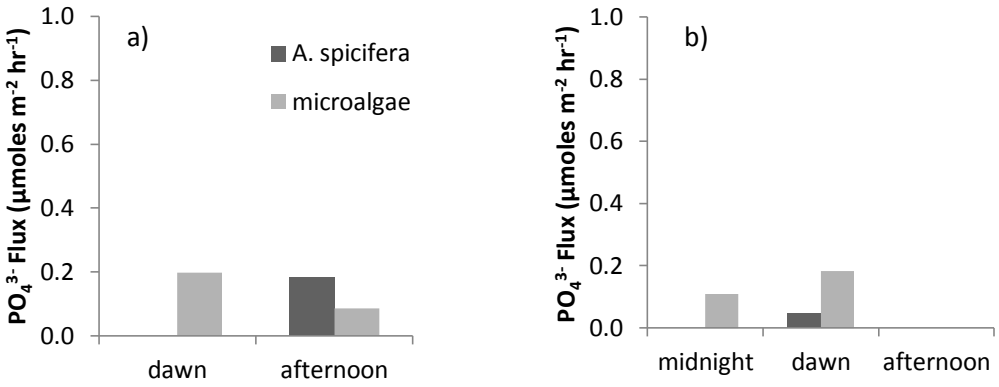

Figure 2.9: Flux of phosphate from the sediment into the water column for a) the muddy facies and b) the sandy facies. No flux occurred during numerous time points, as indicated by regions without bars.

Discussion

Oxygen availability drives numerous biotic and abiotic processes. Oxygen is utilized in microbial respiration, during the breakdown of organic matter. When oxygen becomes limited other oxidized species, including nitrate (Payne 1973), manganese and iron oxides (Nealson and Saffarini 1994) and sulfate (Jørgensen 1982), are used by microbes to oxidize organic matter, which releases N_2, Mn^{2+}, Fe^{2+} and H_2S to the surrounding pore water (Figure 2.1). The depth of oxygen penetration into sediments influences the vertical stratification of the dominant microbial metabolisms, with a deeper oxygen penetration depth driving less energetically favorable reactions deeper into sediments (Sørensen and Jørgensen 1987). Additionally, oxic conditions influence abiotic processes, by enabling the formation of iron and manganese oxides, which remove Mn^{2+} and Fe^{2+} from pore water and also remove dissolved phosphate due to

sorption onto metal oxides. The availability of oxygen also impacts nutrient cycling, with low oxygen conditions favoring nitrate reduction processes, such as denitrification and ammonification (Herbert 1999), and creating reducing conditions suitable for the release of phosphate from the reductive dissolution of iron oxyhydroxides (Chambers and Odum 1990, McManus et al. 1997, Colman and Holland 2000).

The availability of oxygen for biotic and abiotic processes varies over a day-night cycle, with higher concentrations of oxygen occurring during the day, as the rate of photosynthesis is typically greater than that of respiration. Under day time oxic conditions, the pore water concentration maxima of reduced species, such as ammonium, Mn^{2+} and Fe^{2+}, are expected to occur deeper in the sediment than at night, when redox zones shoal and pore water concentrations of reduced species increase. Redox dynamics should be especially apparent in regions colonized by *A. spicifera*, as macroalgae are capable of reducing the availability of oxygen at the SWI due to self-shading (D'Avanzo and Kremer 1994), increasing microbial respiration (Alber and Valiela 1994, Smith et al. 2006), and decreasing flow of water through the canopy (Escartin and Aubrey 1995).

Diel changes in water column oxygen

Diel oscillations in the concentration of oxygen were evident in both the sandy and muddy facies during this study. Water column oxygen concentrations within the sandy facies ranged between 100 - 340 µM (Figure 2.2 a and b) and in the muddy facies between 40 and 300 µM (Figure 2.2 c and d) over the diel cycle. As expected, periods of

active photosynthesis during the day were characterized by higher dissolved oxygen (DO) concentrations than at night, when only respiration was occurring (Table 2.1). Night time benthic respiration was evident in both the sandy and muddy facies, as observed by the nearly 150 µM decrease in the concentration of oxygen in the water column between the air-surface interface and the SWI during the night. These results are consistent with previous work in He‘eia Fishpond, in regions devoid of *A. spicifera*, where similar diel changes in the concentration of oxygen (60 - 220 µM) were observed (Briggs 2011).

Differences in oxygen concentrations in the sandy site, between the microalgal and *A. spicifera* dominated regions, also corresponded to differences in water temperature. During the night, the temperature of the water within the *A. spicifera* canopies was warmer than the water in the adjacent microalgal site. Differences in water column temperature and oxygen concentrations provide evidence that the water column is not homogenously mixed, and suggest the macroalgae is decreasing water flow within the canopy. Numerous studies have shown decreased flow through macroalgal canopies (Escartin and Aubrey 1995, Hurd 2000, and Nepf 2012). Reduced flow through the *A. spicifera* canopies is likely causing the oxygen and temperature differences observed within the canopy, compared to adjacent regions without the macroalgae.

During the day, DO concentrations were similar between sandy and muddy regions, however the sandy facies had the highest DO concentrations at the SWI (330 µM) and the lowest in surface waters (250 µM), while in the muddy facies DO concentrations were highest at the depth of the top of the *A. spicifera* canopy (300 µM)

and lowest at the SWI (~220 µM). Differences in day time water column DO concentrations between the sandy and muddy facies suggest that in sandy facies benthic photosynthesizers were a source of oxygen to the fishpond, while in the muddy facies more respiration was occurring at the SWI. Higher benthic respiration in sediments from the muddy facies, relative to the sandy facies, was likely due to a higher concentration of labile organic matter in muddy facies sediments, caused by their close proximity to input from He‘eia Stream (Briggs 2011). Organic matter remineralization is probably the major factor decreasing dissolved oxygen concentrations at the SWI.

Enhanced respiration in the muddy facies was further illustrated by the extended length of time (3 additional hours) that the SWI beneath the *A. spicifera* canopy was exposed to low oxygen conditions. Despite being exposed to three hours of light prior to the morning sampling, the water column at the base of the *A. spicifera* canopy remained at low, overnight oxygen levels (Table 2.1). Self shading is known to occur in macroalgae (D’Avanzo and Kremer 1994), reducing the availability of light and thus decreasing the rate of photosynthesis at lower canopy locations. Low SWI DO within the *A. spicifera* canopy, while the concentration was 200 µM higher at the SWI in the adjacent non-colonized region, suggests that in the morning the macroalga is self-shading.

At night, the concentration of DO in the water column was highest in surface waters and lowest at the SWI, highlighting the importance of night time benthic respiration to oxygen consumption. Night time DO was also affected by the type of dominant benthic primary producer (Table 2.1). During the night in the sandy facies, DO

was similar in the surface waters of both sites, but the *A. spicifera* site had lower canopy and SWI DO concentrations. In the muddy facies, DO was lower in the *A. spicifera* site at all water column locations. Reducing conditions in the water column of the *A. spicifera* site are consistent with the observations reported in other studies (Lavery and McComb 1991, Krause-Jensen et al. 1999). Low oxygen concentrations in macroalgal canopies has been attributed to increased microbial respiration within the canopy, caused by the release of OM from the macroalgae (Alber and Valiela 1994, Smith et al. 2006), and reduced water movement through the canopy (Escartin and Aubrey 1995). Night time respiration by *A. spicifera* is an additional oxygen sink within the canopy, and likely contributes to the observed differences in DO between sites. The dominant oxygen sink, however, is microbial respiration..

Diel changes in sediments

Nitrogen

Biotic nitrogen cycling favors the presence of nitrate during the day, when photosynthesis creates oxic conditions, and ammonium during the night, when nitrification is inhibited due to the loss of oxygen by respiration. Despite visible diel variation in water column DO, water column NH_4^+ concentrations remained similar throughout the day and night and nitrate remained BDL. Within the sediments, the sandy facies demonstrated the expected diel nitrogen trend, with increased ammonium concentrations at night, and increased nitrate concentrations during the day (Table 2.2). Within the *A. spicifera* site, diel oscillations in ammonium concentrations may be

magnified by the preferential uptake of ammonium during the day, as opposed to at night, as has been shown for *Gracilaria tikvahiae* (Peckol and Rivers 1995).

Although we expected the concentration of ammonium to be higher in the water column at the *A. spicifera* site than at the microalgal site, due to the lower DO concentrations observed in the macroalgal canopy, this was not the case. Similar water column ammonium concentrations were observed at both the microalgal and *A. spicifera* sites (Figure 2.3) in both facies. Increased pore water ammonium in regions dominated by macroalgae has been attributed to reduced oxygen availability at the SWI (Sundback et al. 1990), which decreases nitrification. The similar water column ammonium concentrations between microalgal and *A. spicifera* dominated sites in our study suggest that either there was no measurable increase in ammonium production, or decrease in nitrification, within the *A. spicifera* dominated sites, or that the macroalga is taking up ammonium as it becomes available. Benthic efflux has been shown to provide the major source of nitrogen to macroalgae (Sundback et al. 2003), which is consistent with the notion that macroalgal ammonium uptake may drive concentrations down at the macroalgal sites, such that they are similar at the two sites.

Pore water ammonium concentrations and flux rates provide further evidence that the reason for similar SWI water column ammonium concentrations between regions dominated by the macroalgae and non-colonized regions is macroalgal ammonium uptake. A higher concentration of ammonium was present in the pore water of the *A. spicifera* sites than the microalgal sites (Table 2.2 and 2.3). These results are consistent with previous studies (Sundback et al. 1990, Viaroli et al. 1996) which suggest the

increase in ammonium concentrations are due to organic matter remineralization. Additionally, the flux of ammonium from the sediment to the water column was higher for sites dominated by the invasive macroalgae (Figure 2.8). Higher flux rates coupled with similar water column concentrations (Figure 2.3) support the conclusion that more ammonium is being produced in the sites with invasive macroalgae, and the macroalga is taking up the excess ammonium.

Phosphorus

Pore water TDP was higher in the *A. spicifera* site than the microalgal site in the sandy facies (Figure 2.4a), while no difference in TDP occurred between sites in the muddy facies (Figure 2.4b). TDP is comprised of both the organic (DOP) and inorganic (DIP) fractions of dissolved phosphate, and since DIP was BDL for all samples, the TDP reported here primarily represents DOP. While DIP can be directly taken up by algae, algae are also capable of using DOP to satisfy growth requirements through the use of alkaline phosphatase enzymes (Kuenzler and Perras 1965). Macroalgae are known to excrete dissolved organic matter (Khailov and Burlakova 1969, Alber and Valiela 1994, Smith et al. 2006), and in the sandy facies, the difference in TDP between the two sites may be caused by the excretion of dissolved organic matter by *A. spicifera*. The higher concentration of TDP in the muddy microalgal site compared to the sandy microalgal site suggests that organic matter input from He‘eia Stream does not travel far enough to impact the sandy facies. The concentration of TDP at the *A. spicifera* site in the sandy facies was similar to that found at both sites in the muddy facies, suggesting the invasive

algae has a greater effect on TDP concentrations in the sandy facies than the muddy facies.

In the water column, DIP was BDL, and pore water DIP concentrations were low to undetectable throughout the entire study (BDL - 1 μM), with concentrations similar to those previously observed in the pond (Briggs 2011). One of the mechanisms influencing DIP availability in pore water is sorption of phosphate to iron oxyhydroxides under oxidized conditions, and desorption under reducing ones (Krom and Berner 1981, McManus et al. 1997, Coleman and Holland 2000). We expected to find increased DIP concentrations at night, especially within *A. spicifera* sites, due to the low DO concentrations at the SWI. However, despite the observed reducing conditions, as shown by the presence of dissolved iron and Mn^{2+} in pore waters, DIP concentrations remained low, and no diel pattern was observed. Flux calculations do illustrate diel cycling in the microalgal sites for both sediment facies (Figure 2.9). The flux of phosphate from the sediment into the water column was highest at dawn and lowest in the afternoon in microalgal sites, however phosphate flux was low, as expected from the low phosphate concentrations in pore water.

A relationship was found between the concentration of dissolved iron and DIP in the muddy facies, but not in the sandy facies. In the muddy sites, the maximum concentration of dissolved iron and DIP occurred at the same depth in two of the four cores. These two cores also had the highest total dissolved iron concentration (≥ 90 μM)

observed throughout the entire study (10 total cores). The dissolved iron to phosphate ratios calculated for the muddy facies were 122 (Microalgae: dawn, -1.75 cm) and 150 (*A. spicifera*: afternoon, -0.75 cm). Previous work demonstrated that Fe:P are higher in freshwater (0.7 to 280) than marine (0.008 to 1.1) pore waters, and suggested that the Fe:P difference was due to the formation of iron sulfides in marine environments (Gunnars and Blomqvist 1997). Based on the difference in Fe:P between freshwater and marine sediments, the muddy facies in He‘eia Fishpond is more characteristic of freshwater than marine sediments. However, the down core salinity in these sediments ranges between 15-20 (Briggs 2011), indicating that these sediments are not fresh. Rather, it is likely that the high iron content of He‘eia sediments is inhibiting phosphate availability; however, without analysis of detailed solid-phase iron and phosphate speciation we cannot know for certain the mechanism causing low pore water phosphate concentrations.

Iron

Iron redox cycling was observed in He‘eia Fishpond, as shown by the changes in the concentration of dissolved iron over the diel cycle (Figure 2.6). In addition to retaining phosphate, iron in sediments impacts the redox dynamics of manganese and sulfur. Iron oxyhydroxides are important electron acceptors during the microbial oxidation of organic matter (Lovley and Phillips 1988, Sørensen 1982). During microbial iron reduction, Fe^{3+} is reduced to Fe^{2+}, releasing adsorbed phosphate to the surrounding pore water. Additionally, iron reacts rapidly with H_2S to form pyrite and

other iron-sulfide minerals, a process that removes Fe^{2+} from pore water and prevents the flux of sulfide from the sediment to the water column (Nealson and Saffarini 1994, Thamdrup et al. 1994).

In the muddy facies of the pond, total dissolved iron and Mn^{2+} maximum concentrations occurred at the same depth (Table 2.3), whereas they occur at different depths in the sandy facies. The observed overlap in redox zonations in the muddy facies, but not the sandy ones, suggests that manganese oxides may play a role in the oxidation of Fe^{2+} in sediments from the muddy facies (Lovely and Phillips 1988 and Thamdrup et al. 1994), according to Equation 2.1:

$$2\ Fe^{2+} + MnO_2 + 2\ H_2O \rightarrow 2\ FeOOH + Mn^{2+} + 2\ H^+ \qquad (2.1)$$

If the total dissolved iron pool was composed entirely of Fe^{2+}, there would be a higher concentration of iron at night, due to the more reducing conditions occurring at that time. In the muddy facies, a higher concentration of total iron was observed in the afternoon than at dawn, suggesting that Fe^{3+} is also present in the pore water. Colloidal iron is known to scavenge phosphate (Gunnars et al. 2002 and sources there in), therefore the presence of Fe^{3+} in pore waters is likely contributing to the low DIP pore water concentrations observed in this study.

Manganese

If diel manganese variations were occurring in the sediment, Mn^{2+} concentrations should be highest before dawn, when the sediment is most reducing, and lowest in the afternoon, after photosynthesis has increased the concentration of oxygen at the SWI. Diel variations in the concentration of Mn^{2+} occurred in all sites (Figure 2.5) and were especially apparent in the *A. spicifera* sandy site where the Mn^{2+} concentration decreased from 23 µM at dawn to 5 µM in the afternoon. The higher concentration of Mn^{2+} during the night, and lower concentration during the day, supports our hypothesis that diel variations in redox species are occurring in the pond. Although the microalgal sandy site displayed a similar diel pattern, maximum Mn^{2+} concentrations (6 - 13 µM) had less variability than those observed in the adjacent *A. spicifera* site. The higher night time concentration of Mn^{2+} in the *A. spicifera* site is consistent with the oxygen data, which indicated that the SWI beneath the macroalgal canopy was exposed to lower oxygen conditions than the adjacent microalgal site. Thus water column oxygen appears to be affecting the concentration of Mn^{2+} in pore water.

The effect of SWI oxygen concentrations on pore water Mn^{2+} concentrations is further supported by the similarity in maximum Mn^{2+} concentrations in the sandy facies when SWI oxygen concentration were also similar, between the *A. spicifera* and microalgal sites in the afternoon and at midnight when. In the water overlying the sandy cores, Mn^{2+} was detectable when SWI oxygen concentrations were approximately 130 µM, only 6 hours after SWI oxygen levels were near 300 µM. Previous work from an incubation study, designed to examine the effect of varying degrees of low oxygen at the

SWI on redox cycling, observed similar pore water Mn^{2+} concentrations to those reported in our study, but a longer time was required for Mn^{2+} to move from the sediment to the overlying water (Kristensen et al. 2002). Kristiansen et al. (2002) reported that when the overlying water was devoid of oxygen the first release of Mn^{2+} from sediment cores to the water column occurred after three days, and when the concentration of oxygen at the SWI was 85 µM, the initial Mn^{2+} flux took six days (Kristensen et al. 2002). The observations from He'eia Fishpond suggest that *in situ* fluxes of reduced species occur on a more rapid time scale than predicted by laboratory studies, which is likely caused by the dynamic nature of *in situ* conditions, including bioturbation and turbulent water motion.

Diel changes in pore water Mn^{2+} concentrations were observed over the course of this study (Figure 2.5); however the mechanism for this change is uncertain. The production and removal of Mn^{2+} in sediments is driven by the reduction and oxidation of manganese oxides, which can occur via biotic and abiotic processes. The formation of Mn^{2+} can be attributed to the biotic reduction of Mn-oxides (Nealson and Saffarini 1994) or by the abiotic reduction of manganese oxides by Fe^{2+} and H_2S (Burdige and Nealson 1986, Thamdrup et al. 1994). The reduction of Mn-oxides by H2S is biologically important as this process removes toxic hydrogen sulfide from the pore water, preventing the flux of H2S from the pore water into the overlying water column. Regardless of the mechanism, the larger shifts in the concentration of Mn^{2+} in the *A. spicifera* site support the hypothesis that the invasive alga is altered sediment redox dynamics by creating more reducing conditions in surface sediments.

Conclusion

The goal of this study was to examination of the effects of an invasive macroalga on sediment redox chemistry and nutrient dynamics over diel cycles to determine whether the invasive alga is altering local environmental conditions. Diel cycles were clearly observed in sandy facies where higher pore water concentrations of the reduced species Mn^{2+} and ammonium occurred during the night than during the day. For both sediment facies, the influence of the diurnal cycle was most pronounced in water column DO concentrations. In the sandy site, DO concentrations at the SWI were similar between microalgal and *A. spicifera* sites, and increased from 100 µM at midnight to 340 µM in the afternoon. Unlike the sandy sites, muddy sites displayed a large difference in DO concentrations between sites with and without the macroalgae. For example, in the morning, the DO concentration at the SWI in the muddy microalgal site was 220 µM higher than at the same time and depth in the *A. spicifera* site.

Dissolved iron and manganese were observed in the pore water of surface sediments throughout the study. The availability of iron and manganese oxides may prevent the escape of sulfide from the sediment to the overlying water column, even under the reducing conditions observed at the SWI in the pond. Despite the high concentration of dissolved iron in pore waters, phosphate concentrations were low, with maximum concentrations ranging between 0.5 and 1 µM. Low phosphate is likely due to the presence of iron oxyhydroxides in surface sediments, and subsequent sorption of

phosphate; further solid-phase speciation is required to confirm this as the reason for low phosphate in sediment pore waters.

Vertical oscillations in redox transition zones were observed during the study, and changes in the concentrations of oxygen, ammonium and Mn^{2+} provide additional evidence that diel redox cycling occurs in the pond. Comparison between microalgal and *A. spicifera* dominated sites revealed differences in water column oxygen and ammonium concentrations. *Acanthophora spicifera* had a more pronounced influence on sediment redox chemistry in the sandy facies than in the muddy facies. *Acanthophora spicifera* sites had higher ammonium concentrations and higher fluxes of ammonium from the sediment to the water column than adjacent microalgal sites in both sediment facies. Compared to microalgal dominate regions, the invasive macroalgae is altering redox conditions in the fishpond, however little difference in water column nutrients were observed between sites. Further work in the pond is needed to determine whether the similarity in nutrient concentrations between sites arises from rapid uptake by the invasive macroalgae, or other factors, because the changes in redox conditions are having no effect on water column nutrients.

Chapter 3

Oscillations in oxidation-reduction chemistry within an *Acanthophora spicifera* canopy:

Implications for oxygen-sulfide cycling

(He‘eia 2011)

Abstract

Invasive macroalgae threaten the diversity and function of ecosystems. This study compared the effect of an invasive alga, *Acanthophora spicifera*, on sediment oxidation-reduction chemistry and water column nutrient concentrations over diel cycles in He‘eia Fishpond, Hawai‘i. Eleven out of twelve i*n situ* electrochemical profiles through two *A. spicifera* canopies revealed that oxygen concentrations in the lower few centimeters within *A. spicifera* canopies was less than 5 µM. The water column within *A. spicifera* canopies also had higher concentrations of sulfide than adjacent non-colonized regions of bare sediment. Additionally, beneath one of the *A. spicifera* canopies, anoxic conditions persisted at the SWI for 12 hours of the diel time frame, while the SWI in the adjacent region of bare sediment was only anoxic for six hours. Over the course of the study, oxygen flux from the water column to the sediment ranged between 0 and 93 µmoles O_2 m^{-2} h^{-1}, and sulfide flux from the sediments ranged between 0 and 5.2 µmoles H_2S m^{-2} h^{-1}. Profiles showed the presence of sulfide and oxygen in close proximity to one another, indicating that oxygen is an important oxidizer of sulfide within He‘eia Fishpond. Water column ammonium concentrations were higher in areas colonized by the invasive alga than in adjacent regions of bare sediment. Even though reducing conditions were observed, as evidenced by the detection of hydrogen sulfide, Mn^{2+} and dissolved iron at the sediment-water interface, dissolved inorganic phosphate was below the detection limit (0.5 µM) throughout the entire study. The detection of Mn^{2+} and dissolved iron, both in surface waters and at the sediment water interface, provide evidence that colloidal

Fe^{3+} and manganese oxides are likely sorbing phosphate and contributing to the low phosphate concentrations within He‘eia Fishpond.

Introduction

Invasive algal species are a well known threat to ecosystem function (Schaffelke et al. 2006, Williams and Smith 2007), and invasive algae cost the United States millions of dollars each year in lost revenue (Hoagland et al. 2002). Canopy forming benthic macroalgae are capable of altering the environment physically, biologically, and chemically. Physically, macroalgal canopies alter water flow by reducing water velocity within the canopy (Escartin and Aubrey 1995, Forster et al. 1996, Nepf 2012), and increasing flow over the top of the canopy (Escartin and Aubrey 1995). The presence of macroalgae also reduces light availability at the sediment water interface (SWI) causing a decline in benthic microalgal abundance and reducing the concentration of oxygen at the SWI (Sundback et al. 1990, Corzo et al. 2009). Biologically, invasive macroalgae compete for habitat with native species. It is also true that invasive macroalgae, provide shelter for macrofauna, and can be a source of food, which are positive factors.

Physiologically, macroalgae are complex organisms, capable of chemically altering the environment. Macroalgae inhabiting the SWI can intercept the movement of nutrients from the sediment to the overlying water column (Lavery and McComb 1991, Larned and Atkinson 1997, Sundback et al. 2003, Engelsen et al. 2008), and often compete with benthic microalgae (Corzo et al. 2009) and microorganisms for nutrients

such as nitrate (Dalsgaard 2003). During the day, macroalgae produce more oxygen than needed for their respiration processes, creating an increase in water column oxygen concentrations. At night, when photosynthesis is no longer occurring, macroalgal respiration decreases oxygen availability in the water column. Diel oscillations in the concentration of oxygen within macroalgal canopies highlight the dynamic nature of shallow coastal environments and the importance of macroalgae in influencing water column oxygen concentrations (D'Avanzo and Kremer 1994). Additionally, the senescence of macroalgae provides a large organic matter flux to the benthic community, increasing microbial respiration and reducing the concentration of oxygen (Sfriso et al. 1987, Sundback et al. 1990, Lavery and McComb 1991). Macroalgal canopies also decrease water column oxygen concentrations through increased microbial respiration caused by algal senescence (Krausse-Jensen et al. 1999, Viaroli et al. 2008), and the release of dissolved organic carbon within canopies (Hauri et al. 2010), which results in an alteration of nutrient availability (Larned 1998, Rozan et al. 2002). Thus, the ability of benthic macroalgae to alter oxygen concentrations in shallow coastal waters has implications for the redox chemistry and nutrient cycling of both the water column and sediments.

Redox reactions alter the availability of biologically important chemical species, including sulfide, phosphate, and nitrate. Metabolically, oxygen is the most energetically favorable oxidant, and when available oxygen is used preferentially by microbes for the oxidation of organic matter. Abiotic oxidation of reduced species, such as hydrogen sulfide and Fe^{2+}, also take place under oxic conditions. Abiotic oxidation processes

transform hydrogen sulfide into sulfate (or intermediates) and oxidize Fe^{2+} to Fe^{3+}, which then forms insoluble iron oxyhydroxides. Hydrogen sulfide is toxic to most aquatic life, at varying concentrations depending upon the organism (Bagarinao 1992 and sources therein), while sulfate is abundant in seawater. Hydrogen sulfide is removed from pore water through oxidation or precipitation with iron in surface sediments and at the SWI, which is biologically favorable for aquatic organisms such as benthic macroalgae and benthic animals. The oxidation of Fe^{2+} to iron oxyhydroxide is also a biologically important process because unlike Fe^{2+}, iron oxyhydroxides are known to sorb phosphate, rendering the phosphate biologically unavailable (Krom and Berner 1980, Sundby et al. 1986, Chambers and Odum 1990, Jensen et al. 1995, Gunnars and Blomqvist 1997, Blomqvist and Elmgren 2004). Under oxidizing conditions, phosphate is removed from sediment pore waters and the water column in the presence of iron oxyhydroxides to levels that are potentially limiting the growth of primary producers. Thus, the oxidation of hydrogen sulfide is beneficial to organisms such as macroalgae, while the oxidation of Fe^{2+} can be detrimental.

The availability of oxygen also influences biotic nitrogen cycling. Nitrogen is stable in numerous oxidation states, and biological processes in sediments transform nitrogen between the various forms. The remineralization of organic matter in sediments under aerobic and anaerobic conditions is the primary source of ammonium in sediments (Herbert 1999). In the presence of oxygen, ammonium is transformed by nitrifying bacteria, via a two step process, to nitrite and finally nitrate (Henricksen and Kemp 1988). Abiotic conditions provide an environment suitable for denitrification, where

bioavailable nitrate is reduced to nitrogen gas and is lost from the system. The availability of oxygen at the SWI determines which microbial nitrogen transformations can occur in surface sediments and influences whether ammonium or nitrate is available at the SWI.

Study Site

This study was conducted in Heʻeia Fishpond, located on the windward side of the island of Oʻahu, Hawaiʻi. Heʻeia Fishpond is an 88-acre brackish pond, located at the land-sea interface between the town of Kāneʻohe and Kāneʻohe Bay. The pond is separated from the ocean by a rock wall, however freshwater and ocean water move into and out of the pond through six gates in the wall. The pond is currently being restored to function as it did during ancient times by the not-for-profit group, Paepae O Heʻeia. Paepae is working to strengthen and rebuild the wall around the pond and remove predatory fish and invasive species, including the red algae *Acanthophora spicifera* and *Gracilaria salicornia* and mangrove *Rhizophora mangle*, from the pond. The pond is shallow, with an average depth of 1 m, and sediments in the pond range from fine grained near the stream inputs to coarse grained at the ocean gates. This study was conducted in fine grained sediments at the south-west side of the pond.

The pond and adjacent Kāneʻohe Bay are dominated by the invasive macroalgae, *Acanthophora spicifera*. This species was introduced to Oʻahu in the early 1950s as a hull fouler (Doty 1961) and has since become prevalent around all the main Hawaiian

Islands. *Acanthophora spicifera* forms a dense canopy structure and is one of the most common non-indigenous algal species found in Hawai‘i (Smith et al. 2002).

The purpose of this study was twofold. The first objective was to compare and contrast diel changes in the concentration of water column nutrients, oxygen and sulfide between an area of sediment colonized by the invasive macroalga, *A. spicifera*, and an adjacent non-colonized region of bare sediment. The second objective was to compare diel changes in the spatial and temporal concentration of redox species, including oxygen, manganese, and sulfide, between two *A. spicifera* canopies.

Methods

Experimental Design

The study was conducted in He‘eia Fishpond over a two day period, in May 2011. Dates were chosen during a neap tide to minimize the influence of tides on the study. On the first day, we sampled an area with a small *A. spicifera* canopy, and an adjacent region of bare sediment. The small *A. spicifera* canopy was approximately 2 m in diameter with a height ranging between 0.1 to 0.2 m tall. Electrochemical profiles (see below) were conducted at each site, every six hours, over a 24 hour period. Profiling began at 04:00, 10:00, 16:00, and 22:00, for a total of eight profiles over the diel cycle. In order to compare oxygen distribution and penetration depth between sites, profiles were conducted as temporally close together as possible. The first profile began at one of the

above listed times in the *A. spicifera* dominated site. Immediately following the completion of the *A. spicifera* profile, a profile was conducted in the adjacent site with bare sediment. At each time point water was collected from both the *A. spicifera* and bare sediment sites for nutrient analysis (see below).

The second objective of the study was to characterize short term diel vertical oscillations in the oxic and anoxic transition zones within an *A. spicifera* canopy and compare redox chemistry between two *A. spicifera* canopies. On the second day, profiles were conducted throughout a large *A. spicifera* canopy, 4 meters across and 0.2 m tall, beginning every 2 to 4 hours. Profiles were started at: 00:00, 04:00, 07:00, 10:00, 12:00, 14:00, 16:00, and 20:00 and took place at random places throughout the canopy. When referring to the *A. spicifera* canopies in the subsequent discussion, we will refer to the smaller canopy from the first day as the small *A. spicifera* canopy and the larger canopy from the second day as the large *A. spicifera* canopy.

Electrochemistry

In situ water column and sediment oxygen and sulfide measurements were conducted using voltammetry, a technique involving the measurement of electrochemically active species through the application of a voltage across a three-celled system. A solid state, gold-mercury (Au/Hg) amalgam working electrode is coupled with a silver/silver-chloride (Ag/AgCl) reference electrode and a platinum (Pt) counter electrode (Brendel and Luther 1995). *In situ* voltammetry has been used in coastal studies (Rozan et al 2002), the Chesapeake Bay (Lewis et al 2007), the Black Sea (Glazer

et al 2006), and deep sea sediment studies (Luther et al 1999) because it allows the simultaneous measurement of numerous dissolved and aqueous chemical species *in situ* (e.g. Luther et al. 2008 for review). For this study, we focused on the concentration of oxygen, Mn^{2+}, Fe^{2+} and sulfide to focus on the oscillation of oxic and anoxic redox transition zones (Table 3.1). Electrochemical analysis was performed using a DLK60 (AIS Inc.).

The working electrodes were constructed in the lab, using 100 µm gold wires encased in epoxy and PEEK tubing, as described by Luther et al. (2008). In previous studies, working electrodes were constructed from 3 mm diameter PEEK tubing, however for this study, in order to reduce environmental disturbance, 1.6 mm outer diameter PEEK tubing was used to fabricate the electrodes (Figure 3.1). Working electrodes encased in drawn glass, rather than PEEK, have been used in microbial mats (Glazer et al. 2002) and sediment cores (Briggs 2011), however these electrodes are fragile and not suitable for *in situ* sediment work in carbonate sediments. The working electrodes used in this study reduced the electrode surface area, similar to using drawn glass, while maintaining the durability of the PEEK electrodes.

Table 3.1: Electrode reactions for select species at the gold-mercury working electrode verse the saturated calomel electrode (adapted from Luther et al. 2008).

Electrode Reaction	**$E_p(E_{1/2})$ (V)**	**Detection limit (µM)**
$O_2 + 2H^+ + 2e^- \rightarrow H_2O_2$	-0.33	5
$H_2O_2 + 2H^+ + 2e^- \rightarrow H_2O$	-1.23	5
$Mn^{2+} + Hg + 2e^- \leftrightarrow Mn(Hg)$	-1.55	5
$Fe^{2+} + Hg + 2e^- \leftrightarrow Fe(Hg)$	-1.43	10
$Fe^{3+} + e^- \leftrightarrow Fe^{2+}$	-0.2 to -0.9	molecular species
$FeS + 2e^- + H^+ \leftrightarrow Fe(Hg) + HS$	-1.15	molecular species
$HS^- + Hg \rightarrow HgS + H^+ + 2e^-$	-0.6	0.1
$HgS + H^+ 2e^- \leftrightarrow HS^- + Hg$	~ -0.6	0.1

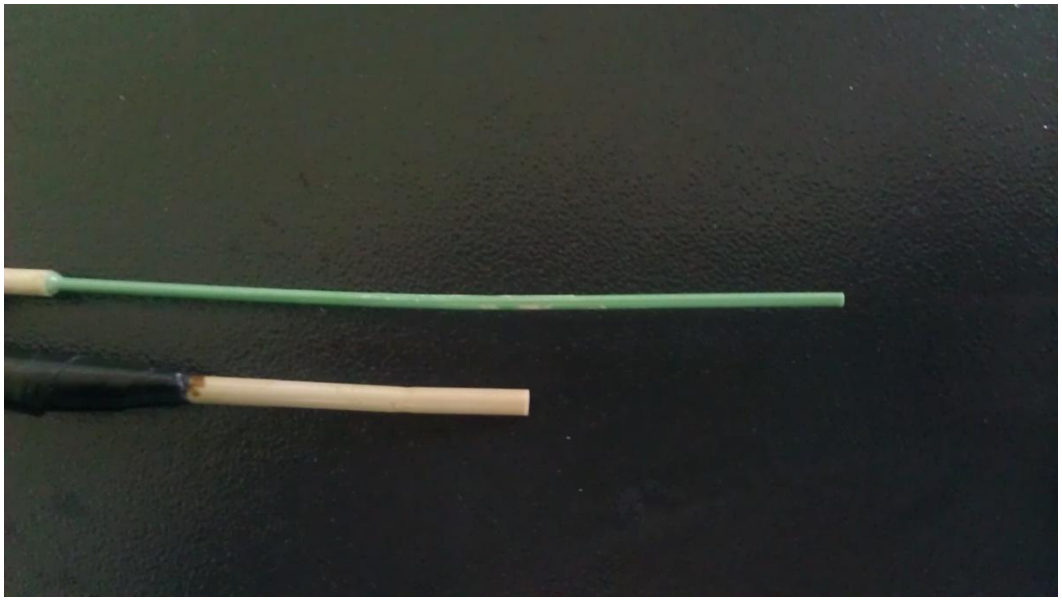

Figure 3.1: Photograph of 1.6 mm PEEK electrode above a 3 mm PEEK. The longer PEEK and narrower body allow for a decreased algal canopy and sediment disturbance during profiling.

Profiles

In situ electrochemical profiles were conducted by attaching a solid state Au/Hg amalgam electrode to a submersible micromanipulator. The micromanipulator consists of three adjustable legs and a motor that turns a threaded rod causing an arm to move up or down. The working electrode is attached to the arm of the micromanipulator. At the start of each profile the micromanipulator was placed over an undisturbed region in the pond. Profiles began in the overlying water column and the electrode was moved in increments between 0.25 and 1.0 cm, down through the water column and into the sediment. Movements in the finer 0.25 cm range occurred in regions where the real-time data indicated changes in the concentration of redox species were occurring. Once a profile was complete, the site where the profile was conducted was marked to ensure it was not profiled again.

Flux

The flux of oxygen and hydrogen sulfide based on each profile was calculated using on Fick's first law of diffusion (Equation 3.1).

$$J = (\phi)(D_{sed})(dC/dz) \qquad (3.1)$$

$$D_{sed} = D_{sw}/\Theta^2 \qquad (3.2)$$

For each profile, a least squares regression line was fit to the concentration profile of each species to determine the change in concentration with depth (dC/dz). The sediment diffusivity (D_{sed}) of oxygen and hydrogen sulfide was calculated using the diffusivity of each species in seawater (D_{sw}) (Boudreau 1997) and tortuosity (Equation 3.2). Tortuosity (Θ^2) was determined based on sediment porosity (ø) from values in Boudreau (1997). Briggs (2011) determined the porosity of the sediment in this region of the pond to be 0.61.

Water column nutrients

Water column samples were collected from the site with the small *A. spicifica* canopy and an adjacent bare sediment site at 4:00, 10:00, 16:00 and 22:00 on the first day of the experiment to allow for the comparison of water column nutrients between *A. spicifera* colonized and non-colonized locations. The water sampler consisted of a 60-cc syringe attached to Teflon© tubing and a three-way stop cock. The stop cock allowed the tubing to be purged of air before sample collection. This sampling design targeted specific areas in the water column and minimized the oxidation of the water before it was filtered. Water was collected from the surface, approximately 0.1 m below the air-water interface, and at the SWI for each sampling time point. After collection, the water was filtered through 0.2 µm Whatman polycarbonate filters and stored in acid clean HDPE bottles. Subsamples for iron, manganese, dissolved inorganic phosphate (DIP) and total dissolved phosphate (TDP) were acidified to a pH of 1, while subsamples for ammonium

and nitrate were placed in separate, non-acidified bottles. Until analysis, acidified samples were stored at 4°C, and non-acidified samples were frozen at -20°C.

Water samples were analyzed using standard colorimetric techniques. Manganese was determined using the method of Tebo (2007). Briefly, a formaldoxime reagent, consisting of 20 parts 10% hydroxylamine-HCl combined with 1 part 37% formaldehyde was made. Samples were combined in a 7:1 ratio with the formaldoxime reagent and read at 450 nm. Total dissolved iron was measured by mixing samples with a 0.2 M hydroxylamine solution in a 10:1 ratio. After 12 hours, samples were run using the ferrozine-acetate method described by Stookey (1970).

Ammonium colorimetric analysis was completed within 12 h of sample thawing, using the Indophenol Blue Method (Koroleff 1979). In order to measure nitrate, the nitrate was first reduced to nitrite using the nitrate reductase enzymatic reaction (Campbell et al. 2006), followed by standard nitrite colorimetric determination (Grasshoff et al. 1983). To measure TDP, a 1.0 mL subsample was combined with 40 µL of $Mg(NO_3)_2$, dried and then combusted at 550 °C. Following combustion, 400 µL of 1 N HCl was added and samples were shaken for 24 h to hydrolyze and solubilize sediment phosphorus (Monaghan and Ruttenberg 1999). After adjusting the pH of each sample to 1.0, using HCl and NaOH as required, the samples were colorimetrically analyzed using the molybdate blue method (Grasshoff et al. 1983). All colorimetric analyses were conducted on a Synergy HT BioTek Multi-Mode Microplate Reader using Thermo Scientific Nuc 96-well Optical Bottom Microplates©.

Results

Small *A. spicifera* canopy and bare sediment

Electrochemistry

Electrochemical profiles conducted throughout the small *A. spicifera* canopy and adjacent bare sediment showed that oxygen was consistently highest in surface waters (Figure 3.2 and 3.3). At the site with the small *A. spicifera* canopy the concentration of oxygen at the SWI was below the instrument detection limit (BDL) of 5 µM for three of the four profiles. In these three profiles, the concentration of oxygen dropped to BDL more than 5 cm above the SWI (Table 3.2). For the 10:00 profile, the single profile with oxygen at the SWI, 22 µM of oxygen was present at the SWI, before dropping to BDL between the SWI and 0.5 cm into the sediment. In the adjacent bare sediment site, oxygen was present at the SWI at 10:00 (130 µM) and 16:00 (210 µM) and BDL during the 04:00 and 23:00 time points. The maximum oxygen penetration depth was deeper in the bare sediment site than the adjacent small *A. spicifera* site during all four sampling times.

The vertical location and size of the suboxic zone, the region in the sediment or water column where oxygen was absent but before hydrogen sulfide began to accumulate, varied over the course of the study. Between the small *A. spicifera* canopy and the bare sediment sites, the suboxic zone was larger in the *A. spicifera* site for all time points. In the small *A. spicifera* site, the suboxic zone ranged in vertical extent from

a minimum of 0 cm at 23:00 to a maximum of 2.8 cm at 04:00 (Table 3.2). In the bare sediment site, the vertical extent of the suboxic zone was 0 cm for all time points except 04:00 (0.5 cm). The suboxic zone in the small *A. spicifera* site was larger and more variable than the adjacent bare sediment site.

The depth of first appearance of sulfide varied at each site over the diel cycle. Sulfide was present in the overlying water column for four of the eight profiles, during the 04:00 and 16:00 time points for the small *A. spicifera* site and at the 23:00 time point for both sites. Fe^{3+} was present in the majority of profiles, beginning near the depth of sulfide appearance. The concentration of Fe^{3+} cannot be determined using electrochemical methods because it is not possible to determine the Fe^{3+} complexes formed in the field. No correlation was found between the depth at which oxygen concentrations dropped to BDL and the depth at which sulfide first appeared.

Oxygen flux from the water column into the sediment ranged between 15 and 60 µmoles O_2 m^{-2} hr^{-1} (Figure 3.4a). The flux of oxygen was always from the water column into the sediments. In the small *A. spicifera* canopy, flux only occurred during the day at 10:00. For the remainder of the profiles through the small *A. spicifera* canopy oxygen concentrations dropped to BDL in the water column above the SWI. In the bare sediment site, oxygen flux from the water column to the sediment was highest at 16:00 (60 µmoles O_2 m^{-2} hr^{-1}) and lowest at 4:00 (0 µmoles O_2 m^{-2} hr^{-1}). Hydrogen sulfide flux ranged from 0.11 to 0.76 µmoles H_2S m^{-2} hr^{-1} (Figure 3.4b). In the small *A. spicifera* canopy, flux from the sediment to the water column only occurred at 10:00. At 4:00 and

22:00 hydrogen sulfide was present in the overlying water column at a higher concentration than in surface sediments, and at 16:00, the first appearance of hydrogen sulfide in sediments did not occur until greater than 1.5 cm below the SWI. In the bare sediment site, hydrogen sulfide flux from the sediment to the water column occurred at all times. Flux was highest at 16:00 (0.76 μmoles H_2S m^{-2} hr^{-1}) and lowest at 10:00 (0.15 μmoles H_2S m^{-2} hr^{-1}).

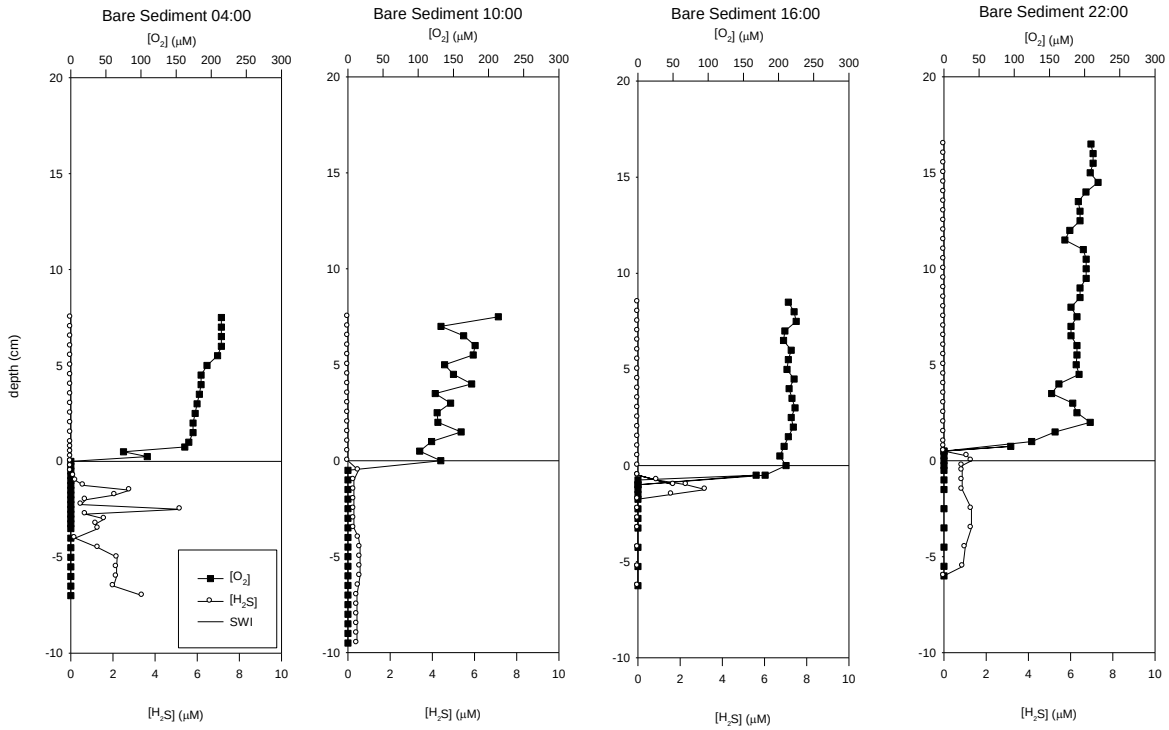

Figure 3.2: Electrochemical profiles through the water column and into the sediment at the bare sediment site. The solid line in each plot is the location of the SWI.

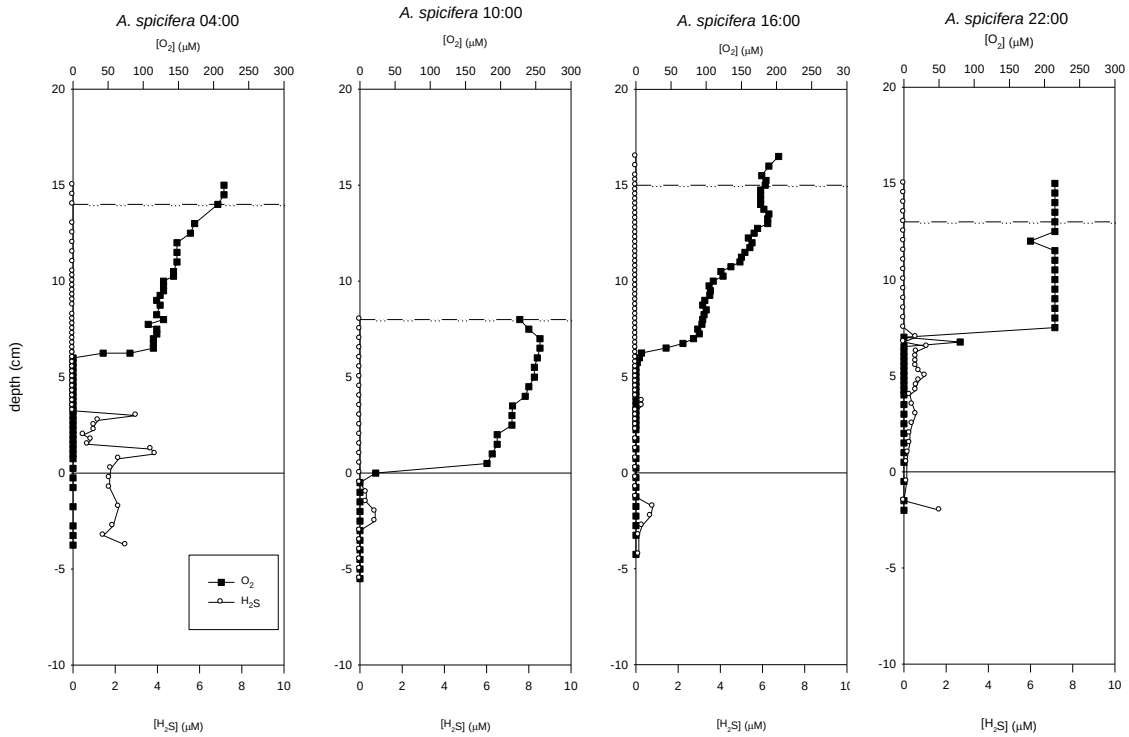

Figure 3.3: Electrochemical profiles through the water column and sediment at the site with the small *A. spicifera* canopy. The solid line in each plot is the location of the SWI, and the dashed line represents the height of the *A. spicifera* canopy.

Table 3.2: Comparison between the small *A. spicifera* site and the adjacent bare sediment site for the depth at which oxygen dropped to BDL, the depth of the first appearance of sulfide, and the vertical extent of the suboxic zone. Positive numbers correspond to the height above the SWI, zero is at the SWI, and negative numbers are locations below the SWI, in the sediment.

	Profile	Max. O_2 penetration depth (cm)	Depth of sulfide appearance (cm)	Vertical extent of the suboxic zone (cm)
Small canopy A. spicifera	**4:00**	6.0	3.0	3.0
	10:00	0.0	-1.0	1.0
	16:00	5.5	-1.8	7.3
	22:00	7.0	6.5	0.5
Bare sediment	**4:00**	0.0	-0.8	0.8
	10:00	-0.5	-1.0	0.5
	16:00	-0.5	-1.0	0.5
	22:00	0.5	0.3	0.2

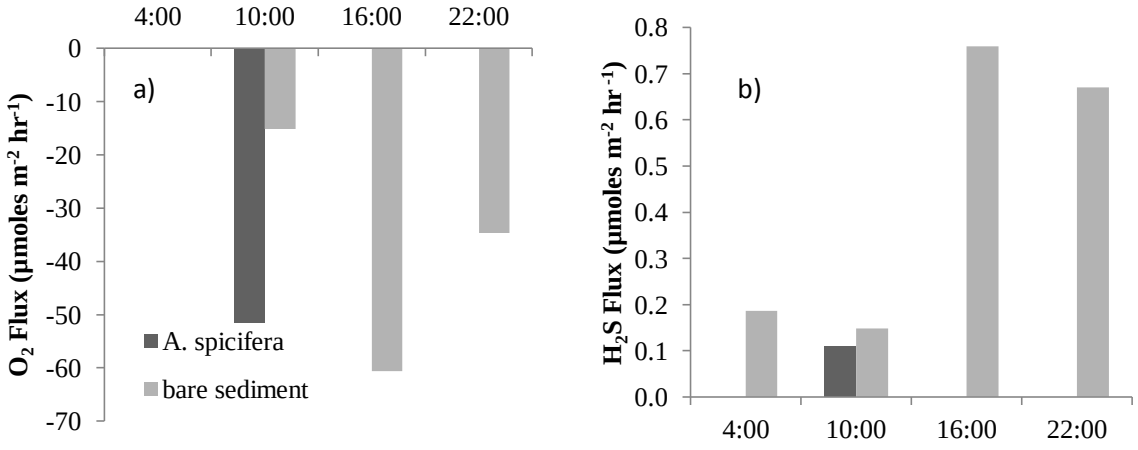

Figure 3.4: Flux of (a) oxygen and (b) hydrogen sulfide across the SWI for the small *A. spicifera* canopy (dark bars) the bare sediment (light bars). Positive numbers indicate species movement from the sediment into the water column, and negative numbers indicate movement from the water column to the sediment. No flux occurred during numerous time points, as shown by regions without bars.

Water column nutrients

Nutrient concentrations (nitrate, ammonium, DIP, TDP, total dissolved iron and manganese) were quantified in order to compare water column conditions between the site dominated by the small *A. spicifera* canopy and the adjacent bare sediment. Nitrate was BDL (0.5 µM) for all samples. Ammonium was only detected in the *A. spicifera* site: in surface waters at 10:00 (2.6 µM) and at the SWI at 10:00 (0.5 µM) and 16:00 (1.6 µM). DIP was BDL (0.5 µM) for all samples, and TDP was BDL (0.5 µM) for all samples except at the SWI in the bare sediment site at 04:00 (2.8 µM). In the surface water, manganese was only detectable in the *A. spicifera* sites, and was detected at 04:00, 10:00 and 16:00, while at the SWI manganese was detectable in both sites at all time points (Figure 3.5). Total dissolved iron was detectable at all sites and time points (Figure 3.6). The highest total dissolved iron concentrations at the SWI were observed for both sites during the 04:00 and 22:00 sampling. Higher concentrations of reduced species were present in the *A. spicifera* dominated site than in the adjacent bare sediment.

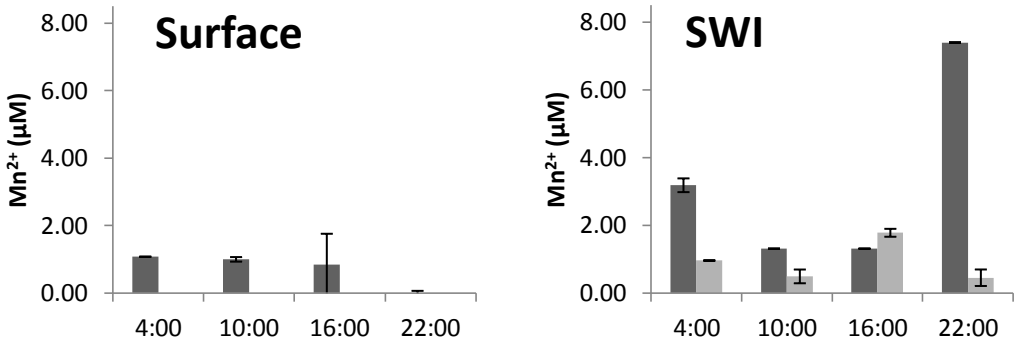

Figure 3.5: Water column Mn^{2+} concentration for water from the surface and at the SWI. The dark bars are for the small *A. spicifera* site and the light bars are for the bare sediment. Time points appearing to be without error bars have bars less than 0.1 µM (n=3 analytical replicates; error bars represent +/- 1 SD).

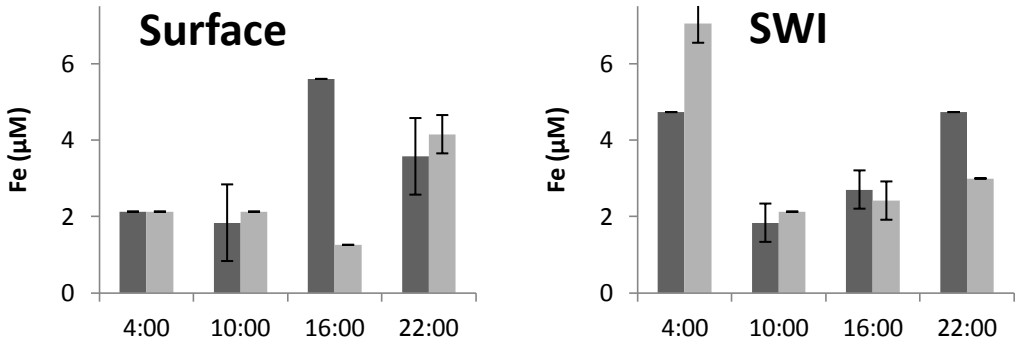

Figure 3.6: Water column total dissolved iron concentration for the water at the surface and the SWI. The dark bars are for the small *A. spicifera* site and the light bars are for the bare sediment. Time points appearing to be without error bars have bars less than 0.1 µM (n=3 analytical replicates; error bars represent +/- 1 SD).

Large *A. spicifera* canopy

Fluctuations in the concentration of oxygen occurred within the large *A. spicifera* canopy over the 24 hour study period (Figure 3.7). Oxygen did not penetrate into the sediment beneath the canopy during any of the eight profiles (Table 3.3). In the canopy, the oxygen penetration depth ranged between 0.8 and 7.8 cm above the SWI. Sulfide was present in the water column within the large *A. spicifera* canopy during 6 of the 8 profiles, with the 12:00 and 14:00 profiles being the only ones where the first appearance of sulfide did not occur until the sediment. Fe^{3+} was detected, starting near the depth of the first appearance of sulfide, during all profiles. A good correlation (R^2=0.95) between the depth at which oxygen dropped to BDL and the depth where sulfide begins was observed for all profiles, except the one taken at 14:00 (Figure 3.8).

Table 3.3: Comparison within the large *A. spicifera* canopy over the 24 hour period of the depth oxygen dropped to BDL, the depth the first sulfide appearance, and the vertical extent of the suboxic zone. Positive numbers correspond to the height above the SWI, zero is at the SWI, and negative numbers are locations low the SWI, in the sediment.

Profile	Maximum O_2 penetration depth (cm)	Depth of first sulfide appearance (cm)	Vertical extent of the suboxic zone (cm)
0:00	3.5	3.5	0
4:00	3	3	0
7:00	3.8	3.8	0
10:00	7.8	7.5	0.3
12:00	1.3	-0.3	1.5
14:00	0.8	-8.8	9.5
16:00	1.3	1.3	0
20:00	3.8	3.8	0

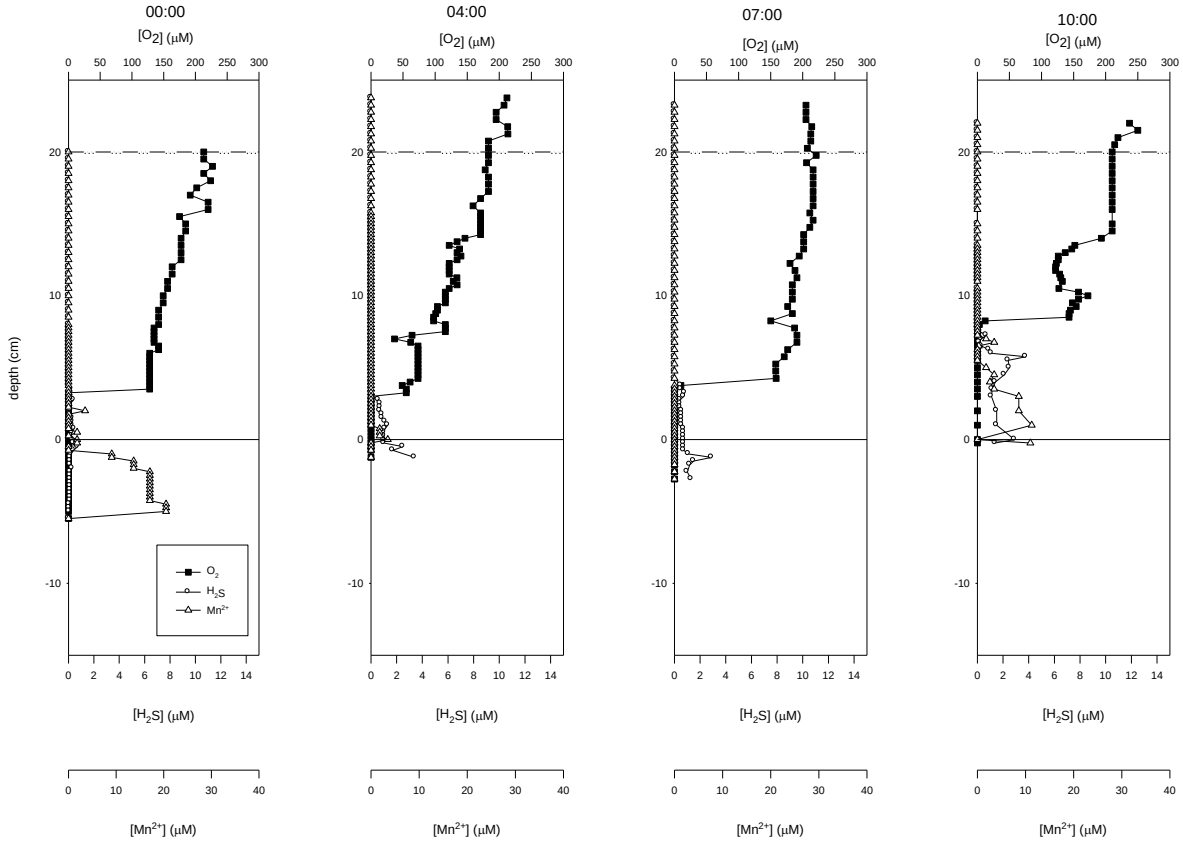
00:00
04:00
07:00
10:00
[O2] (μM)
depth (cm)
[H2S] (μM)
[Mn2+] (μM)
O2
H2S
Mn2+

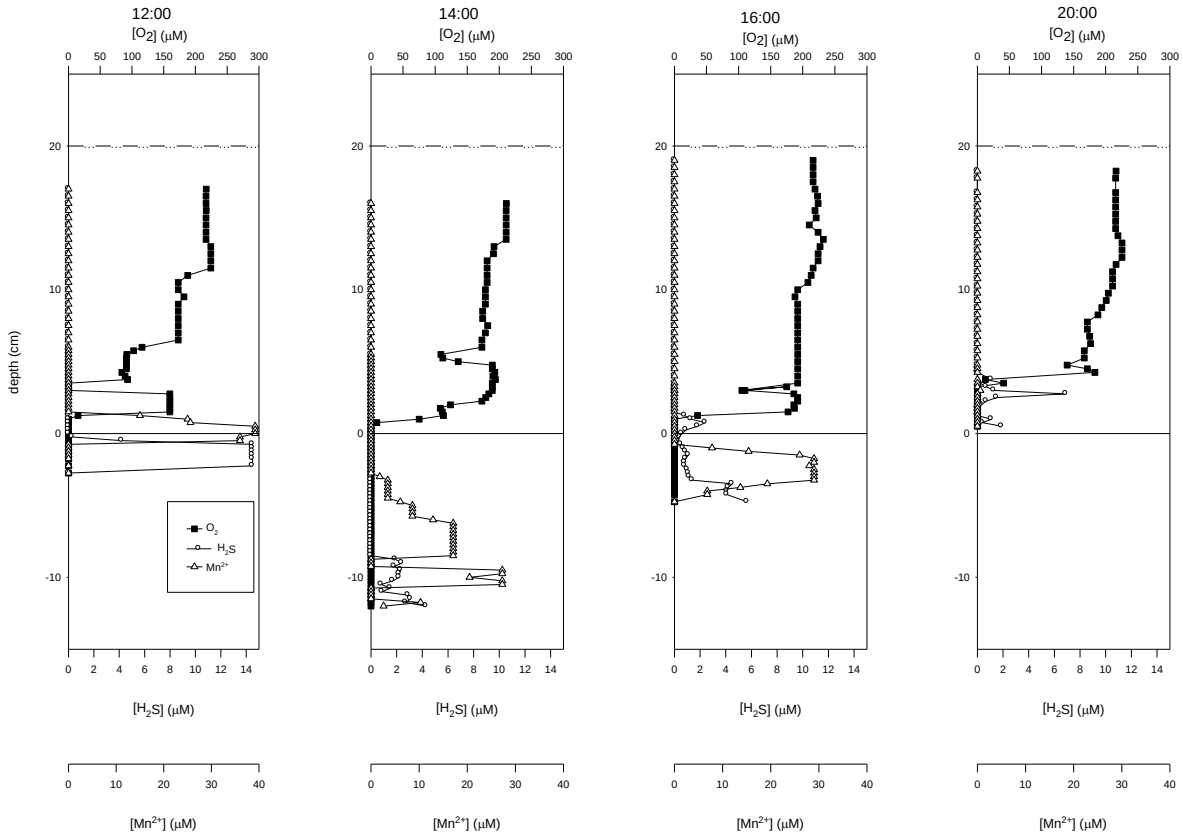

Figure 3.7: Electrochemical profiles through the water column and sediment at the site with the large *A. spicifera* canopy. The solid line in each plot is the location of the SWI, and the dashed line represents the height of the *A. spicifera* canopy.

The 14:00 profile was conducted following a brief, less than 30 minute, rain event. There are numerous characteristics about the 14:00 profile that make it different from the other profiles conducted during this study. The 14:00 profile had a large, 9.5 cm, suboxic zone compared to all other profiles in the large canopy, which averaged 0.25 cm. This profile also had the deepest oxygen penetration depth, to a depth of 0.75 cm above the SWI. For these reasons, we consider the 14:00 profile to be significantly different from the others and will interpret it separately from the other profiles. The 14:00 profile did show clear redox zonations within the sediment, suggesting bioturbation or equipment malfunction were not the cause of the observed difference.

In the large *A. spicifera* canopy, oxygen only fluxed from the water column into the sediments at 12:00 (93 µmoles O_2 m^{-2} hr^{-1}) and 14:00 (42 µmoles O_2 m^{-2} hr^{-1}) (Figure 3.9 a). During the other profiles the concentration of oxygen dropped to BDL in the water column above the SWI. Hydrogen sulfide fluxed from the sediment into the water column during four of the eight profiles, with a maximum flux of 5.2 µmoles H_2S m^{-2} hr^{-1} (Figure 3.9 b). During two of the times at which no flux of sulfide from the sediment to the water column occurred, sulfide was detected in the water column above the SWI (10:00 and 20:00) (Figure 3.7). At 16:00, the concentration of sulfide was higher in the water column that in the sediment, indicating the direction of flux was into the sediment. The other time when sulfide flux was absent occurred at 14:00, following the rain event described above.

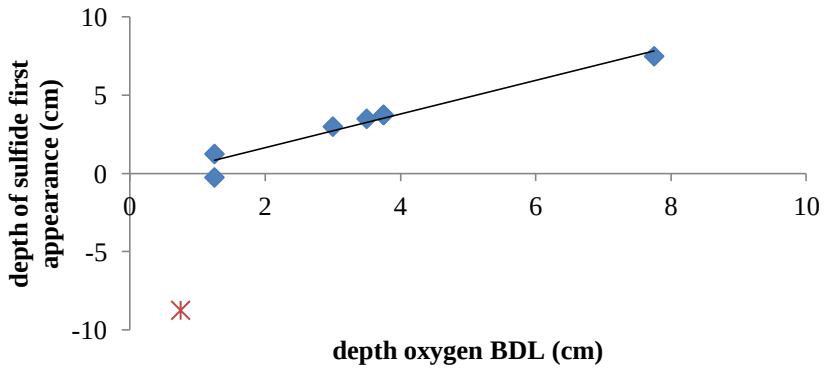

Figure 3.8: Correlation between the depth at which oxygen is BDL and the depth at which sulfide first appears for the profiles conducted within the *A. spicifera* site (R^2= 0.95). Diamonds show the points for the seven profiles used in the correlation. The asterisk is for the 14:00 profile, which occurred following a 30 minute rain event.

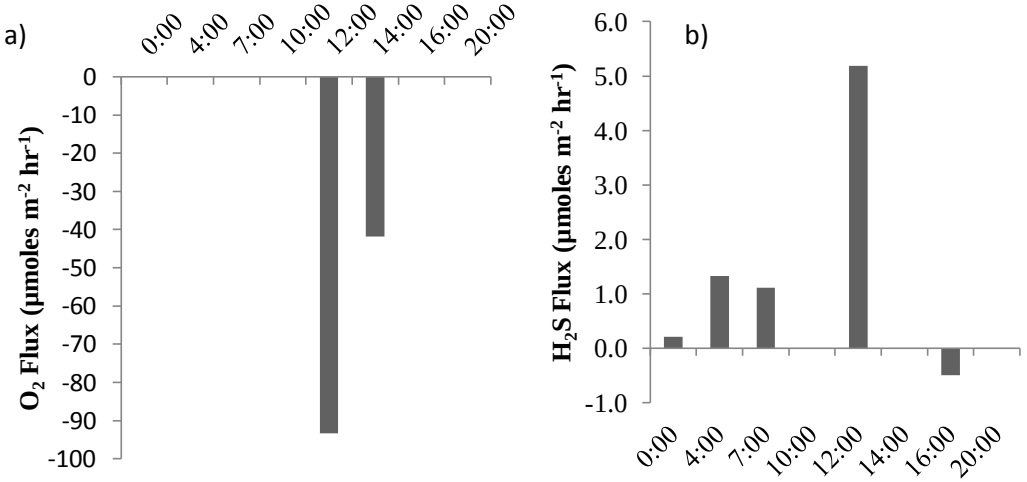

Figure 3.9: Flux of (a) oxygen and (b) hydrogen sulfide within the large *A. spicifera* canopy. Positive numbers indicate species movement from the sediment into the water column and negative numbers indicate movement from the water column into the sediment. No flux occurred during numerous time points, as shown by time points without bars.

Discussion

Invasive benthic macroalgae affect the environment by influencing nutrient availability and changing redox chemistry at and below the SWI. The goals of this study were to: (i) compare water column and sediment oxygen and sulfide concentrations between regions of sediment colonized by an invasive macroalgae (*A. spicifera*) and an adjacent non-colonized area of bare sediment, (ii) compare the availability of water column nutrients between areas dominated by *A. spicifera* and adjacent non-colonized areas, and (iii) compare changes in the availability and depth of redox species between a small (2 m diameter) and a large (4 m diameter) *A. spicifera* canopy over a 24 hour period.

Oxic Zone

Oxygen production occurs during the day, due to photosynthesis, while respiration, oxygen consumption, occurs throughout the diel cycle. The deepest oxygen penetration depth in He‘eia Fishpond was expected to occur in the afternoon, when water column oxygen concentrations are highest, while the shallowest penetration should occur in the early morning, before the onset of photosynthesis, as shown in previous work in the pond (Briggs 2011). In the bare sediment site, without *A. spicifera*, oxygen availability throughout the diel cycle followed the expected trend of penetrating deepest during the day and shallowest at night (Figure 3.2). The diel cycle observed in our study

is thus consistent with previous work and can be attributed to a net loss of oxygen near the SWI at night, when photosynthesis is no longer occurring, and microbial respiration continues in the sediment and in the water column (D'Avanzo and Kremer 1994, Sundback et al. 1991, Briggs 2011).

The concentrations of oxygen within the *A. spicifera* sites were more complex than the bare sediment. In the small canopy, oxygen penetration was deepest at 10:00, while the 16:00 profile had a shallower oxygen penetration depth, similar to the 04:00 and 22:00 profiles (Figure 3.3). We expected the 16:00 profile to have the deepest oxygen penetration depth because the alga would have been exposed to sunlight for the longest period of time, and thus photosynthesis would have increased the water column oxygen concentration. The small canopy in our study had variable heights, ranging from eight to fifteen cm, and the 10:00 profile, which had the deepest oxygen penetration depth (Figure 3.3), occurred in the shortest region of the *A. spicifera* canopy. Previous work within algal canopies attributed variations in oxygen profiles to the heterogeneity of the algal canopy (Corzo et al. 2009), and we suspect the shorter region of the macroalgal canopy profiled at 10:00, is the reason oxygen penetrated the deepest at 10:00, rather than at 16:00.

In the large algal canopy, where profiles were conducted every two to four hours, oxygen profiles were similar to those observed in the bare sediment. As expected, oxygen penetration was deepest into the *A. spicifera* canopy during the 12:00 and 16:00 profiles, while the shallowest oxygen penetration depths were observed during the 10:00

profile (Figure 3.7). This is consistent with previous work in macroalgal canopies in He‘eia Fishpond (Chapter 2), where oxygen levels at 10:00 within an *A. spicifera* canopy were found to be 50 µM, while outside of the canopy oxygen concentrations exceeded. In Chapter 2, we speculated that this discrepancy arose because it takes a longer period of time to oxygenate the water column within *A. spicifera* canopies, after oxygen levels have been drawn down during the night, than adjacent regions without the macroalgae. Additionally, water movement in the canopy is likely slowed, increasing the flushing time of water within the canopy. In the large canopy, the SWI was exposed to less than 5 µM of oxygen for more than twelve hours (Figure 3.7), while the adjacent bare sediment site had an oxygen concentration below 5 µM for less than six hours per 24 hour period (Figure 3.2). McKinnon et al. (2009) observed changes in benthic community composition beneath invasive algal canopies coincident with a similar decrease in the concentration of oxygen, to that observed in He‘eia Fishpond. We thus speculate that the similar pattern of reduced oxygen under *A. spicifera* canopies in He‘eia Fishpond, along with the extended period of suboxic conditions, is likely affecting the benthic community inhabiting He‘eia Fishpond.

A decrease in the concentration of oxygen at the SWI is also affecting the flux of oxygen from the water column into the sediment. Oxygen fluxes were lowest at 4:00, as expected from diel cycling, when night time benthic respiration decreases the concentration of oxygen at the SWI. The flux of oxygen from the water column to the sediment occurred in three of the four profiles in the bare sediment but only one of four in the small *A. spicifera* canopy and two of eight in the large canopy. Within the *A.*

spicifera canopies, oxygen only fluxed into the sediment when it was light out, unlike the bare sediment where oxygen flux into the sediment occurred as late as 22:00. Oxygen flux rates within He‘eia Fishpond were consistent with those observed in previous studies (Reay et al. 1995, Chrisensen et al. 2000). The presence of *A. spicifera* canopies is reducing the flux of oxygen from the water column into the sediment by creating low oxygen conditions in the water column above the SWI, creating an environment suitable for flux of reduced species, including hydrogen sulfide, from the sediment into the water column.

Despite the extended exposure to suboxic conditions in the *A. spicifera* site, compared to the bare sediment site, nitrate was BDL in both sites. Nitrification is performed by chemoautotrophic organisms, and occurs through the oxidation of ammonium using oxygen (Hendriksen and Kemp 1988, and sources therein). The fact that nitrate was BDL in both sites, indicates that *A. spicifera* is not affecting nitrification rates, or in both sites algae are taking up nitrate as it becomes available. Additionally, rates of denitrification may be such that nitrate is rapidly lost from the system as dinitrogen gas, maintaining water column concentrations below our nitrate detection limit of 0.5 µM. Previous work with macroalgae found rates of denitrification to be similar in suboxic macroalgal canopies and adjacent regions with bare sediment (Krause-Jensen et al. 1999). This may be true of the fishpond as well, with the rate of denitrification the same between the water column in the *A. spicifera* canopy and the adjacent bare sediment.

As expected from the reducing environment created by the macroalgae, higher ammonium concentrations occurred at the SWI in the *A. spicifera* site than the bare sediment. Contrary to our hypothesis that ammonium concentrations would be highest at night, because of suppressed nitrification when oxygen concentrations were lowest, ammonium was only detected during the day, not at night. The concentration of nitrate and ammonium in the *A. spicifera* site is complicated by algal uptake rates, as there can be a difference in the rate of macroalgal ammonium uptake between the day and night (Dalsgaard 2003). Additionally, macroalgae take up ammonium at different rates based on carbon to nitrogen ratios in their tissues, which can indicate whether the alga is nutrient-replete (McGlathery et al. 1997). Work in our study suggests that *A. spicifera* takes up ammonium at night, however further physiological work with the macroalgae is needed to determine whether this is actually the reason for the observed difference in ammonium concentrations between the day and night, or if some other component of the nitrogen cycle is responsible for the increased concentration of ammonium during the day.

Suboxic Zone

The suboxic zone occurs where the concentration of oxygen is BDL and the first appearance of sulfide has not yet occurred, a region where organic matter oxidation takes place via nitrate, manganese oxide and iron oxide reduction (Froelich et al. 1979, Berner 1980). The vertical extent of the suboxic zone varied between the three sites, with the largest occurring beneath the small canopy and similar, smaller suboxic regions in the large *A. spicifera* canopy and in the bare sediment (Table 3.2 and 3.3). Suboxic zones

can vary in size due to diel cycling, where increased oxygen during the day penetrates deeper into the canopy, or due to differences in organic matter content (Rozan et al. 2002). In He'eia Fishpond, no discernible diel pattern existed in the variation in the vertical extent of the suboxic zone. Between sites, differences in the vertical extent of the suboxic zone are likely due to algal and organic matter heterogeneity. The density of algae influences oxygen concentrations within algal canopies, by affecting water flow (Escartin and Aubrey 1995) and light penetration (Sundback et al. 1990). The larger suboxic zone within the small *A. spicifera* canopy suggests the canopy has slower OM remineralization than the other two sites, allowing slower oxygen consumption and slower sulfide production within the small canopy.

During the day, SWI concentrations of Mn^{2+} were similar between the small *A. spicifera* site and the bare sediment site (~1 µM); however at night higher concentrations of Mn^{2+} occurred in the small *A. spicifera* site (5 µM) (Figure 3.5). (Water column Mn^{2+} concentrations were BDL(15 µM) using voltammetry.) Higher Mn^{2+} at the SWI of the small *A. spicifera* site is consistent with voltemmetric oxygen data, which show the small *A. spicifera* site had a shallower oxygen penetration depth than the bare sediment site. Thus, the reduced concentration of oxygen at the SWI is altering the concentration of Mn^{2+} in the water column.

For the majority of profiles through the large *A. spicifera* canopy (5 of 7), oxygen became depleted at the same depth as the first appearance of sulfide, and the suboxic zone was nonexistent (Figure 3.7). Despite this overlap between the oxic and anoxic zones, where oxygen and sulfide were present at the same depth, Mn^{2+} was detectable in

6 of the 7 profiles. Mn^{2+} is formed through the microbial reduction of Mn-oxides (Nealson and Saffarini 1994) and the abiotic reduction of Mn-oxides by Fe^{2+} and H_2S (Burdige and Nealson 1986, Thamdrup et al. 1994). These processes release Mn^{2+} into the surrounding water, where it remains until removal through abiotic manganese oxidation, which takes place on the order of hours (Thamdrup et al. 1994). The coincidence of Mn^{2+} and H_2S in the pore water suggests that the abiotic reduction of manganese oxides is a major source of Mn^{2+} to pore waters, and the close proximity of the oxic and anoxic zones in many of the profiles shows that oxygen is also an oxidant for sulfide within the large *A. spicifera* canopy. This is especially apparent in Figure 3.7 at 10:00 and 12:00. During the profile taken at 10:00, both manganese and sulfide were present in the lower half of the large *A. spicifera* canopy; however by 12:00, while manganese was still present in the bottom half of the canopy, sulfide was not detected until beneath the SWI (Figure 3.7). The disappearance of sulfide, but not manganese, between the two profiles can be explained by the abiotic oxidation rate of the two chemical species with oxygen. The abiotic oxidation of sulfide by oxygen is more rapid, on the order of minutes (Cline and Richards 1969), compared to the abiotic oxidation of manganese, which occurs on the order of hours to days (Thamdrup et al. 1994). Based on these profiles, and the oxidation rates of Mn^{2+} and sulfide, the availability of oxygen in the lower canopy controls the concentration of sulfide in the large *A. spicifera* canopy. Given the close proximity of the Mn^{2+} and sulfide peaks in the profiles, the abiotic reduction of manganese oxides by hydrogen sulfide is likely the major source of Mn^{2+} within He‘eia Fishpond.

Iron cycling in He‘eia Fishpond is important for both sulfate and phosphate availability. Iron rapidly reacts with H_2S to form pyrite and other iron-sulfide minerals, a process that decreases the concentration of Fe^{2+} and prevents the flux of toxic hydrogen sulfide from the sediment to the water column (Nealson and Saffarini 1994, Thamdrup et al. 1994). In our study, total dissolved iron was detected in the water column at all sites and at all times. Total dissolved iron is composed of the fraction of iron that passes through a 0.2 µM filter, and thus contains both Fe^{2+} and Fe^{3+}. Dissolved iron concentrations observed at the SWI and surface were similar which implies that the majority of iron detected in the water column was the oxidized form (Fe^{3+}), as the reduced form (Fe^{2+}) is rapidly oxidized in the presence of oxygen, on the order of minutes to hours (Davison and Seed 1983, Kirby et al. 1999). Fe^{3+} was also detected in the majority of electrochemical profiles, beginning near the depth at which sulfide first appeared. The presence of dissolved iron in the water column may also explain why phosphate was BDL for the entire study. Under oxidizing conditions, as we observed in much of the water column, phosphate is removed through sorption onto iron oxyhydroxides (Krom and Berner 1980, Sundby et al. 1986, Chambers and Odum 1990).

Fe^{3+}, when detected, appeared in the pore water near the depth onset of sulfide and co-occurred with sulfide for much of the profile. The overlap between sulfide and Fe^{3+} suggests that pyritization is occurring in the sediment. Pyritization is a rapid reaction between sulfide and iron oxides, as demonstrated by the inability of sulfide to accumulate in pore waters in the presence of iron oxides (Canfield 1989, Canfield et al. 1992). The reactivity of iron oxides with sulfide, however, is dependent upon the iron

oxide mineralogy, with more crystalline forms being less reactive than amorphous forms (Canfield 1989). The detection of sulfide in surface waters, and build up of sulfide in pore waters, suggests that the more easily reducible iron oxides may have already been reduced, and were thus unavailable to react with H_2S and form solid FeS. The coexistence of Mn^{2+} with Fe^{3+} and H_2S, suggests that manganese oxides are oxidizing Fe^{2+} and sulfide in the fishpond.

Anoxic Zone

The depth of the first appearance of sulfide within a profile is a function of local sulfide production and the availability of oxidants, such as oxygen, manganese oxides, and iron oxides, to oxidize the sulfide. Differences in the concentration of hydrogen sulfide in the water column between the small *A. spicifera* site and bare sediment site are revealed by the profiling data. In the bare sediment site, sulfide was only present in the water column during the 22:00 profile (Figure 3.2). The oscillation of the oxic-anoxic transition zone from deeper during the day to shallower at night indicates diel cycling occurs in the bare sediments.

Within the small *A. spicifera* site the depth of the first appearance of sulfide occurred as expected for diel cycling. Sulfide was not detectable in the water column during the day and at night sulfide was present in the water column (Figure 3.3). The shape of many of the sulfide profiles, with larger concentrations of sulfide present in the water column than in the sediment, indicates that the sediment is not the only source of sulfide to the water column, but rather that sulfate reduction is occurring within the *A.*

spicifera canopy. This is confirmed by the flux data. For example, at 04:00 sulfide concentrations at more than one location within the *A. spicifera* canopy were higher than at the SWI. Work by Nedergaard et al. (2002) showed that sulfate reducing bacteria are present on the thallus of the benthic macroalgae *Ulva*, not just in sediments, demonstrating that organisms capable of sulfate reduction live in the water column in close proximity to macroalgae. The presence of in the water column consistent with the flux data from the large *A. spicifera* canopy which indicated that sulfate was fluxing from the water column into the sediment at 16:00. Additionally, macroalgae excrete dissolved organic carbon (Alber and Valadia 1994, Valadia et. al 1997), providing an energy source for local microbial metabolisms. Thus, increased microbial activity from the decomposition of dissolved organic carbon excreted by the algae may explain why in some profiles sulfide was present in the water column within the *A. spicifera* canopy at higher concentrations than in the surface sediment.

Sulfide availability differed between the two *A. spicifera* canopies. In the smaller canopy, sulfide was only present in the overlying water during the night (Figure 3.3), while in the larger canopy sulfide was present in the overlying water for six of the seven profiles, occurring during the day and at night (Figure 3.7). In the larger canopy a correlation occurred between the depths of oxygen depletion and sulfide onset (Figure 3.8), while in the small canopy no such correlation existed. This oxygen-sulfide correlation in the large canopy, coupled with the co-occurrence of oxygen and sulfide at the same depth in five of the profiles suggests that the oxidation of sulfide by oxygen is an important mechanism controlling sulfide concentrations within some of the *A.*

spicifera canopies in the pond. In the small *A. spicifera* canopy a large suboxic zone existed between the depths of oxygen depletion and sulfide onset (Figure 3.3), which suggests that sulfide oxidation is occurring primarily through the reduction of manganese and iron oxides. While Mn^{2+} and dissolved iron can be detected using voltammetry (Table 3.1), colorimetric data indicates that the reason dissolved manganese and iron were not detected in the water column is because the concentrations were BDL. One explanation for the larger suboxic zone in the small canopy is that there is decreased sulfate reduction occurring in this canopy, perhaps due to variability in the oxygen penetration depth throughout the diel cycle. Without using radiotracers, however, the rate of sulfide production and sulfate consumption within the canopies and sediments cannot be accurately calculated. Previous work has shown that different thresholds of algal cover alter biogeochemical cycling within macroalgal communities (Viaroli et al. 2008). Once algal density reaches a minimum threshold, the alga begins affecting biogeochemical cycling. The smaller surface area covered by the small canopy, along with the shorter height, may create regions within the canopy below the threshold required to create the higher sulfide concentrations observed in the larger *A. spicifera* canopy.

The success of other macroalgal species, such as *Caulerpa*, has been attributed to the macroalga increasing the local concentration of sulfide (McGlathery 2001, Holmer et al. 2009). The creation of anoxic conditions in the water column by *A. spicifera* in He‘eia Fishpond may give the alga an ecological advantage by creating a toxic environment that other algae are unable to tolerate. The increased concentration of

sulfide at the SWI within *A. spicifera* canopies provides further evidence of local habitat alteration by the invasive species, and may contribute to success of the algae in He‘eia Fishpond.

The flux of sulfide from the sediment to the water column occurred during three of the four profiles in the bare sediment site. The flux of sulfide from the sediment to the water column in sites colonized by *A. spicifera* was complicated by the production of sulfide within the canopies. Unlike regions of bare sediment in the pond, the macroalgae creates an environment where sulfide can be produced in the water column, allowing a flux of sulfide to take place from the water column into surface sediments.

Previous work in the pond over bare sediments by Briggs (2011) found a larger separation (many cm) of oxygen and sulfide than observed in our study, and concluded that oxygen could not be a direct oxidizer of sulfide. The smaller depth separation between oxygen depletion and sulfide onset in the bare sediment site from our work, especially that observed at 22:00 (Figure 3.2) when sulfide was detected in the overlying water column, indicates that oxygen was likely a sulfide oxidant over the course of our study. Additionally, the data from the large *A. spicifera* canopy, showing overlap of the oxic-anoxic zones provides further evidence that oxygen is an oxidant of sulfide in He‘eia Fishpond. The difference in sulfide oxidation results between our work and that from Briggs (2011) may be attributed to a difference in the organic matter content between sites. Sulfate reducers compete with other microbes for organic matter, and in the presence of large quantities of organic matter the more energetically favorable

oxidants are utilized first, leaving sulfate reduction to oxidize remaining organic matter. The close proximity of our bare sediment site to the macroalgae may have provided labile organic matter to the bare site, increasing benthic respiration. Our results are consistent with work by Jørgensen (1977b) which showed sulfide to be a major consumer of oxygen in coastal sediments.

Rain Event

The profile conducted in the large *A. spicifera* canopy at 14:00 followed a 20 minute rain storm. This profile showed numerous differences in redox characteristics than the other profiles: the depth of the first appearance of sulfide occurred more than 8 cm deeper, oxygen penetrated closest to the SWI, and the depth of the first appearance of Mn^{2+} was the deepest (Figure 3.7). The clear appearance of Mn^{2+} and Fe^{2+} in pore waters at a shallower depth than sulfide suggests that bioturbation or equipment malfunction was not the cause of the observed difference. Rather, the rain event appears to have increased the oxygen penetration depth in the canopy. While this is only a single profile, the large deviation from the surrounding time points indicates that storm events may be important for water column mixing within *A. spicifera* canopies, and further work should examine the significance of rain events on SWI redox chemistry within He‘eia Fishpond.

Fe-S-P Cycling

Under oxidizing conditions, phosphate binds to iron oxyhydroxides, while reducing conditions favor phosphate release to the surrounding water (Krom and Berner 1980, Sundby et al. 1986, Chambers and Odum 1990, Jensen et al. 1995, Gunnars and

Blomqvist 1997, Blomqvist and Elmgren 2004). Sulfide rapidly reduces iron oxides (Dos Santos Afonso and Stumm 1992, Canfield et al. 1992), a reaction that occurs on the order of minutes to days, depending upon the type of iron mineral present (Poulton et al. 2004). High concentrations of iron oxyhydroxides cause little to no sulfide to be present in sediment pore waters due to iron-sulfide interactions (Canfield 1989). Additionally, the reductive dissolution of iron oxides by sulfide, and subsequent formation of iron-sulfide minerals, has been shown to release phosphate and stimulate macroalgal blooms (Rozan et al. 2002). Therefore, when reducing conditions were present in the sediment and at the SWI, we expected to find DIP in He‘eia Fishpond.

The presence of dissolved iron (Fe^{3+} and Fe^{2+} smaller than 0.2 µm), Mn^{2+} and sulfide over the course of our study indicates that reducing conditions existed both in the sediment, and in some cases in the overlying water column. Total dissolved iron was detected in all samples from the water column at all time points, with similar concentrations in surface waters and at the SWI (Figure 3.6). Fe^{2+} is rapidly oxidized by oxygen, on the order of minutes to hours (Davison and Seed 1983, Kirby et al. 1999), and thus the presence of similar concentrations of total iron at the SWI, where oxygen concentrations were low, and in oxygenated surface waters, suggests that the majority of the iron measured during our study was Fe^{3+}. Colloidal Fe^{3+} is a known scavenger of phosphate (Gunnars et al. 2002 and sources therein), and the presence of Fe^{3+} in the surface waters and at the SWI in He‘eia Fishpond indicates this species is likely the dominant actor in sorptive removal of DIP from the water column.

Previous studies in He‘eia Fishpond attributed the low dissolved DIP concentrations in sediment pore waters (less than 2 µM) to phosphate sorption by iron oxyhydroxides (Briggs 2011, Murphy He‘eia 2010). The results from our study support these findings, and further suggest that colloidal iron in the water column is scavenging phosphate. Another possible mechanism for DIP removal is through sorption to manganese oxides (Ingri and Bostrom 1991, Yao and Millero 1996). Dissolved manganese was measured throughout the water column during our study. While the abiotic oxidation of Mn^{2+} by oxygen is slower than that of Fe^{2+} (Davison and Seed 1983, Thamdrup et al. 1994), and phosphate sorption by manganese is less important when iron is present (Yao and Millero 1996), the presence of Mn^{2+} both in surface sediments and in the water column indicates that manganese oxides are prevalent in He‘eia Fishpond. Thus DIP sorption by manganese oxides may be another phosphate removal mechanism in the pond.

In our study, the occurrence of sulfide in the water column within *A. spicifera* canopies provides a source for the reduction of manganese and iron oxides which could release sorped phosphate to the surrounding water, making it available for uptake by the macroalgae. The success of this invasive macroalgae in the fishpond may be due to its ability to create pockets of reducing conditions where iron and manganese oxides are reduced and phosphate is released. If phosphate release takes place in close proximity to the algae, it would allow rapid phosphate uptake by the algae before the phosphate is again sorbed by manganese and iron oxides. Further work on the physiology of *A. spicifera* and mineralogy of surface sediments within He‘eia Fishpond is needed to

determine whether the algal phosphate uptake mechanism just described is operant, and to examine whether part of the success of this invasive species is due to its ability to harvest phosphate from the ecosystem.

Conclusion

The invasive alga, *A. spicifera* is altering the habitat of He‘eia Fishpond by creating reducing conditions above the SWI. Areas in the pond with *A. spicifera* had higher ammonium concentrations than adjacent areas of bare sediment. Sulfide was found in the water column within the *A. spicifera* canopy throughout the diel cycle, while in adjacent regions where macroalgae were absent, sulfide was only present in the water column during the night. The higher concentration of sulfide in sites colonized by *A. spicifera* indicates that increased rates of sulfate reduction are occurring in areas colonized by the invasive alga.

The complex interactions between redox chemistry of manganese, iron, sulfide and phosphate warrants further investigation into the solid phase chemistry of surface sediments to determine what particles are sorbing phosphate in He‘eia Fishpond. Further biological work in the pond should examine the physiology of *A. spicifera* to determine if the alga preferentially takes up ammonium during the day or night and whether manganese or iron oxides are being reduced in close enough proximity to the algae to allow rapid phosphate uptake, before phosphate is resorbed to particles. From a management perspective, the larger patches of *A. spicifera* are more detrimental to the

ecosystem, as these patches create conditions under which extended periods of anoxic conditions can persist at the SWI, when compared to smaller patches and non-colonized areas.

Chapter 4

Dissolved oxygen and hydrodynamics in *Gracilaria salicornia* mats: characterizing a microniche

(Coconut Island)

Abstract

The effect of the invasive alga, *Gracilaria salicornia*, on water column oxygen concentration and water flow were examined by profiling through the water column and into the algal mats using *in situ* voltammetry and an acoustic Doppler velocimeter. Mats of *G. salicornia* reduced water velocity, turbulent kinetic energy and turbulent xRMS compared to adjacent algae free regions. Water column oxygen concentrations were reduced within algal mats, dropping to below the detection limit (5 µM) in the water column for five of the six profiles, and the depth oxygen penetration into the mat was proportional to flow velocity above the mat. The location of suboxic regions within the mat occurred at depths where turbulent xRMS of the dominant flow direction dropped to velocities near 0.001 m/s, indicating that reduced flow in the water column influences the location of suboxic regions within *G. salicornia* mats. Thin, (less than 1 cm) vertically isolated suboxic zones occurred within the otherwise oxic water column in vertical profiles through two of the algal mats. These suboxic microniches provide environmental conditions suitable for oxidation-reduction sensitive nutrient transformations, such as denitrification and reductive solubilization of phosphate bound to iron oxides, to take place. Results of this study illustrate that the biotic and abiotic alteration of local habitats, through reduced flow and shifts in redox transition zones, make *G. salicornia* an ecosystem engineer.

Introduction

Invasive macroalgae comprise a large component of non-indigenous marine species (Schaffelke et al. 2006). In shallow, coastal ecosystems, benthic macroalgae are important primary producers. Blooms and subsequent die offis of macroalgae can lead to water column anoxia from the microbial decomposition of algal tissues (Sfriso et al. 1987), which can stimulate further algal blooms (Rozan et al. 2002). Additionally, blooms of macroalgae, whether native or introduced, negatively affect other benthic organisms, including coral (Lapointe 1997, Smith et al. 2005, Hauri et al. 2010), seagrass (McGlathery 2001, Holmer et al. 2009), and benthic fauna (McKinnon et al. 2009). The ability of an organism to alter a habitat, through biotic or abiotic processes, such that resource availability is altered, makes that organism an ecosystem engineer (Jones et al. 1994, Jones et al. 1997). Thus, the physical and chemical alteration of the environment, benthic macroalgal mats can act as ecosystem engineers.

The presence of a benthic macroalgal mat alters local hydrodynamic conditions (Forster et al. 1996, Nepf 2012). As much as 90% of the water flowing in an area can be diverted around, rather than through, a mat (Escartin and Aubrey 1995). The amount of water diverted around a mat is related to the extent of macroalgal coverage, such that there exists a negative relationship between the macroalgal coverage and current velocity through a mat (Widdows and Brinsley 2002). Local hydrodynamics are further altered in regions with macroalgal mats through the dissipation of eddies and the resulting increase in turbulent energy within the surface of macroalgal mats (Nepf 2012). In many mats, there is enhanced turbulence at the top of the macroalga causing a rapid flushing of mat

surface water and decreased turbulence at the bottom of the mat, resulting in slower turnover of water (Nepf and Vivoni 2000). The reduction in flow through macroalgal mats also influences the movement of water at the sediment water interface (SWI). Reduced SWI flow decreases the rate at which fluids are moved from the sediment into the overlying water column (Huettel et al. 1998). Macroalgal mats increase the size of the benthic boundary layer (Koehl et al. 2003), increasing the distance solutes must travel to escape the benthic boundary layer, and thus decreasing the rate at which diffusion across the sediment-water interface takes place (Jørgensen and Revsbech 1985). Thus, an increased benthic boundary layer slows the movement of nutrients from the sediment to the overlying water and changes oxidation-reduction (redox) conditions in the sediment.

Benthic macroalgal mats also reduce the amount of light at the SWI. By decreasing the amount of light penetrating to surface sediments, macroalgae cause a decline in the abundance of microphytobenthos (Sundback et al. 1990, Corzo et al. 2009). In addition to shading other species, macroalgae can be self-shading, creating regions within the mat where photosynthesis is reduced. D'Avanzo and Kremer (1994) noted that only approximately the top 25% of a mat was photosynthetically active, indicating that for the majority of the mat respiration was the dominant metabolic process. In *Gracilaria salicornia,* Beach et al. (1997) demonstrate the red alga is able to acclimate to reduced light within the self-created mat. A reduction in photosynthesis contributes to the drop in water column oxygen concentrations observed within the lower regions of benthic macroalgae (Sundback et al. 1990, D'Avanzo and Kremer 1994, Hauri et al. 2010). The physical environmental alterations caused by benthic macroalgal mats,

through the decrease in water flow, as well as the reduction of light availability at the SWI, with consequent diminished photosynthetic activity, act together to reduce the concentration of oxygen within mats. Reduced oxygen concentrations in mats alter redox conditions at the SWI, where the remineralization of organic matter generates nutrients, including phosphate and ammonium, and affects the movement of nutrients from the sediment to the water column (Sundback et al. 1990). Thus, reduced concentrations of oxygen, resulting from these physical-biological interactions have the potential to alter redox chemistry occurring at the SWI.

Anoxic sediment conditions promote solubilization of phosphate during the reductive dissolution of iron oxyhydroxides, rendering phosphate biologically available, while oxic sediment conditions render phosphate biologically unavailable due to sorption of phosphate onto iron oxyhydroxides (Krom and Berner 1980, Sundby et al. 1986, Jensen et al. 1995). Thus decreased oxygen concentrations in macroalgal mats, create conditions suitable for enhanced phosphate bioavailability. Macroalgal die-off events, during which bacterial respiration decreases local oxygen concentrations, also provide a mechanism for phosphate release from the sediments to the overlying water column (Rozan et al. 2002).

A decrease in the concentration of oxygen at the SWI also alters nitrogen cycling. Nitrification, the transformation of ammonium to nitrate, cannot take place without oxygen (Henricksen and Kemp 1988). Therefore, reduced oxygen at the SWI creates an environment characterized by increased ammonium and decreased nitrate concentrations

(Sundback et al. 1990). In addition to affecting microbial oxidant availability and nutrient transformations, macroalgae have nutrient growth requirements, and can intercept nutrients diffusing out of sediments and into the overlying water column (McGlathery et al. 1997, Larned 1998, Sundback et al. 2003). Macroalgae also compete for nitrate with microorganisms, such as denitrifiers (Dalsgaard 2003). In summary, the presence of benthic macroalgae alters local nitrogen availability by altering microbial nitrogen cycling and by taking up nitrogen for growth requirements.

Through their effects on flow, light, and nutrient cycling, macroalgal mats have the ability to physically and chemically affect ecosystems and therefore may be considered ecosystem engineers. Benthic mats alter flow regimes by decreasing the speed at which water moves through the mats. Slower water movement, coupled with reduced photosynthesis within the mat due to shading, can create an environment where community respiration occurs at a faster rate than photosynthesis, resulting in a decrease in the concentration of oxygen at the SWI. A reducing environment at the SWI affects nutrient cycling in surface sediments, altering the movement of nutrients from the sediment to the water column.

In Hawai‘i, *Gracilaria salicornia* is a highly successful invasive macroalgal species (Smith et al. 2002), which forms dense mats on coral reefs and the surrounding sandy sediment. The purpose of this study was to determine if *G. salicornia* is physically and chemically altering the local ecosystem and can be considered an ecosystem engineer. In order to determine whether *G. salicornia* is altering local hydrodynamics

and oxygen availability, our study compared flow and oxygen availability in the water column between areas with and without the invasive macroalgae.

Methods

Site Description

Three locations around Coconut Island, in Kāneʻohe Bay, Hawaiʻi, were chosen for study based upon the presence of *G. salicornia*: in a lagoon (lagoon), in a channel at the inlet to the lagoon (channel), and on sand flats located on the southeast side of the island (flats). The sediment around Coconut Island consists of coarse grained sand, and water depths throughout the experiment ranged between 0.5 to 1 m, depending upon the site location. At each location, a patch of *G. salicornia* at least 9 m^2 in size was chosen to conduct *in situ* profiles of chemistry using microelectrodes and flow using an acoustic Doppler velocimeter (ADV). At each site, profiles were taken at three locations: the sand outside of the *G. salicornia* mat (sand), the edge of the mat (edge- less than 0.5 m inside the mat), and in the center of the mat (center). Profiles were conducted with the mat aligned so that flow direction was from the outside, to the edge, towards the center location.

Electrochemistry

The presence and concentration of electrochemically active species can be detected and measured using voltammetry. The use of Au/Hg solid state electrode

sensors (Brendel and Luther 1995) enable the simultaneous measurement of numerous chemical species *in situ*. Redox species that can be quantified by voltammetry include: O_2, H_2S, Fe^{2+}, and Mn^{2+} (Luther et al. 2008) (Table 4.1).

Table 4.1: Electrode reactions for select species at the gold-mercury working electrode verse the saturated calomel electrode (adapted from Luther et al. 2008).

Electrode Reaction	**$E_p(E_{1/2})$ (V)**	**Detection limit (µM)**
$O_2 + 2H^+ + 2e^- \rightarrow H_2O_2$	-0.33	5
$H_2O_2 + 2H^+ + 2e^- \rightarrow H_2O$	-1.23	5
$Mn^{2+} + Hg + 2e^- \leftrightarrow Mn(Hg)$	-1.55	5
$Fe^{2+} + Hg + 2e^- \leftrightarrow Fe(Hg)$	-1.43	10
$Fe^{3+} + e^- \leftrightarrow Fe^{2+}$	-0.2 to -0.9	molecular species
$FeS + 2e^- + H^+ \leftrightarrow Fe(Hg) + HS$	-1.15	molecular species
$HS^- + Hg \rightarrow HgS + H^+ + 2e^-$	-0.6	0.1
$HgS + H^+ 2e^- \leftrightarrow HS^- + Hg$	~ -0.6	0.1

In situ voltammetric profiles were conducted at the 3 locations: lagoon, channel, and flats, and at 3 sites within each location: sand, edge and center, for a total of 9 profiles. A DLK60 (AIS Inc.) coupled with a submersible micromanipulator were used to collect the *in situ* voltammetric data (Figure 4.1a). The micromanipulator consists of a stepper motor, mounted on three adjustable legs, that turns a threaded precision rod and

causes an arm to move up or down. The working electrode is attached to the arm of the micromanipulator, and for this study the electrode was moved in 0.1 to 0.5 cm increments. For each profile, a 0.3 cm diameter Au/Hg PEEK electrode (Luther et al. 2008) was attached to the micromanipulator and profiled from the water column, through the *G. salicornia* mat, when present, and into the sandy sediment (Figure 4.1b). Each profile took approximately 1 hour to complete. The concentration of oxygen at the surface of the water, below the air-sea interface, was measured using an oxygen optode (Aanderaa Data Instruments, 4330), and these values were used to confirm voltammetric oxygen data.

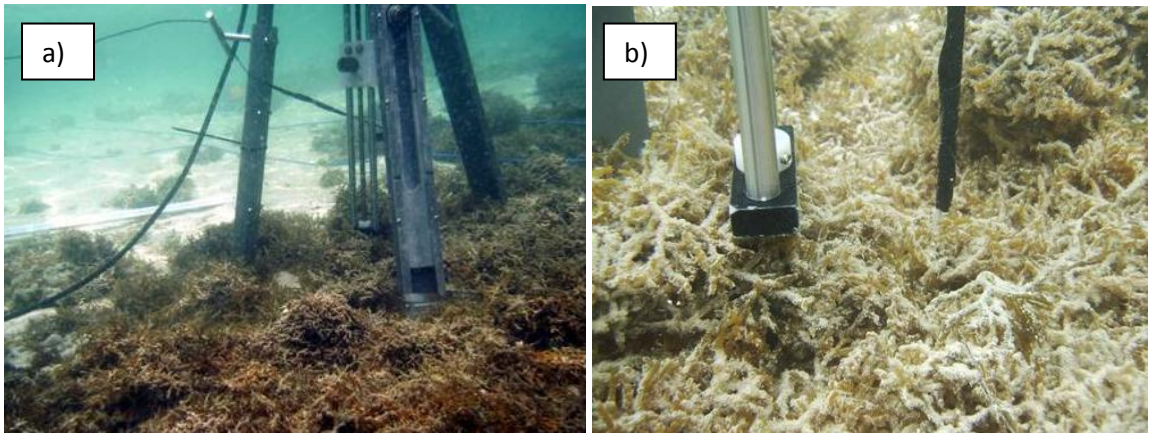

Figure 4.1: (a) The micromanipulator in the edge of a *G. salicornia* mat. (b) Close up of the electrode being inserted into the center of a *G. salicornia* mat.

ADV

After completing the electrochemical profile, a Nortek Vectrino II ADV (acoustic Doppler velocimeter) was used to collect water column flow data. Electrochemical and ADV profiles could not be conducted simultaneously due to the electrical interference caused by the ADV on the electrochemical signals. The Vectrino II was attached to a stand with spring clamps, allowing rapid repositioning of the ADV within the water column. For each profile, the initial collection occurred near the surface of the water and subsequent measurements were taken in 1 to 10 cm increments down through the water column. At each depth, data were collected for approximately 5 minutes before the ADV was repositioned deeper in the water column. For profiles through regions containing *G. salicornia*, it was necessary to cut a small hole into the macroalgal mat to allow insertion of the ADV, due to the dense, tough nature of the algal mat, which introduces error. Profiles were successfully conducted at 8 of the nine sites, and data were collected at a minimum of 5 depths per site. We were unable to collect ADV data from the edge of the lagoon site because of equipment malfunction.

Data from the ADV were analyzed based on the spectral analysis described in Stainsen and Sundby (2001). The energy spectrum from each depth was broken down into wave and turbulent components for the x, y and z directions, with x corresponding to the primary flow direction (m s^{-1}). The root mean square (RMS) for each directional component was then calculated to determine the velocity of water motion at each depth.

Turbulent RMS for each directional component was then used to calculate the turbulent kinetic energy (TKE) (Equation 4.1) at each depth, resulting in units of $m^2 s^{-2}$.

$$TKE = 0.5 * (TxRMS^2 + TyRMS^2 + TzRMS^2) \qquad (4.1)$$

The short time frame over which data were collected at each depth prevented the determination of the wave component. Wind waves in this area typically have periods of 6 – 10 s (Falter et al. 2004).

Results

Lagoon

In the lagoon, oxygen penetrated into the sediment in the bare sand site only (-0.5 cm) (Figure 4.2). In the two locations with *G. salicornia*, oxygen dropped to below the detection limit (BDL) of the electrode (5 µM) within the water column inside of the mat, at varying depths. The profile conducted at the edge of the mat indicated there was an increase in the concentration of oxygen at the surface of the mat, followed by a steady decline in oxygen until a depth of 6.9 cm above the SWI, at which point the oxygen concentration dropped to BDL. In the center profile, some variance was noted in the concentration of oxygen above the mat; however, unlike the edge, the center did not display much of an increase in oxygen at the surface of the mat. Similar to the edge, the center site had a rapid decline in the concentration of oxygen once inside the mat, and dropped to BDL 8.3 cm above the SWI. The profile through the center of the mat was unique in that after the initial depth where oxygen had dropped to BDL in the surface of

the mat, two additional peaks in the oxygen concentration were observed in the water column above the sediment (Figure 4.2c). Thus the profile of oxygen at the center reveals the existence of suboxic pockets intercalating with oxic regions in the *G. salicornia* mat.

The size of the suboxic zone, the zone in which neither oxygen nor sulfide are detectable, and depth of the first appearance of sulfide varied between lagoon sites. The vertical suboxic zone was small in the bare sand site (0.5 cm) compared to the sites within *G. salicornia* (edge = 9 cm, center =13 cm). In the bare sand site, sulfide appeared at the shallowest depth, 1 cm below the SWI, and more than 15 µM of sulfide was detected 2 cm below the SWI. At the edge of the mat, sulfide was BDL for the entire profile, which penetrated 5 cm below the SWI. In the center site, sulfide was first detected (0.5 µM) at a depth of 5 cm below the SWI, but then dropped to BDL until 10 cm beneath the SWI, where sulfide was once again detected at low concentrations.

Channel

In the channel, oxygen profiles varied between sites (Figure 4.3). The bare sand site had a relatively constant water column oxygen concentration before dropping to BDL at 2.5 cm below the SWI. The two profiles conducted within the *G. salicornia* mat displayed a complete loss of oxygen in the mat well above the SWI. At the edge of the *G. salicornia* mat, the oxygen concentration dropped to BDL 4.7 cm above the SWI, then increased 1 cm above the SWI to near overlying water concentrations, and finally

dropped to BDL 1 cm into the sediment. The profile conducted in the center of the mat showed near constant oxygen concentrations in the surface of the mat, before rapidly decreasing to BDL 5.3 cm above the SWI.

The size of the suboxic zone varied between the three sites. Similar to the lagoon location, the channel bare sand site had the smallest suboxic zone (1 cm), while the center had the largest (7 cm). The edge site had two distinct suboxic zones, one in the water column (5 cm) and a smaller one in the sediment (1 cm). Unlike the lagoon location, the first appearance of sulfide occurred deepest in the bare sand site (-3.5 cm), followed by the edge (-2.0 cm), with the center having the shallowest first appearance of sulfide (-1.0 cm).

Flats

Oxygen penetrated into the sediment at the bare sand site (-1.2 cm) and at the edge of the *G. salicornia* mat (-1.5 cm) in the flats location (Figure 4.4). In the bare sand site, the concentration of oxygen was constant until the SWI, where there was a slight increase, followed by a rapid decrease in the sediment. The profile at the edge of the algal mat showed a slight increase in the concentration of oxygen at the surface of the *G. salicornia* mat, followed by a slight decrease in oxygen concentration within the mat, and then a rapid decrease at the SWI. The profile in the center of the mat had a slight increase in the concentration of oxygen at the surface of the mat, followed by a rapid decrease, such that it was BDL 5.3 cm above the SWI. Similar to the lagoon-center site,

the bottom half of the mat at the flats-center site had two areas of low oxygen within an otherwise suboxic region.

For the bare sand and edge sites, where oxygen penetrated 1 cm into the sediment, the suboxic zone was small (1 and 0.8 cm respectively) compared to the size of the suboxic zone in the center of the mat (4 cm). The first appearance of sulfide occurred at similar depths for the bare sand and edge sites (-2.1 and -1.8 cm respectively), while in the center of the mat sulfide was not detectable until deeper in the sediment (-5.0 cm).

Table 4.2: Summary of data for sites with *G. salicornia*.

site		**mat height (cm)**	**height above SWI where oxygen is BDL* (cm)**	**depth from surface of mat where oxygen drops BDL* (cm)**
lagoon	edge	10.5	6.9	3.6
	center	11	8.8	2.2
channel	edge	8	4.7	3.3
	center	15	5.3	9.7
flats	edge	5.5	-1.5	7
	center	8	5.3	2.7

*BDL = Below the detection limit

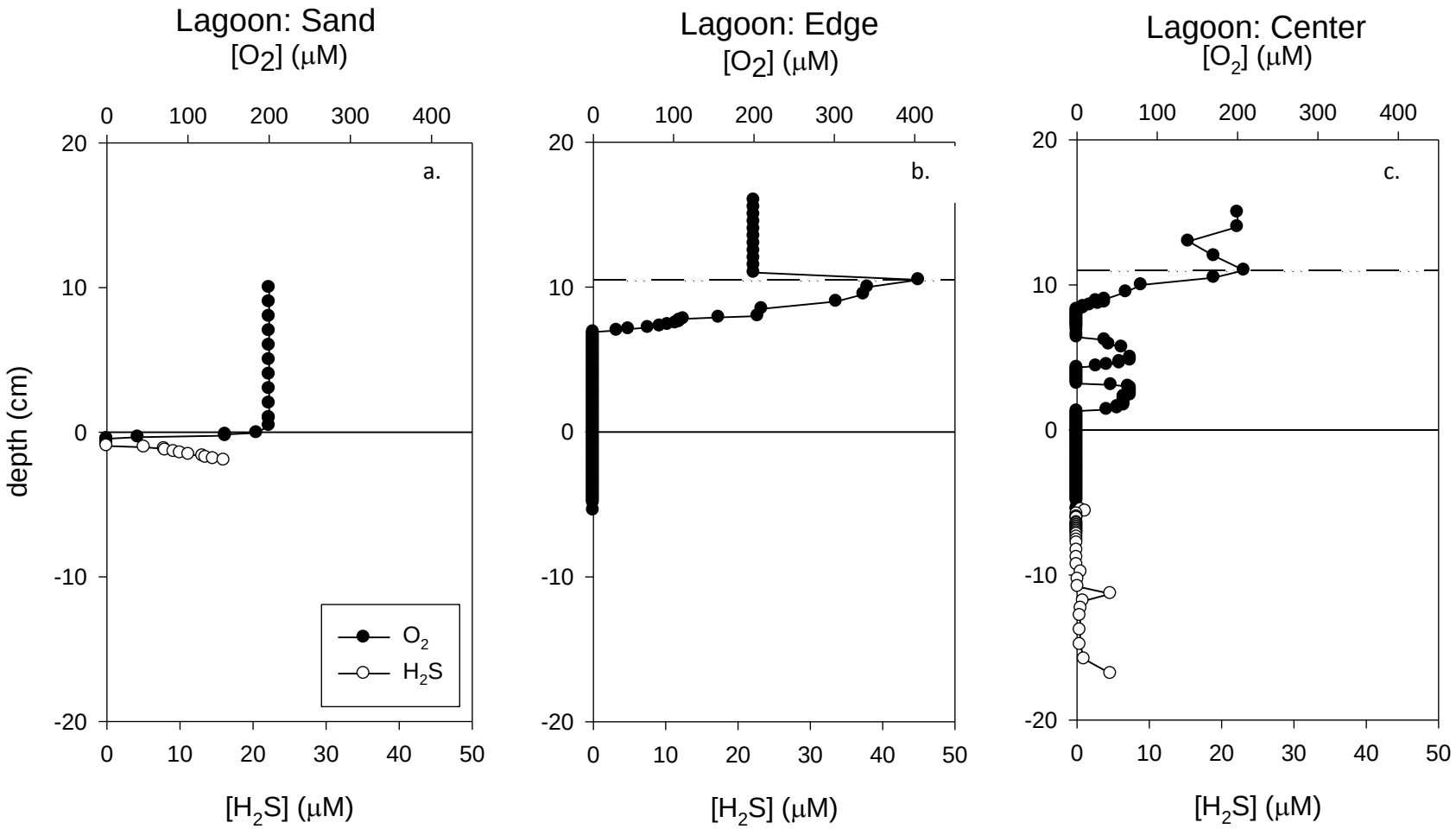

Figure 4.2: Oxygen and sulfide profiles for the three sites at the lagoon location. Depth is positive in the water column and negative below the sediment water interface (SWI), with the SWI occurring at 0. Oxygen is displayed as filled in circles and sulfide as open circles. The location of the top of the *G. salicornia* mat is indicated by the dashed line.

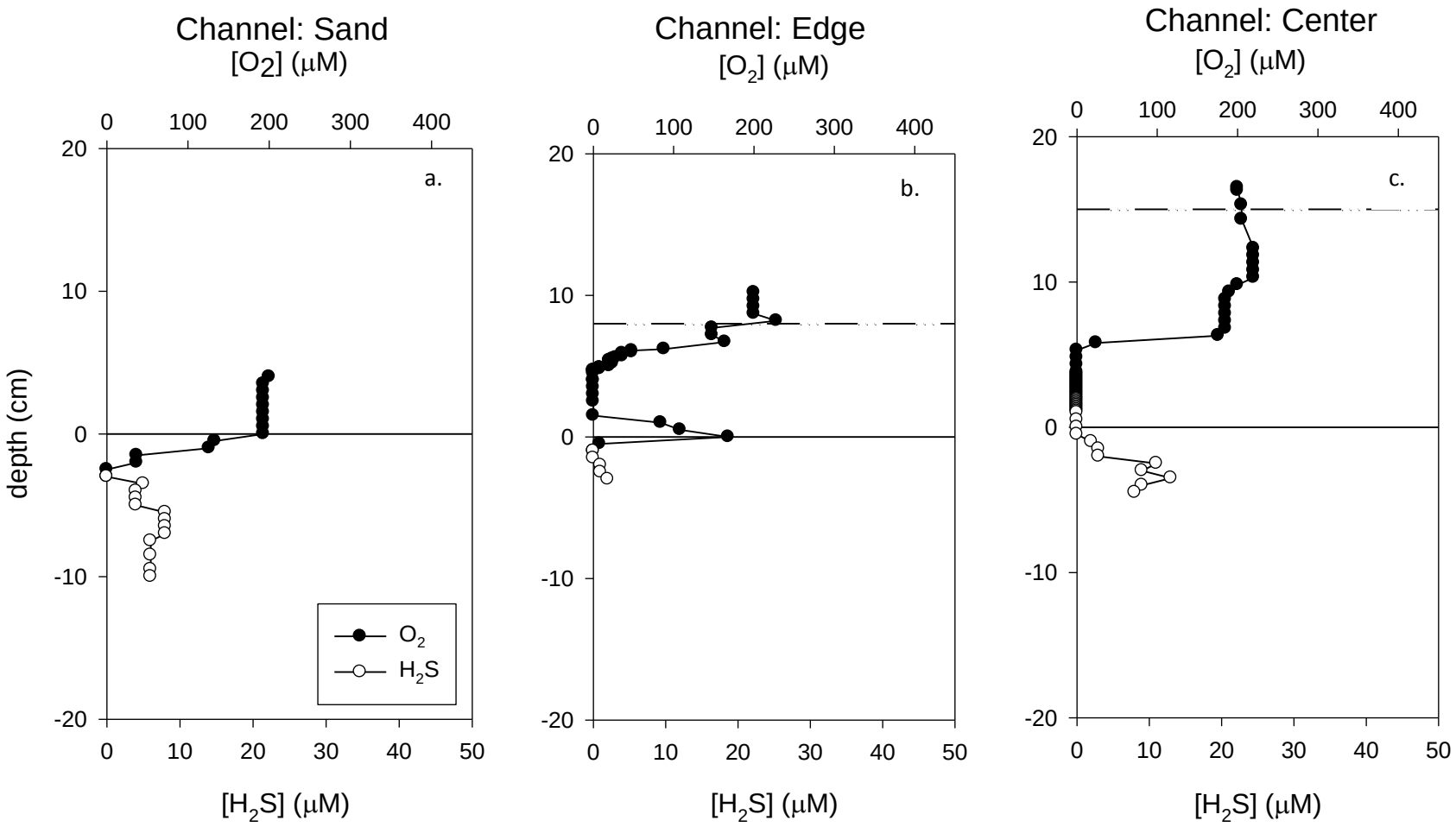

Figure 4.3: Oxygen and sulfide profiles for the three sites at the channel location. Depth is positive in the water column and negative below the sediment-water interface (SWI), with the SWI occurring at 0. Oxygen is displayed as filled in circles and sulfide as open circles. The location of the top of the *G. salicornia* mat is indicated by the dashed line.

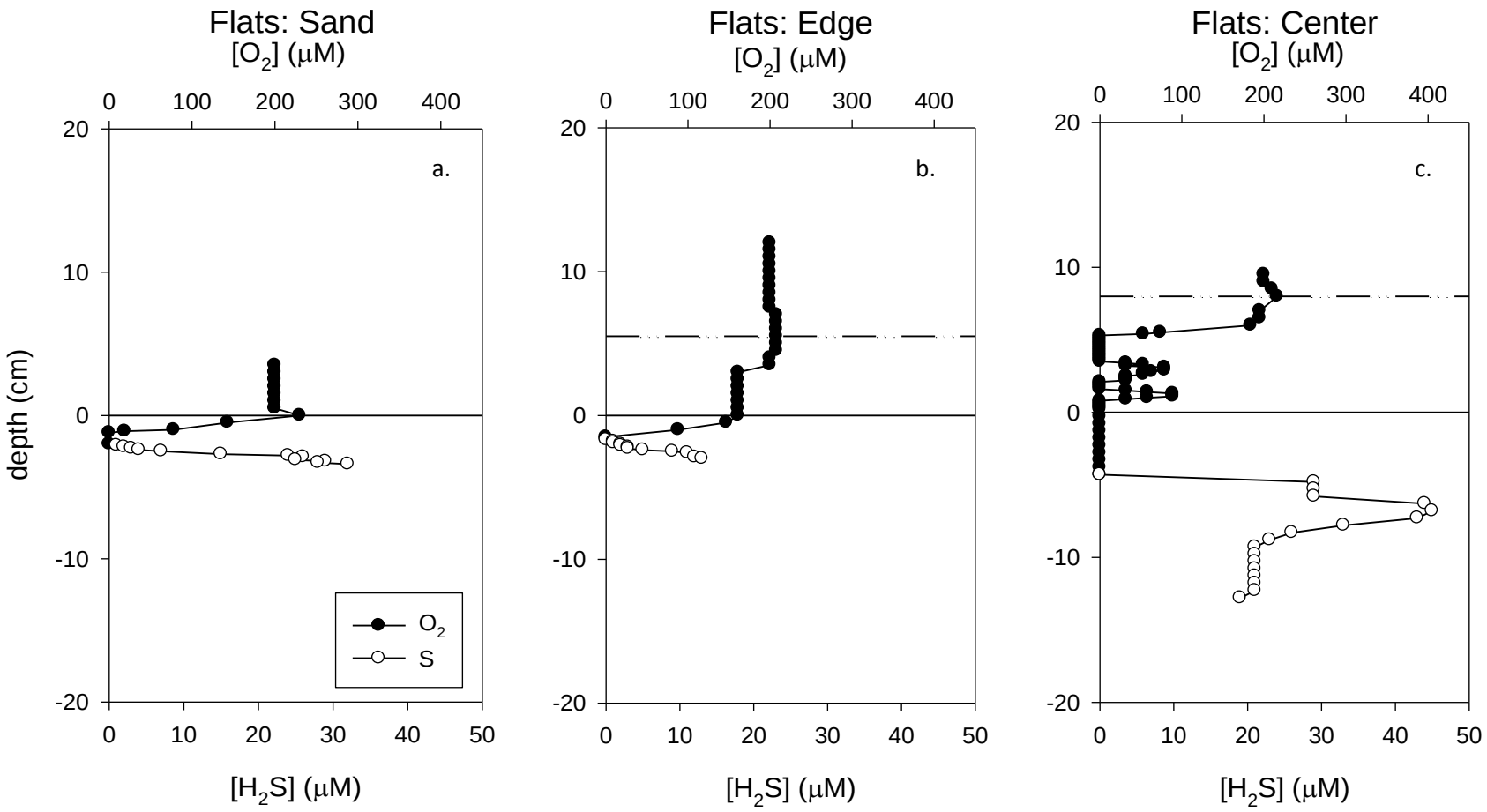

Figure 4.4: Oxygen and sulfide profiles for the three sites at the flats location. Depth is positive in the water column and negative below the sediment-water interface (SWI), with the SWI occurring at 0. Oxygen is displayed as filled in circles and sulfide as open circles. The location of the top of the *G. salicornia* mat is indicated by the dashed line.

Hydrodynamics

When comparing the lagoon, channel and sand flats locations, turbulent kinetic energy was highest at the sand flats location and lowest in the lagoon. Water flow was compared within each location, between the bare sand, edge and center of the mat, to examine differences in the hydrodynamics in areas with and without *G. salicornia*. For each of the three locations, the maximum water velocity at the bare sand site was higher than the maximum velocity at the adjacent sites with *G. salicornia*. Water velocities were slower within the *G. salicornia* mats when compared to velocities at similar heights in the adjacent bare sand sites (Figure 4.5). Between locations, the overall lowest site averaged TKE occurred in the lagoon and the highest in the flats. Additionally, for all locations TKE was higher in the water column above the mats than within the mats (Figure 4.6).

A positive relationship was observed between turbulent water velocity and the concentration of oxygen for profiles conducted in the center of the *G. salicornia* mats (Figure 4.7). Within the mat, the reduction in turbulent xRMS corresponded to a reduction in the concentration of oxygen at a similar depth. Additionally, the onset of suboxic conditions within the macroalgal mat occurred at approximately the same depth at which turbulent xRMS slowed, approaching 0.001 m/s. No relationship between the concentration of oxygen and turbulent xRMS was observed for sites within the center of the mat and did not occur for profiles conducted at the edge of the mat.

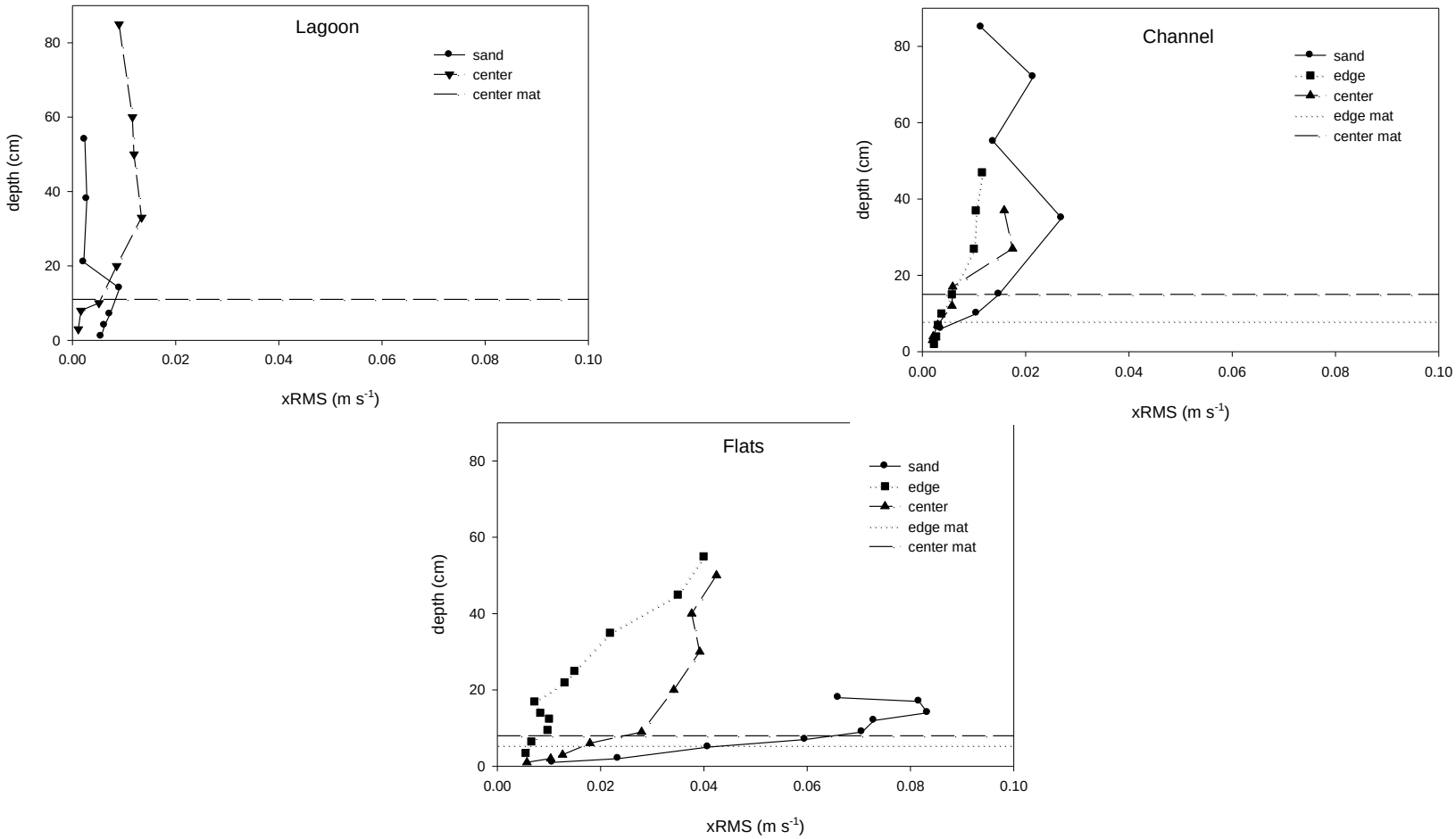

Figure 4.5: XRMS for each of the three locations: Lagoon, Channel, and Flats. Symbols represent different sites within each location: circle (bare sand), square (mat edge), and triangle (mat center). The dotted line is the height of the *G. salicornia* at the edge of the mat, and the dashed line is the height of the *G. salicornia* in the center of the mat.

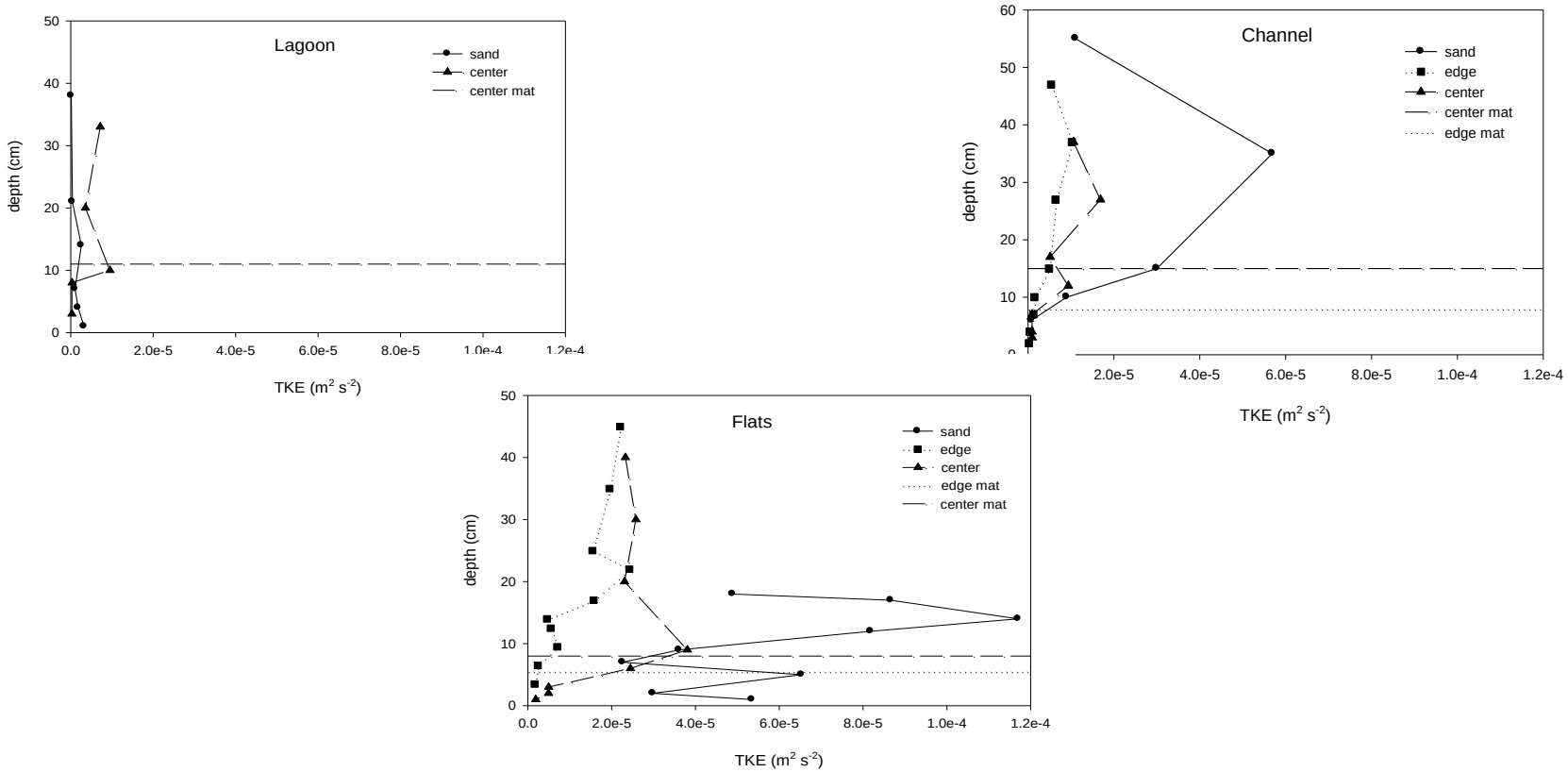

Figure 4.6: Turbulent kinetic energy for each of the three locations: Lagoon, Channel and Flats. Symbols represent different sites within each location: circle (bare sand), square (mat edge), and triangle (mat center). The dotted line is the height of the *G. salicornia* at the edge of the mat, and the dashed line is the height of the *G. salicornia* in the center of the mat

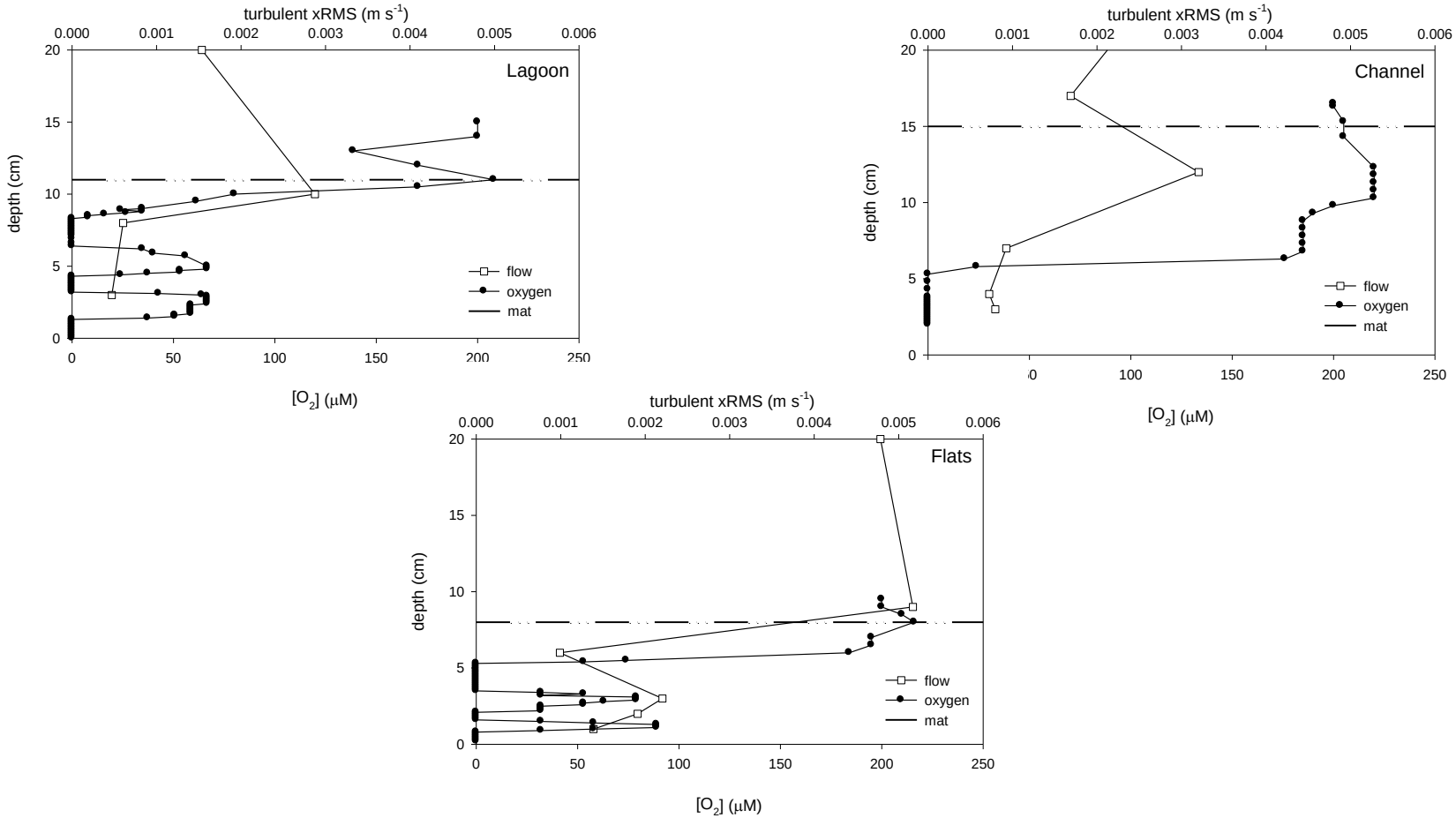

Figure 4.7: Water column profile taken at the center of the *G. salicornia* mats, where a depth of zero represents the SWI. Open squares represent turbulent xRMS, filled circles represent oxygen concentration, and the dashed line indicates the location of the top of the *G. salicornia* mat.

Discussion

The purpose of this study was to examine the interaction between water flow, TKE and water column chemistry in sandy regions with and without *G. salicornia*, to determine whether the invasive alga is altering local conditions. Based upon the changes in flow velocity and oxygen availability within the *Gracilaria salicornia* mats, we provide evidence that the macroalgae is an ecosystem engineer, capable of altering the physical and chemical properties of local systems.

Oxygen and Flow

Oxygen dropped to BDL (5 µM) in the water column during five of the six *G. salicornia* profiles, while oxygen was always present throughout the water column in sites without the macroalgae. The loss of oxygen in the water column can be caused by a number of factors, including: reduced macroalgal photosynthesis caused by self shading (D'Avanzo and Kremer 1994), and/or a decrease in water exchange between the mat and the surrounding area (Escartin and Aubrey 1995). If self shading were the only reason for a loss of oxygen within the mats, we would expect oxygen to decrease at approximately the same depth beneath the surface of the mat at each site, with slight variation due to heterogeneity in the density of the mat. For our profiles, the distance from the surface of the mat to where the oxygen concentration dropped to BDL ranged between 2 and 10 cm (Table 4.2). Therefore, self shading is probably not the dominant mechanism controlling oxygen depletion within the *G. salicornia* mats. This is consistent with the work of Beach et al. (1997) which found *G. salicornia* acclimates to lower light levels within the mat.

Numerous relationships between water flow and oxygen penetration depth were found within the *G. salicornia* mats. Flow velocity influenced the depth of oxygen penetration into the mats at all three locations: lagoon, channel and flats (Figure 4.5). In the lagoon location, flow was slowest, and oxygen dropped to BDL farthest above the SWI for both the edge and center sites (Table 4.2). The flats-edge site, which had the highest flow rate, had the deepest oxygen penetration depth, while the lagoon-edge site, which had the lowest flow rate, had the shallowest oxygen penetration depth. These results are similar to those observed in porous sediments, where higher flow velocities cause deeper water advection, increasing the concentration of oxygen and the oxygen penetration depth within sediments (Booij et al. 1991).

Oxygen persisted to greater depths within the macroalgal mats at the edge of the mat, relative to those in the center (Figures 4.2 – 4.4), indicating horizontal water movement also influences oxygen penetration depth within *G. salicornia* mats. Around the perimeter of submerged vegetation there is an edge-effect, where a rapid attenuation of flow velocity occurs inside the edge of a canopy, as has been shown in sea grass meadows by Peterson et al. (2004). The extent of this effect is likely dependent upon the density of the algal mat and water velocity, making a direct comparison between edge and center sites difficult. At the flats location, the velocity was higher above the mat at the center site than the edge site (Figure 4.4). We attribute this difference to the orientation of our site selection within the macroalgal mat with respect to wave driven flow. At the flats site, waves encountered the center location of the mat before the location selected to be the edge of the mat, which likely resulted in the dissipation of

wave energy before encountering the edge location (Hurd 2000 and sources there in). Wave dissipation as the cause for the differences between locations is further supported by the higher TKE in the surface of the mat at the center than the edge location. In the channel site, there was also a difference in TKE and water flow between the edge and center location (Figure 4.6). We suggest this may be due to acceleration over the top of the canopy and the resulting creation of eddies and flow instabilities (Hurd 2000). Additionally, it was necessary to cut a hole in the canopy to make ADV measurements, which introduces error to the measurement. Environmental variability makes it difficult to compare the hydrodynamic results between the center and edge locations in the canopy, however, when flow is compared at similar depths between the bare sand sites and those with the macroalgae, flow is slower within the macroalgal mats (Figure 4.5).

The lower concentration of oxygen observed within the *G. salicornia* mats at slower flow rates may signify a shift from advection to diffusion dominated transport within the mats, decreasing the speed at which oxygen is transported through the water column (Escartin and Aubrey 1995, Forster et al. 1996). Another possibility for the low oxygen concentrations within the mats is an increase in the size of the boundary layer around the algae. Solutes required for macroalgal growth, including nutrients, must pass through a boundary layer around the alga in order to be taken up. Increased flow velocities decrease the size of boundary layers around macroalgae, thus increasing the rate of solute uptake (Wheeler 1980). The rate of solute transport, and therefore the size of the boundary layer, in macroalgal canopies influences photosynthetic rate (Gonen et al. 1995). In addition to self shading, photosynthesis within the *G. salicornia* mat may be

decreased because of an increase in the size of the boundary layer created by reduced flow in the mat.

The channel-edge site had a unique oxygen profile (Figure 4.3b). At this site oxygen dropped to BDL in the mat and then returned to near fully saturated conditions at the SWI. We suspect the increase in oxygen at the SWI is due to either a gap between the algae and the sediment, or some other aspect of algal morphology at the base of the mat which allows more rapid water penetration into the lower portion of the mat, near the SWI, than into the middle of the mat. Previous work in algal mats attributed irregular oxygen profiles to heterogeneity in the structure of the algae (Corzo et al. 2009). Additionally, Nepf and Vivoni (2000) determined that is a maximum local water velocity at the SWI for submerged macroalgal mats. Unfortunately water flow data was not collected at a height of 1 cm above the SWI, where the local oxygen maximum occurred, which would have allowed us to determine to if an increase in flow at the SWI was the cause of the increased oxygen; however we suspect this is the case.

Turbulent kinetic energy at all sites was higher above the mats than within them. Similar results were found in a flume experiment using *Caulerpa* canopies (Hendriks et al. 2009) and in an *in situ* seagrass meadow (Gambi et al. 1990), where maximum TKE occurred above the mat and decreased inside of the mat due to the disruption of flow at the canopy-water interface. The reduction in TKE within the algal mats may further explain the existence of suboxic regions within the *G. salicornia* mats. Macroalgae excrete large quantities of dissolved organic matter (Khailov and Burlakova 1969), which

create regions of increased microbial activity (Alber and Valiela 1994, Smith et al. 2006). Under reduced turbulence, the rate at which chemical species, including oxygen and dissolved organic matter, are transported is decreased. Thus the macroalgal mats create an environment with reduced advection, decreasing the rate of water exchange, and increased microbial activity, increasing the rate of oxygen consumption. We conclude that the environment of slowed water exchange and increased microbial respiration creates suboxic regions in the water column within the *G. salicornia* mats.

The largest suboxic regions were observed in profiles through the center of the *G. salicornia* mats. For these sites, the concentration of oxygen in the water column followed a trend similar to the turbulent xRMS recorded in the mats (Figure 4.7). At depths with increased turbulent xRMS, oxygen concentrations were higher, providing further evidence that water motion within the macroalgal mats influences the concentration of oxygen. Another component to the turbulent xRMS-oxygen relationship occurred in the center of the mats, where the suboxic zone appeared as the turbulent xRMS approached 0.001 m/s (Figure 4.7). This relationship was especially apparent at the flats location, where two suboxic pockets were present, and the turbulent xRMS profile showed a decrease in water velocity near the depth of each of the suboxic regions. The relationship between turbulent xRMS and oxygen concentration, along with the appearance of a suboxic zone as turbulent xRMS diminishes, approaching 0.001 m/s, suggests that turbulent xRMS is an important factor in transporting oxygenated water to the center of the algal mats, and contributes to the dispersion of oxygen through the mat.

In summary, the relationship between flow rates and oxygen penetration depth provides evidence that water flow is an important component in determining the concentration of oxygen within *G. salicornia* mats. Reduced photosynthesis, combined with the decrease in water flow rates within macroalgal mats are responsible for the loss of oxygen within the water column. The existence of suboxic zones within *G. salicornia* mats creates microniches within the water column and may provide a competitive advantage for the invasive algae.

Microniches

Microniches have been observed in sediment burrows (Aller 1983), fecal pellets (Alldredge and Cohen 1987) and around high concentrations of OM in marine sediments (Jørgensen 1977a). Previous work with macroalgal canopies has identified the existence of low oxygen zones (Sundback et al. 1990) and anoxic water conditions beneath canopies (Krause-Jensen et al. 1999); however to our knowledge the existence of suboxic pockets, or microniches, within macroalgal structures has not been previously reported. Suboxic zones are important both biologically and chemically because of the ecological conditions they create and the nutrient transformations that take place within them. The suboxic layers within *G. salicornia* mats provide an environment in which microbial processes that otherwise would be confined to the sediment can occur, potentially increasing the local transport and uptake of nitrogen and phosphorus, as described below, and providing a competitive advantage to the invasive algae.

The existence of suboxic pockets within *G. salicornia* mats alters the location of redox reactions. Shoaling of the oxic-suboxic redox transition zone shifts the location of biotic and abiotic nutrient transformations from the sediment to the overlying water column. Solutes travel faster in water than in sediments, and therefore the shoaling of the oxic-suboxic boundary into the water column increases the transport rate of the products of redox reactions. The suboxic pockets within the *G. salicornia* mat also creates multiple oxic-suboxic boundaries, potentially increasing the rate of reactions taking place at the oxic-suboxic boundary due to the increased surface area over which these reactions can take place. As described below, suboxic microniches within *G. salicornia* create an environment conducive to increased nutrient transformations and nutrient transport.

Nitrogen is stable under numerous redox states, existing primarily as dinitrogen gas, ammonium, or nitrate, depending on local microbial transformations. Nitrification, the oxidation of ammonium to nitrate, is a strictly aerobic process (Henricksen and Kemp 1988). Denitrification, the reduction of nitrate to dinitrogen gas, is an anaerobic metabolism, typically occurring at or below the SWI in a thin layer beneath the oxic zone where nitrate is present (Christensen et al. 1989). Suboxic water column conditions cause denitrification to shoal from the sediments into the water column, a process that has been observed in the lower suboxic portion of *Chaetomorpha linum* at a similar rate to that found in adjacent sediments (Krause-Jensen et al. 1999).

The existence of multiple oxic and suboxic zones within the *G. salicornia* mat observed during our study creates an environment of double diffusion layers, suitable for

enhanced denitrification and nitrification. The rate of nitrification is influenced by oxygen and ammonium concentrations, while denitrification rates are dependent on suboxic conditions and the availability of nitrate (Rysgaard et al. 1994). Ammonium concentrations are usually higher under macroalgal mats due to the remineralization of organic matter (Sundback et al. 1990, Larned 1998). Unlike the *C. linum* mat in Krause-Jensen et al.'s (1999) study, the *G. salicornia* mats from our study had numerous (up to five) oxic-suboxic interfaces. The suboxic pockets within *G. salicornia* mats are likely regions of enhanced organic matter remineralization, creating ammonium that can be used for nitrification in the adjacent oxic regions. Suboxic pockets may be advantageous for the macroalgae because these low-oxygen regions provide a localized source of nitrate and ammonium for growth, and may decrease the release of nitrate and ammonium to the surrounding water column.

Redox chemistry influences phosphorus cycling indirectly, through the interaction of phosphate with iron. Oxic conditions favor the sorption of phosphate to iron oxyhydroxides, rendering the phosphate biologically unavailable, and reducing conditions promote the release of phosphate from iron oxyhydroxides to the surrounding water (Krom and Berner 1980). The release of phosphate from iron minerals typically takes place in the suboxic zone of sediments, and previous studies have observed phosphate in the lower portion of macroalgal mats due to the creation of reducing conditions at the SWI (Lavery and McComb 1991). Suboxic pockets within the *G. salicornia* mat create an environment favorable for the reduction of phosphate at more than one location within the algal mat. Reducing conditions within the *G. salicornia* mat,

in contrast to reductive solubilization of iron-bound phosphate in the sediment below, provide a pathway for phosphate release in close proximity to the algae. This is advantageous for the macroalgae, as phosphate would become available within the mat, rather than in the sediments, where the macroalgae would have to compete for phosphate with abiotic sorption processes and benthic photosynthesizers.

Conclusion

Gracilaria salicornia is an ecosystem engineer, physically and chemically altering the environment it invades. Within *G. salicornia* mats, we observed a decrease in TKE and flow rates compared to adjacent regions without the macroalgae. The invasive mats create suboxic regions within the water column, and in a few locations oxic pockets were found interspersed in suboxic regions of the mat. Decreased TKE in the macroalgal mats corresponded to a decrease in the concentration of oxygen, and as turbulent xRMS approached 0.001 m/s the concentration of oxygen in mats fell to below the detection limit. *Gracilaria salicornia* mats also create suboxic microniches, which may be advantageous to the macroalgae by altering the location of nutrient transformations, including ammonification and reductive solubilization of iron-bound phosphate, from the sediment to the water column within the mat. The closer proximity to nutrient release provides a competitive advantage to *G. salicornia*, and future research

should examine this as a possible mechanism contributing to the success of this invasive species.

Chapter 5

Ocean Acidification: The role of CO_2

By: Jennifer Murphy and Chris Measures

Purpose of Activity

- Understand how water absorbs gases
- Understand why increasing the amount of carbon dioxide in the atmosphere is decreasing the pH of the oceans.
- Understand what pH measures.
- Learn why pH is important for corals, and other organisms that build their skeletons using calcium carbonate.

Audience

The laboratory activity was designed to be used with college freshmen and sophomores, mostly non-science majors. Depending upon the number of calculations included in the laboratory exercise, the activity could be adapted for high school students or more advanced undergraduates or graduate students.

Background

For the past 250 years humans have been increasing the amount of carbon dioxide (CO_2) in the atmosphere through the combustion of fossil fuels and changing land-use activities. At the beginning of the industrial revolution, atmospheric CO_2 were in the range of 270-280 ppmv (Wigley 1983). Over the past 50 years, weekly measurements at Mauna Loa have revealed an increase in atmospheric CO_2 from 317 ppm in 1960 to 390 ppm in 2011 (Tans and Keeling) (Figure 5.1).

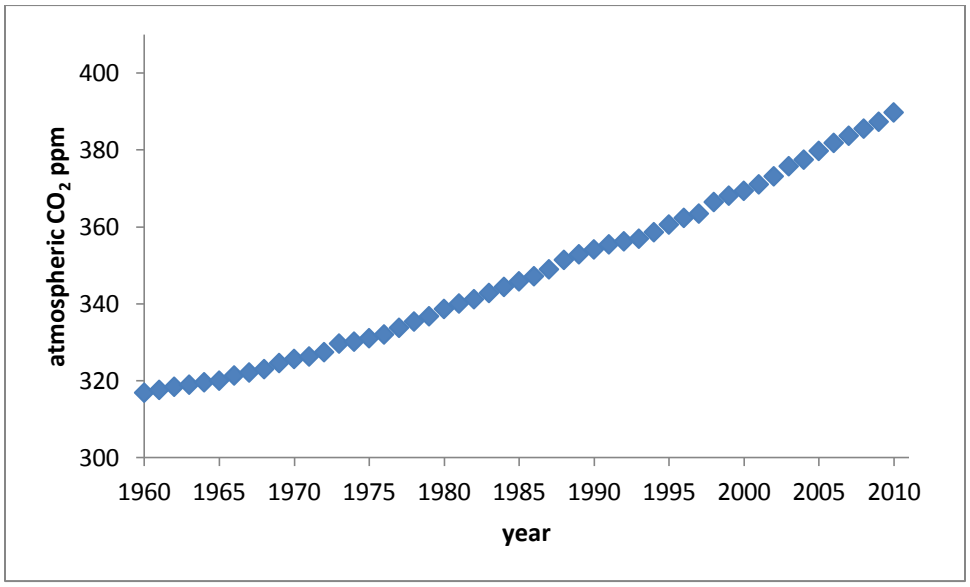

Figure 5.1: Atmospheric CO_2 record from Mauna Loa, Hawai‘i.

Carbon reservoirs

The carbon on the planet is stored in different forms and places, and these are called reservoirs (Table 5.1). It is important to note that the amount of total carbon on the planet is not changing; it is merely being moved between these different reservoirs. From Table 5.1 it is clear that the majority of the carbon on Earth is stored in the carbonate sediments reservoir. Carbonate sediments are composed of the discarded shells and skeletons of plants and animals that lived in the ocean, and inorganic carbon precipitated from seawater. The former process is the most important in the modern oceans. While alive, these organisms take up carbon and calcium from the water and by combining them

build structures of the compound calcium carbonate ($CaCO_3$); this process is called calcification. When these organisms die, their $CaCO_3$ shells and skeletons slowly sink to the bottom of the ocean. In transit, much of the $CaCO_3$ is dissolved in the water column, but about 35% of it is buried in sediments. The burial of $CaCO_3$ is an example of a CO_2 sink, because carbon is being removed from the ocean and atmosphere reservoirs and is being added to the carbonate sediment reservoir. This reservoir, and most of the others, change on very long time-scales (e.g. thousands to millions of years) and are not playing a role in the recent changes in atmospheric CO_2 concentrations. (It is important to note that each time an organism produces 1 mole of $CaCO_3$ in the ocean, 1 mole of CO_2 is also produced- exactly how much of that CO_2 remains dissolved in the ocean and how much is released into the atmosphere is a function of the temperature of the ocean and the partial pressure of CO_2 in the overlying atmosphere.) All evidence to date indicates that as CO_2 concentrations in the atmosphere rise and the oceans become more acidic, calcification rates will slow and the strength of this positive feedback to rising atmospheric CO_2 will weaken. Also, changes in this biological pump may occur on time scales of human generations.

Table 5.1: Amount of carbon in different reservoirs on Earth (Open University Team). Units are in 10^{12} tonnes of CO_2 equivalent- although most Earth Scientists use units of C, we use CO_2 to facilitate comparison with the lab exercise.

Reservoir	**Quantity**
carbonate sediments	150000
organic carbon in soils	25000
dissolved in oceans/freshwater	140
living biological material	30
fossil fuels	27
atmosphere	2

The observed increase in atmospheric CO_2 concentration (Figure 5.1) is due to the movement, by humans, of carbon between two of the smaller reservoirs, from the fossil fuels reservoir to the atmospheric one. Looking at the Table 5.1, notice that burning all of the fossil fuels, and therefore releasing that CO_2 into the atmosphere, could potentially increase the amount of CO_2 in the atmosphere more than ten times! As humans continue to burn fossil fuels, and move carbon between these different reservoirs, we need to understand how the climate and geochemical cycles of the planet are going to be affected.

An increase in the concentration of atmospheric CO_2 has an influence on both global temperatures and the chemistry of the ocean. It is well established that CO_2 is a greenhouse gas that traps some of the infrared radiation leaving the surface of the planet

to space, and thereby resulting in increased heating of the Earth. While comprising only 0.04% of the atmosphere, CO_2 is very important in regulating surface temperatures. However, a large part of the CO_2 that goes into the atmosphere will dissolve in the surface ocean as a result of Henry's Law (see later), resulting in another set of problems (see below).

Chemistry

When CO_2 dissolves in the ocean it partitions into several different forms, some of which alter pH. The vast majority (400:1) of the CO_2 forms CO_{2aq} which has no effect on pH, but the rest reacts with the water to form the diprotic acid H_2CO_3, which then partitions into the various species shown in Equations 5.1-5.4. Exactly which of the various species shown in these equations is dominant depends upon the pH of the solution. The pH of a solution is a measure of the number of free hydrogen atoms (H^+) available: the more H^+, the more acidic is a solution. Solutions are classified as acidic (pH < 7), neutral (pH = 7) or basic (pH > 7) based on the number of free H^+ ions present.

$$CO_{2\,(g)} \leftrightarrow CO_{2\,(aq)} + H_2O \leftrightarrow H_2CO_3 \qquad (5.1)$$

$$H_2CO_3 \leftrightarrow HCO_3^- + H^+ \qquad (5.2)$$

$$HCO_3^- + H^+ \leftrightarrow CO_3^{2-} + 2H^+ \qquad (5.3)$$

The net overall reaction in seawater is:

$$CO_{2\,(g)} + CO_3^{2-} + H_2O = 2HCO_3^- \qquad (5.4)$$

The average pH of surface seawater, is 8.1, slightly alkaline. At pH 8.1, the presence of HCO_3^- is favored over the other two chemical species (H_2CO_3 and CO_3^{2-}), and therefore every time one of the molecules of H_2CO_3 from the dissolved CO_2 turns into HCO_3^-, one H^+ molecule is released. Thus the dissolution of CO_2 in water causes a decrease in pH as the number of H^+ in solution is increased.

The pH of a solution not only influences the direction and equilibrium point of chemical reactions, but also the saturation state of seawater with respect to $CaCO_3$. Decreasing the pH of the ocean decreases the $CaCO_3$ saturation state within seawater making it harder for organisms such as corals to form their $CaCO_3$ shells.

As CO_2 is being added to the atmosphere through the combustion of fossil fuels and land use activities, that CO_2 then moves from the atmosphere to the oceans by diffusion and turbulent mixing (waves), in an attempt to reach an equilibrium dictated by Henry's Law (see below). Chemically, the ocean is a complex system being controlled by physical, biological and chemical processes. Biological respiration decreases pH, physical mixing provides ocean-atmospheric gas exchange, and chemical buffering reactions provide some stability in the environment. The buffering capacity of the ocean is in part due to the ability of the salts dissolved in seawater to take up and release excess protons. Without this buffering, the pH of the ocean would change even more rapidly.

Questions

Why does the increase in atmospheric CO_2 change the pH of the ocean?

Does temperature influence the amount of CO_2 water is able to take up?

Materials

10 Tire valve stems- screw together type with gaskets (not the snap in type)

10 plastic 1 L soda bottles with plastic caps

500 mL graduated cylinders

small CO_2 cylinder with pressure regulator, hose and tire chuck (the tire chuck can be bought at most hardware stores)

Hot water container

Cold water container

Methyl Red pH indicator dye ($C_{15}H_{15}N_3O_2$ in 0.1% ethanol, VWR catalog number AA38698-AE CAS # 493-52-7)

pH paper strips

Tire pressure gauge

1000 mL seawater at room temperature (or baking soda dissolved in tap water as a buffering agent)

Drill press (to make holes in the soda caps)

Activity

Before the laboratory, build the bottle cap assembly (Figure 5.2). Drill out the plastic bottle caps and insert the tire valves so that there is a rubber gasket on the top and

bottom of the cap. The drill bit should be slightly larger than the valve stem to ensure easy assembly. Use a wrench to tighten the tire valves on the caps to prevent leaking during the activity.

Figure 5.2: Pieces required for the bottle caps. The clamp-in tire valves can be purchased at an auto-parts store.

Demonstration

Methyl red is a pH indicator that is yellow under neutral or basic conditions and red under acidic conditions. Place approximately 1 mL of indicator dye into each 1 L bottle, one containing approximately 1000 mL of freshwater and the other approximately 1000 mL of sea water (actual volumes vary slightly by bottle type). Due to variations in

the volume of the bottle used, as well as pH and buffering capacity of the local water source, the required headspace volume required for this demonstration will vary. We suggest experimenting with your water supply to determine the actual volume of headspace you will require. (For a simple way to demonstrate buffering capacity, or ensure your demonstration is successful, dissolve sodium bicarbonate (baking soda) into the water in the ocean bottle.) Secure the caps (hand tight), and add approximately 30 pounds per square inch (psi) of CO_2 to the headspace of each bottle. If the freshwater bottle is not shaken as the CO_2 is added, it is possible to observe the diffusion of CO_2 from the headspace into the bottle by the formation of tiny red eddies in the surface layer of the freshwater. After observing the diffusion, vigorously shake the bottles to demonstrate turbulent mixing. Depending on the teaching level, ask what processes are controlling the movement of CO_2 from the headspace to the water at each step. After shaking, the freshwater bottle will turn red, while the seawater bottle remains yellow (Figure 5.3).

Figure 5.3: Demonstration of buffering using methyl red indicator dye. The bottle on the left contains saltwater and the one on the right contains freshwater.

Hands-on Activity

How does the temperature of water influence the amount of CO_2 able to dissolve into it? For this activity, students use 1 L soda bottles with modified caps to observe the ability of water to take up CO_2 at different temperatures. Add 0.8 L of warm water (approximately 50°C) to one bottle and 0.8 L of cold water (approximately 10°C) to another bottle. If using pH paper, have the students take a pH reading before the CO_2 addition. Loosely screw on the caps and squeeze the bottles to remove all air from the

headspace. Then tightly screw on the caps. Depending on the audience, now is a great time to make a few assumptions and ask students questions. For example, we assume only water is in the bottle (i.e. no CO_2 has dissolved into the water) and ask students to calculate the pH (7.0) and number of moles of CO_2 in the bottle (0 moles). Finally, the bottles are brought to the instructor to be filled with 30 psi of CO_2 from the gas tank.

After filling, students should touch the bottles, and notice their firmness. Students can then take the initial pressure of the bottles using a hand held tire pressure gauge. Be aware that a good seal with the tire pressure gauge is necessary to avoid excessive loss of gas from the bottle, and the pressure should only be measured once, as this process will cause some loss of gas from the bottle. At this point, it is possible to calculate the number of moles of CO_2 in the bottles using the ideal gas law (see later for a detailed description).

To observe the effect of water temperature on CO_2 uptake, shake the bottles vigorously. A large pressure drop can be observed in both bottles. The cold bottle actually collapses as the CO_2 dissolves into the water, while the warm one becomes noticeably less pressurized (Figure 5.4). The amount of CO_2 taken up by each liquid, and therefore the number of moles of H^+ released into each bottle and subsequent pH can then be calculated. If using the pH strips, students can take the post CO_2 addition reading and reflect on why the calculated and actual pH vary (Table 5.2). (The actual change in pH will depend on the temperature and water used.)

Figure 5.4: The bottle on the left contains warm water and the one on the right contains cold water. After removing all air from the headspace, the two bottles were filled with CO_2 and then shaken. Notice the difference in pressure between the two bottles.

Table 5.2: Measured pH before and after CO_2 addition.

	pH pre-CO_2 addition	**pH post-CO_2 addition**
sea water	8.0	5.6
freshwater	8.1	5.5
hot water (50 °C)	8.1	5.2
cold water (12 °C)	8.1	5.0

We provide our students with a percent uptake for each bottle, but more advanced students could also measure the change in bottle volume to approximate the quantity of CO_2 dissolved into the water (Table 5.3). Unfortunately it is not possible to measure the pressure inside the bottles after shaking with the tire pressure gauges to obtain a more exact volume.

Table 5.3: Change in bottle volume with the hot and cold water additions.

	Change in volume	**Percent change**
10 °C	100 cm^3	50 %
60 °C	20 cm^3	10 %

Humans and CO_2

In addition to understanding the effects of CO_2 on ocean pH, this lab provides an opportunity for students to consider how human activities are contributing to atmospheric CO_2 concentrations. To begin, we ask students to list different ways they create CO_2. Answers vary from using cars and electricity to breathing. The students are then led through a series of exercises to put into perspective how much CO_2 different processes release. For example, a human respires approximately 1 kg of CO_2 each day, which is equivalent to 22.7 moles of CO_2 per day. Students can also examine the influence of fossil fuels on atmospheric CO_2. If we assume the combustion of one gallon of gasoline releases 8.8 kg of CO_2 (EPA Emission Facts), students can evaluate the amount of CO_2

released by cars with different fuel efficiencies. We compare three types of cars, and calculate how much CO_2 each car releases if it is driven 10 miles a day over the course of a year. Depending on the age of students, it may be more beneficial for students to calculate how much CO_2 their car generates driving to and from school. To examine this problem at a larger scale, knowing the United States consumes 18,810,000 barrels of oil each day, students calculate how many moles of CO_2 are released into the atmosphere in one day and in one year.

Another activity involves determining the significance of electricity consumption on CO_2 emissions. Using EPA data on electricity generation and power sources, it is possible to calculate the amount of CO_2 released to the atmosphere using light bulbs and electric appliances. For example, in Hawai‘i, oil is the major source of electricity, and CO_2 is produced at a rate of 0.609 kg CO_2/kWh (EPA eGRID). By knowing the number and wattage of light bulbs in the classroom, students are asked to calculate how much CO_2 is released to power the lights for the length of our class. This could also be extrapolated to calculate the amount of CO_2 released for numerous electronic devices.

Calculating the actual change in ocean pH due to increased atmospheric CO_2 concentrations is beyond the scope of this laboratory exercise. In order to easily quantify the process, there are numerous simplifying assumptions required: the ocean is uniformly mixed, there is no CO_2 uptake by biological organisms, and the ocean lacks any buffering capacity. Rather than make these simplistic assumptions, we suggest

challenging students to discuss whether or not the bottle exercise provides a good model of oceanic CO_2 uptake and pH change.

Theory

Henry's Law states that at constant temperature the amount of gas in solution is proportional to the partial pressure of the gas in equilibrium with the liquid (i.e. in the headspace above it). Increasing the headspace pressure of a gas increases its solubility, while increasing the temperature of the solution decreases the solubility of the gas. This lab demonstrates the temperature aspect of Henry's Law, a decrease in the water temperature increases the solubility of the CO_2 in solution. It would also be possible to demonstrate the pressure aspect, by using the same temperature water and altering the pressure of the gas injected into the headspace.

The ideal gas law can be used to calculate the number of moles of CO_2 in the headspace.

$$P \times V = n \times R \times T \qquad (5.5)$$

In Equation 5.5: P= pressure (kPa), V = volume (L), n = moles, R = the gas constant, 8.431 (J moles^{-1} K^{-1}), and T = temperature (K). Knowing the volume of the headspace in the 1 L bottle, the room temperature and the atmospheric pressure the moles of gas in the headspace of the bottle can be calculated. At 1 atmosphere (101.3 kPa or 14.7 psi) and 25°C, 1 mole of gas has a volume of 23.9 L. It is important to note that the volume of an

ideal gas is 22.4 L at STP (0°C). Equation 5.6 shows how to calculate the moles of gas in the headspace of the 1 L bottle after 0.8 L of water has been added.

$$\frac{0.2\ L\ in\ headspace \times 1\ mole\ gas}{23.9\ L} = 0.008\ moles\ gas\ in\ headspace\ of\ 0.2\ L \quad (5.6)$$

After the addition of CO_2 to the headspace by the gas cylinder, the pressure in the bottle is approximately doubled (room pressure is 14.7 psi, and we increase it to approximately 30 psi). Therefore the number of moles of gas in the headspace is also doubled.

The pH of a solution is the number of protons (H^+) available, and the more H^+ the lower the pH of the solution. Mathematically, pH is calculated in Equation 5.7.

$$pH = - \log [H^+] \quad (5.7)$$

Therefore, in pure water at 25°C, where $[H^+] = 1.0 \times 10^{-7}$ M, the pH of the solution is 7.0.

For the lab activity, after calculating the moles of CO_2 in the headspace of each bottle, we first assume all of the CO_2 dissolves from the headspace into the water and calculate what the pH of the water in the bottle would be (Equation 5.8).

0.008 moles of gas in headspace at atmospheric pressure x 2 (we doubled the pressure with pure CO_2 from the tank) = 0.016 moles of CO_2 in the headspace of the bottle. (5.8)

If we assume all of the gas dissolved into the water then 0.02 moles per liter H^+ was released into the water (Equation 5.9).

$$0.016 \text{ moles } H^+ / 0.8 \text{ L} = 0.02 \text{ M } H^+ \quad (5.9)$$

Add this to the concentration of H^+ present, $[H^+] = 1.0 \times 10^{-7} + 0.02 = 0.02$, and the pH of the water would be 1.7. (Note the addition of the $[H^+]$ from the water does not change the pH of the water in this example due to the large $[H^+]$ from the dissociation of H_2CO_3.) This is only true if all of the dissolved CO_2 becomes HCO_3^-. As mentioned previously, the majority of CO_2 gas dissolving in water becomes $CO_{2\,(aq)}$, with only 1 in 400 actually becoming HCO_3^- and releasing a proton. Therefore, to accurately calculate the pH in our exercise, it is necessary to divide our calculated $[H^+]$ by 400.

If all the CO_2 from the headspace dissolved into the water, pH is calculated using Equations 5.10 through 5.12.

$$0.016 \text{ moles } CO_{2\,(g)} \text{ in headspace} \rightarrow 0.016 \text{ moles } CO_{2\,(aq)} \quad (5.10)$$

$$\frac{0.16\ moles\ CO_{2\,(aq)}}{} \times \frac{1\ mole\ H_2CO_3}{400\ moles\ CO_{2\,(aq)}} \times \frac{1\ mole\ HCO_3}{1\ mole\ H_2CO_3} \times \frac{1\ mole\ H^+}{1\ mole\ HCO_3} = 4 \times 10^{-5} \text{ moles } H^+ \quad (5.11)$$

$$pH = -\log (4 \times 10^{-5} \text{ moles } H^+ / 0.8 \text{ L}) = 4.3 \quad (5.12)$$

The change in pH for the different water temperatures can be calculated using the percent change given in Table 5.3 (Equations 5.12 and 5.14).

$$4 \times 10^{-5} \text{ moles } H^+ \times 10\% \text{ (at 50 °C)} = 4 \times 10^{-6} \text{ moles } H^+, \text{ pH} = 5.3 \quad (5.13)$$

$$4 \times 10^{-5} \text{ moles } H^+ \times 50\% \text{ (at 10 °C)} = 2 \times 10^{-5} \text{ moles } H^+, \text{ pH} = 4.6 \quad (5.14)$$

Useful web resources

http://www.epa.gov/climatechange/fq/emissions.html

http://cdiac.ornl.gov/pns/faq.html

Chapter 6

Conclusion

Gracilaria salicornia and *Acanthophora spicifera* are two common and successful invasive species in Hawai‘i (Smith et al. 2002). The goal of this dissertation was to evaluate the effect of invasive algae on water flow, diel redox cycling and nutrient availability. After completing the work for this dissertation, we propose that the success of these invasive algae is due, in part, to the ability of the algae to alter local redox conditions, creating an environment that enhances algal growth.

Invasive macroalgae are a major component of non-indigenous marine species (Schaffelke et al. 2006). Whether native or invasive, benthic macroalgae biologically, physically, and chemically alter local ecosystems. Biologically, macroalgae negatively impact other benthic organisms, including coral (Lapointe 1997, Smith et al. 2005, Hauri et al. 2010), seagrass (McGlathery 2001, Holmer et al. 2009) and benthic infauna (McKinnon et al. 2009). Macroalgae increase the availability of organic matter (Khailov and Burlakova 1969), which increases rates of microbial respiration (Alber and Valiela 1994, Smith et al. 2006), and reduces the concentration of oxygen in the water column. Physically, macroalgal canopies and mats reduce local flow conditions (Escartin and Aubrey 1995, Forster et al. 1996, Nepf 2012) and decrease the amount of light that penetrates to the sediment water interface (SWI) (Sundback et al. 1990, Corzo et al. 2009). Chemically, a reduction in the concentration of oxygen at the SWI increases the availability of phosphate, due to desorption from iron oxyhydroxides (Krom and Berner 1980, Sundby et al. 1986, Slomp et al. 1996a and b, Jensen et al. 1995, Blomqvist and

Elmgren 2004), and increases ammonium concentrations, because nitrification can no longer occur.

In He‘eia Fishpond, *A. spicifera* canopies decrease the concentration of oxygen at the SWI and compared to non-colonized regions in the pond, the invasive algae extend the length of time oxygen is absent at the SWI (Chapters 2 and 3). Enhanced diel cycling was observed at the SWI beneath the *A. spicifera* canopies, where oxygen concentrations were higher during the day and lower at night than in adjacent non-colonized regions (Chapter 2). Areas with the invasive algae also had higher ammonium concentrations (Chapters 2 and 3) and higher rates of ammonium flux from the sediment into the overlying water column (Chapters 2) than sediments without the macroalgae (Chapters 2 and 3). Water column nitrate was below the detection limit (BDL) in sites with and without the macroalgae, suggesting that denitrification rates are similar between colonized and non-colonized regions (Krause-Jensen et al. 1999) or nitrate was being rapidly taken up. *Acanthophora spicifera* created reducing conditions at the SWI, as shown by the presence of Mn^{2+} (Chapters 2 and 3), dissolved iron (Chapters 2 and 3) and sulfide (Chapter 3) in the lower few centimeters of the algal canopy and at the SWI. Despite the reducing conditions observed in the algal canopy and in sediments, dissolved inorganic phosphate was below the detection limit (0.5 µM) during the majority of samplings events, as previously reported for fishpond sediments (Briggs 2011).

Phosphate is particle-reactive, capable of sorbing to iron oxides, and the reductive dissolution of iron oxides releases phosphate to the surrounding water. The Fe:P ratio

was calculated at sediment depths when the maximum concentrations of iron and phosphate coincided (Chapter 2). We found the Fe:P ratio to be in the range for freshwater, not marine, systems, indicating less sulfide was available in the sediments than required for FeS formation (Gunnars and Blomqvist 1997).

Reduced forms of manganese and iron were observed in the surface sediments of the fishpond. Manganese oxides are abiotically reduced by sulfide and ferrous iron (Burdige and Nealson 1986, Thamdrup et al. 1994), and sulfide is the primary abiotic reducer for iron oxides (Nealson and Saffarini 1994, Thamdrup et al. 1994). These reduction reactions are fast, occurring on the order of minutes to hours, depending upon the types of minerals available (Cline and Richards 1969, Davison and Seed 1983, Kirby et al. 1999). Previous work has demonstrated that the rapid iron-sulfide interaction causes sulfide to be absent from sediment pore waters when iron oxides are abundant (Canfield 1989). Sulfide was present in pore waters both in He‘eia Fishpond (Chapter 3) and around Coconut Island (Chapter 4). Within He‘eia Fishpond, the detection of sulfide at the SWI in the pore waters within fine grained, terrigenous facies, is surprising given the high iron content in Hawaiian soils. The occurrence of sulfide in the presence of iron oxides suggests sulfate reduction is occurring so rapidly that sulfide accumulates in the pore water even in the presence of iron oxides. Alternatively, the type of iron oxide present may be such that the sulfide-iron oxide reaction is occurring at a slower rate than sulfide production.

Our work in He‘eia Fishpond found that unlike idealized pore water profiles, dissolved iron, dissolved manganese and sulfide overlap in sediment pore waters. The co-occurrence of dissolved manganese and sulfide provides evidence that in addition to reducing iron oxides, sulfide is likely reducing manganese oxides in these sediments (Chapter 3). There are two potential reasons sulfide was detected in the water column of the fishpond. One, the rate of sulfate reduction in the sediment beneath *A. spicifera* canopies is so high that excess sulfide diffuses into the water column before it can react with available oxidants in the sediment. Two, the mineralogy of the sediments is such that iron-sulfide reactions cannot occur fast enough for all of the sulfide to be oxidized, and therefore other oxidants, including manganese oxides are being reduced. Regardless of the mechanism, the presence of both manganese and iron in the sediments and water column of the pond provides a scavenging mechanism for phosphate, likely causing the low phosphate concentrations found in the pore water and contributing to the low levels of phosphate in the water column in He‘eia Fishpond. Additionally, the higher concentration of sulfide in areas dominated by the macroalgae provides evidence of environmental alteration by the invasive algae.

The relationship between redox chemistry and water flow was examined within and around *G. salicornia* mats (Chapter 4). As previously reported for porous sediments (Booij et al. 1991), we found that higher flow rates corresponded to deeper oxygen penetration depths in the macroalgal mats (Figure 4.5). A comparison between turbulent kinetic energy and oxygen availability revealed that when TKE is below 0.001 m/s suboxic pockets appear in the center of mats (Figure 4.7), suggesting that an increase in

the size of diffusive boundary layers influences the production and concentration of oxygen in the mats. Compared to non-colonized regions, the *G. salicornia* created reducing conditions at the SWI, as observed through the decreased concentration of oxygen at the SWI.

The work completed for this dissertation has shown that the invasive macroalgae *A. spicifera* and *G. salicornia* create regions of low oxygen in the water column and cause reducing environments at the SWI (Chapters 2, 3 and 4). We expected reducing conditions at the SWI beneath the macroalgae to increase the concentrations of ammonium and dissolved inorganic phosphate, however only ammonium concentrations were found to be higher beneath the macroalgae (Chapters 2 and 3). We propose the existence of reducing conditions in close proximity to the macroalgae create microniches, within which processes such as reductive dissolution of iron-oxides and subsequent phosphate release are occurring, and that these conditions provide an ecological advantage for the invasive macroalgae.

References

Alber, M. and I. Valiela. 1994. Production of microbial organic aggregates from macrophyte-derived dissolved organic material. *Limnology and Oceanography*. 39: 37-50.

Alldredge, A. and Y. Cohen. 1987. Can microscale chemical patches persist in the sea? Microelectrode study of marine snow, fecal pellets. *Science*. 235: 689-691.

Aller, R. 1983. The importance of the diffusive permeability of animal burrow linings in determining marine sediment chemistry. *Journal of Marine Research*. 41: 299-322.

Aller, R. 1994. Bioturbation and remineralization of sedimentary organic matter: effects of redox oscillation. *Chemical Geology*. 114: 331-345.

An, S., and S. B. Joye. 2001. Enhancement of coupled nitrification-denitrification by benthic photosynthesis. *Limnology and Oceanography*. 46:62-74.

Anschutz, P., S. Zhong, and B. Sundby. 1998. Burial efficiency of phosphorus and the geochemistry of iron in continental margin sediments. *Limnology and Oceanography*. 43: 53-64.

Bagarinao, T. 1992. Sulfide as an environmental factor and toxicant: tolerance and adaptations in aquatic organisms. *Aquatic Toxicology*. 24: 21-62.

Beach, K., H. Borgeas, N. Nishimura and C. Smith. 1997. In vivo absorbance spectra and the ecophysiology of reef macroalgae. *Coral Reefs*. 16: 21-28.

Berner, R. A. 1980. Early diagenesis: A theoretical approach. Princeton University Press.

Blomqvist, S., and R. Elmgren. 2004. Why the limiting nutrient differs between temperate coastal seas and freshwater lakes: A matter of salt. *Limnology and Oceanography*. 49: 2236-2241.

Booij, K., W. Helder, and B. Sundby. 1991. Rapid redistribution of oxygen in a sandy sediment induced by changes in the flow velocity of the overlying water. *Netherlands Journal of Sea Research*. 28: 149-165.

Boudreau, B.P. 1997. Diagenic models and their implications. 1 ed. Springer.

Boyle, K. A., K. Kamer, and P. Fong. 2004. Spatial and temporal patterns in sediment

and water column nutrients in a eutrophic Southern California estuary. *Estuaries*. 27: 378-388.

Brendel, P. J. and G. W. Luther. 1995. Development of a gold amalgam voltammetric microelectrode for the determination of dissolved Fe, Mn, O_2, and S(-II) in porewaters of marine and freshwater sediments. *Environmental Science & Technology*. 29: 751-761.

Briggs, R.A. 2011. Evaluating the influence of organic matter (OM) source, lability and episodic variations in OM abundance and sediment redox conditions on remineralization efficiency and nutrient regeneration in nearshore sediments. Ph D Dissertation. University of Hawai‘i at Manoa.

Burdige, D.J. and K.H. Nealson. 1986. Chemical and microbial studies of sulfate-mediated manganese reduction. *Geomicrobiology Journal*. 4: 361-387.

Burkepile, D. and M. Hay. 2006. Herbivore vs. nutrient control of marine primary producers: context-dependent effects. *Ecology*. 87: 3128-3139.

Campbell, W.H., P. Song, and G.G. Barbier. 2006. Nitrate reductase for nitrate analysis in water. *Environmental Chemistry Letters*. 4: 69-73.

Canfield, D. 1989. Reactive iron in marine sediments. *Geochimica et Cosmochia Acta*. 53: 619-623.

Canfield, D., R. Raiswell and S. Bottrell. 1992. The reactivity of sedimentary iron minerals toward sulfide. *American Journal of Science*. 292: 659-683.

Canfield, D.E. and R.A. Berner. 1987. Dissolution and pyretization of magnetite in anoxic marine sediments. *Geochimica et Cosmochimica Acta.* 51: 645-659.

Canfield, D.E., B. Thamdrup, and E. Kristensen. 2005. *Aquatic Geomicrobiology: Advances in Marine Biology.* Volume 48. San Diego, CA: Elsevier Academic Press.

Canfield, D.E., B.B. Jørgensen, H. Fossing, R. Glud, J. Gundersen, N.B. Ramsing, B. Thamdrup, J.W. Hansen, L.P. Nielsen, and P.O.J. Hall. 1993. Pathways of organic carbon oxidation in three continental margin sediments. *Marine Geology*. 113: 27-40.

Capone, D., and R. Kiene. 1988. Comparison of microbial dynamics in marine and freshwater sediments: Contrasts in anaerobic carbon catabolism. *Limnology and Oceanography.* 33: 725–749.

Chambers, R. M. and W. E. Odum. 1990. Pore water oxidation, dissolved phosphate and the iron curtain: Iron-phosphorus relations in tidal freshwater marshes. *Biogeochemistry.*

10: 37-52.

Chambers, R. M., J. Fourqurean, S. Macko, and R. Hoppenot. 2001. Biogeochemical effects of iron availability on primary producers in a shallow marine carbonate environment. *Limnology and Oceanography.* 46: 1278-1286.

Christensen, P., L. Nielsen, N. Revsbech, and J. Sorensen. 1989. Microzonation of denitrification activity in stream sediments as studied with a combined oxygen and nitrous oxide microsensor. *Applied Environmental Microbiology*. 55: 1234-1241.

Christensen, P., S. Rysgaard, N. Sloth, T. Dalsgaard, and S. Schwaerter. 2000. Sediment mineralization, nutrient fluxes, denitrification and dissimilatory nitrate reduction to ammonium in an estuarine fjord with sea cage trout farms. *Aquatic Microbial Ecology*. 21: 73-84.

Cline, J. and F. Richards. 1969. Oxygenation of hydrogen sulfide in seawater at constant salinity, temperature, and pH. *Environmental Science and Technology*. 3: 838-843.

Colman, A. S., and H. D. Holland. 2000. The global diagenetic flux of phosphorus from marine sediments to the oceans: Redox sensitivity and the control of atmospheric oxygen levels, in Marine Authigenesis: From Global to Microbial, edited by C. R. Glenn, pp. 53– 75, Soc. for Sed. Geol.

Corzo, A., S.A. Van Bergeijk, and E. Garcia-Robledo. 2009. Effects of green macroalgal blooms on intertidal sediments: net metabolism and carbon and nitrogen contents. *Marine Ecology Progress Series*. 380: 81-93.

D'Avanzo, C. and J. Kremer. 1994. Diel oxygen dynamics and anoxic events in a eutrophic estuary of Waquoit Bay, Massachusetts. *Estuaries*. 17: 131-139.

Dalsgaard, T. 2003. Benthic primary production and nutrient cycling in sediments with benthic microalgae and transient accumulation of macroalgae. *Limnology and Oceanography.* 48: 2138-2150.

Davison, W. and G. Seed. 1983. The kinetics of the oxidation of ferrous iron in synthetic and natural waters. *Geochimica et Cosmochimica Acta.* 47: 67-79.

Dos Santos Afonso, M. and W. Stumm. 1992. Reductive dissolution of iron(III) (hydr)oxides by hydrogen sulfide. *Langmuir*. 8: 1671-1675.

Doty, M.S. 1961. *Acanthophora*, a possible invader of the marine flora of Hawai'i. *Pacific Science.* 11: 547-552.

Engelsen, A., S. Hulth, L. Pihl, and K. Sundback. 2008. Benthic trophic status and nutrient fluxes in shallow-water sediments. *Estuaries, Coastal and Shelf Science*. 78: 783-795.

EPA eGRID. http://www.epa.gov/cleanenergy/documents/egridzips/eGRID2010V1_1_year07_SummaryTables.pdf

EPA Emission Facts. http://www.epa.gov/otaq/climate/420f05002.htm

Eppley, R. and B. Peterson. 1979. Particulate organic matter flux and planktonic new production in the deep ocean. *Nature*. 282: 677-680.

Escartín, J., and D. Aubrey. 1995. Flow structure and dispersion within algal mats. *Estuarine, Coastal and Shelf Science.* 40: 451-472.

Falkowski, P. G., T. Fenchel, and E.F. Delong. 2008. The microbial engine that drives earth's biogeochemical cycles. *Science.* 320: 1034-1039.

Falter, J., M. Atkinson, and M. Merrifield. 2004. Mass-transfer limitation of nutrient uptake by a wave-dominated reef flat community. *Limnology and Oceanography*. 49: 1820-1831.

Fisher, T., P. Carlson, and R. Barber. 1982. Sediment nutrient regeneration in three North Carolina estuaries. *Estuarine, Coastal and Shelf Science*. 14: 101-116.

Forster, S., M. Huettel, and W. Ziebis. 1996. Impact of boundary layer flow velocity on oxygen utilization in coastal sediments. *Marine Ecology Progress Series*. 143: 173-185.

Froelich, P. 1988. Kinetic control of dissolved phosphate in natural rivers and estuaries: A primer on the phosphate buffer mechanism. *Limnology and Oceanography* 33: 649–668.

Froelich, P., G. Klinkhammer, M. Bender, N. Luedtke, G. Heath, D. Cullen, P. Dauphin, D. Hammond, B. Hartman, and V. Maynard. 1979. Early oxidation of organic matter in pelagic sediments of the eastern equatorial Atlantic: suboxic diagenesis. *Geochimica et Cosmochimica Acta*. 43: 1075-1090.

Gambi, M., A. Nowell, and P. Jumars. 1990. Flume obxervations on flow dynamics in *Zostera marina* (eelgrass) beds. *Marine Ecology Progress Series.* 61: 159-169.

Glazer, B., S. Cary, L. Hohmann, and G.W. Luther III. 2002. Sulfur speciation and microbial characterization of an intertidal salt marsh microbial mat. In: *Environmental*

Electrochemistry: Analysis of trace element biogeochemistry. Taillefert, M and Rozan, TF eds. *American Chemical Society Symposium Series.* 811: 283-304.

Glazer, B.T., G.W. Luther (III), S.K. Konovalov, G.E. Friederich, D.B. Nuzzio, R.E. Trouwborst, B.M. Tebo, B. Clement, K. Murray, and A.S. Romanov. 2006. Documenting the suboxic zone of the Black Sea via high-resolution real-time redox profiling. *Deep-Sea Research II*. 53: 1740-1755.

Gonen, Y. and M. Friedlander. 1995. Diffusion boundary layer transport in *Gracilaria conferta* (Rhodophyta). *Journal of Phycology*. 31: 768-773.

Grasshoff, K., M. Ehrhardt, and K. Kremling (Eds). 1983. Methods of seawater analysis, 2nd ed. Verlag Chemie.

Gunnars, A. and S. Blomqvist. 1997. Phosphate exchange across the sediment-water interface when shifting from anoxic to oxic conditions: An experimental comparison of freshwater and brackish-marine systems. *Biogeochemistry*. 37: 203-226.

Gunnars, A., S. Blomqvist, P. Johansson, and C. Andersson. 2002. Formation of Fe(III) oxyhydroxide colloids in freshwater and brackish seawater, with incorporation of phosphate and calcium. *Geochimica et Cosmochimica Acta.* 66: 745-758.

Hauri, C., K. Fabricius, B. Schaffelke, and C. Humphrey. 2010. Chemical and physical environmental conditions underneath mat- and canopy- forming macroalgae, and their effects on understory corals. *PLoS ONE*. 5: 1-9.

Hecky, R. and P. Kilham. 1988. Nutrient limitation of phytoplankton in freshwater and marine environments: a review of recent evidence on the effects of enrichment. *Limnology and Oceanography.* 33: 796–822.

Hendriks, I., T. Bouma, E. Morris, and C. Duarte. 2009. Effects of seagrasses and algae of the *Caulerpa* family on hydrodynamics and particle-trapping rates. *Marine Biology*. 157: 473-481.

Henricksen, K. and W. Kemp. 1988. Nitrification in estuaries and coastal marine sediments. In: *Nitrogen Cycling in Coastal Marine Environments*. T.H. Blackburn and J. Sorenen Eds. John Wiley and Sons Ltd. p. 207-249

Herbert, R.A. 1999. Nitrogen cycling in coastal marine ecosystems. *FEMS Microbiology Reviews*. 23: 563-590.

Hoagland, P., D. Anderson, Y. Kaoru, and A. White. 2002. The economic effects of harmful algal blooms in the United States: Estimates, assessment issues, and information

needs. *Estuaries.* 25: 819-837.

Holmer, M., N. Marba, M. Lamote, and C. Duarte. 2009. Deterioration of sediment quality in seagrass meadows *(Posidonia oceanica*) invaded by macroalgae (*Caulerpa sp.*). *Estuaries and Coasts*. 32:456-466.

Huettel, M., W. Ziebis, S. Forster and G. Luther. 1998. Advective transport affecting metal and nutrient distributions and interfacial fluxes in permeable sediments. *Geochimica et Cosmochimica Acta*. 62: 613- 631.

Hupfer, M. and J. Lewandowski. 2008. Oxygen controls the phosphorus release from lake sediments – a long-lasting paradigm in limnology. *International Review of Hydrobiology.* 93: 415-432.

Hurd, C. 2000. Water motion, marine macroalgal physiology, and production. *Journal of Phycology*. 36: 453-472.

Ingri, J., R. Lofvendahl, and K. Bostrom. 1991. Chemistry of suspended particles in the southern Baltic Sea. *Marine Chemistry*. 32: 73-87.

Jensen, H., P. Mortensen, F. Andersen, E. Rasmussen, and A. Jensen. 1995. Phosphorus cycling in a coastal marine sediment, Aarhus Bay, Denmark. *Limnology and Oceanography.* 40: 908–917.

Jones, C., J. Lawton, and M. Shachak. 1994. Organisms as ecosystem engineers. *Oikos*. 69: 373-386.

Jones, C., J. Lawton, and M. Shachak. 1997. Positive and negative effects of organisms as physical ecosystem engineers. *Ecology*. 78: 1946-1957.

Jørgensen, B. 1977a. Bacterial sulfate reduction within reduced microniches of oxidized marine sediments. *Marine Biology*. 41: 7-17.

Jørgensen, B. 1977b. The sulfur cycle of a coastal marine sediment (Limfjorden, Denmark). *Limnology and Oceanography*. 22: 814-832.

Jørgensen, B. 1982. Mineralization of organic-matter in the sea bed-the role of sulfate reduction. *Nature.* 296: 643–645.

Jørgensen, B. 1983. Processes at the sediment-water interface. B. Bolin and R. Cook [eds.]. In: *The Major Biogeochemical Cycles and Their Interactions,* SCOPE 21. p. 478-509.

Jørgensen, B. and N. Revsbech. 1985. Diffusive boundary layers and the oxic uptake of sediments and detritus. *Limnology and Oceanography*. 30: 111-122.

Khailov, K. and Z. Burlakov. 1969. Release of dissolved organic matter by marine seaweeds and distribution of their total organic production in inshore communities. *Limnology and Oceaongraphy.* 14: 521-527.

Kirby, C., H. Thomas, G. Southam, and R. Donald. 1999. Relative contributions of abiotic and biological factors in Fe(II) oxidation of mine drainage. *Applied Geochemistry*. 14: 511-530.

Kleeberg, A., J. Kohler, T. Sukhodolova, and A. Sukhodolov. 2010. Effects of aquatic macrophytes on organic matter deposition, resuspension, and phosphorus entrainment in a lowland river. *Freshwater Biology*. 55: 326-345.

Klump, J. and C. Martens. 1987. Biogeochemical cycling in an organic rich coastal marine basin- II. Nutrient sediment-water exchange processes. *Geochimica et Cosmochimica Acta*. 45: 101-121.

Koehl, M., P. Jumars and L. Karp-Boss. 2003. Algal biophysics. pp. 115-130 in T.A. Norton, Ed. *Out of the Past*. British Phycological Association, Belfast.

Koretsky, C., C. Moore, K. Lowe, C. Meile, T. Dichristina, and P. Van Cappellen. 2003. Seasonal oscillation of microbial iron and sulfate reduction in saltmarsh sediments (Sapelo Island, GA, USA). *Biogeochemistry.* 64: 179–203.

Koroleff, F. 1979. Phosphorus. In: Grasshoff, R., Ehrhardt, M., and Kremling, K. (eds.) *Methods of Seawater Analysis*. Verlag Chimie, Weinheim, NY.

Krause-Jensen, D., P. Christensen, and S. Rysgaard. 1999. Oxygen and nutrient dynamics within mats of filamentous macroalga *Chaetomorpha linim*. *Estuaries*. 22: 31-38.

Kristiansen, K.D., E. Kristensen, and M.H. Jensen. 2002. The influence of water column hypoxia on the behavior of manganese and iron in sandy coastal marine sediment. *Estuarine, Coastal and Shelf Science*. 55: 645-654.

Krom, M., and R. Berner. 1980. Adsorption of phosphate in anoxic marine sediments. *Limnology and Oceanography*. 25: 797–806.

Krom, M., and R. Berner. 1981. The diagenesis of phosphorus in a nearshore marine sediment. *Geochimica et Cosmochimica Acta*. 45: 207–216.

Kuenzler, E. and J. Perras. 1965. Phosphatases of marine algae. *Biological Bulletin*. 128(2): 271-284.

Lapointe, B. 1997. Nutrient thresholds for bottom-up control of macroalgal blooms on coral reefs in Jamaica and southeast Florida. *Limnology and Oceanography*. 42: 1119-1131.

Larned, S. 1998. Nitrogen- versus phosphorus-limited growth and sources of nutrients for coral reef macroalgae. *Marine Biology*. 132: 409-421.

Larned, S. T. and M. J. Atkinson. 1997. Effects of water velocity on NH_4 and PO_4 uptake and nutrient-limited growth in the macroalga *Dictyosphaeria cavernosa*. *Marine Ecology Progress Series.* 157: 295-302.

Lavery, P.S. and A.J. MacComb. 1991. Macroalgal-sediment nutrient interactions and their importance to macroalgal nutrition in a eutrophic estuary. *Estuarine, Coastal and Shelf Science*. 32: 281-295.

Lewis, B.L., B.T. Glazer, P.J. Montbriand, G.W. Luther (III), D.B. Nuzzio, T. Deering, S. Ma, and S. Theberge. 2007. Short-term and interannual variability of redox-sensitive chemical parameters in hypoxic/anoxic bottom waters of the Chesapeake Bay. *Marine Chemistry.* 105: 296-308.

Lovley, D.R. and E.J. Phillips. 1988. Manganese inhibition of microbial iron reduction in anaerobic sediments. *Geomicrobiology Journal*. 6: 145-155.

Luther, G. W., B. Glazer, S. Ma, R. Trouwborst, T. Moore, E. Metzger, C. Kraiya, T. Waite, T. Shank, B. Lewis, P. Brendel, G. Druschel, B. Sundby, M. Taillefert, and D. Nuzzio. 2008. Use of voltammetric solid-state (micro)electrodes for studying biogeochemical processes: Laboratory measurements to real time measurements with an *in situ* electrochemical analyzer (ISEA). *Marine Chemistry*. 108: 221-235.

Luther, G. W., C. Reimers, D. Nuzzio, and D. Lovalvo. 1999. *In situ* deployment of voltammetric, potentiometric, and amperometric microelectrodes from a ROV to determine dissolved O_2, Mn, Fe, S(−2), and pH in pore waters . *Environmental Science & Technology.* 33: 4352-4356.

Marba, N., C. Duarte, M. Holmer, M. Calleja, E. Alvarez, E. Diaz-Almela, and N. Garcias-Bonet. 2008. Sedimentary iron inputs stimulate seagrass (*Posidonia oceanica*) population growth in carbonate sediments. *Estuarine, Coastal and Shelf Science.* 76: 710-713.

McGlathery, K. 2001. Macroalgal blooms contribute to the decline of seagrass in

nutrient-enriched coastal waters. *Journal of Phycology*. 37: 453-456.

McGlathery, K., D. Krause-Jensen, S. Rysgaard, and P.B. Christensen. 1997. Patterns of ammonium uptake within dense mats of the filamentous macroalga *Chaetomorpha linum*. *Aquatic Botany.* 59: 99-115.

McKinnon, J., P. Gribben, A. Davis, D. Jolley, and J. Wright. 2009. Differences in soft-sediment macrobenthic assemblages invaded by *Caulerpa taxifolia* compared to uninvaded habitats. *Marine Ecology Progress Series*. 380: 59-71.

McManus, J., W. Berelson, K. Coale, K. Johnson, and T. Kilgore. 1997. Phosphorus regeneration in continental margin sediments. *Geochimica et Cosmochimica Acta.* 61: 2891–2907.

Monaghan, E. and K. Ruttenberg. 1999. Dissolved organic phosphorus in the coastal ocean: Reassessment of available methods and seasonal phosphorus profiles from the Eel River Shelf. *Limnology and Oceanography*. 44: 1702-1714.

Mortimer, C.H. 1941. The exchange of dissolved substances between mud and water in lakes. *Journal of Ecology*. 29: 280-329.

Mortimer, C.H. 1942. The exchange of dissolved substances between mud and water in lakes. *Journal of Ecology*. 30: 147-201.

Muehe, E. S. Gerhardt, B. Schink, and A. Kappler. 2009. Ecophysiology and the energetic benefit of mixotrophic Fe(II) oxidation by various strains of nitrate-reducing bacteria. *FEMS Microbiology Ecology*. 70: 335-343.

Myers, C.R. and K.H. Nealson. 1988. Bacterial manganese reduction and growth with manganese oxide as the sole electron acceptor. *Science*. 240: 1319-1321.

Nealson, K. and D. Saffarini. 1994. Iron and manganese in anaerobic respiration: Environmental Significance, Physiology, and Regulation. *Annual Review of Microbiology.* 48: 311-343.

Nedergaard, R., N. Risgaard-Petersen, and K. Finster. 2002. The importance of sulfate reduction associated with *Ulva lactuca* thalli during decomposition: a mesocosm experiment. *Journal of Experimental Marine Biology and Ecology*. 275: 15-29.

Nepf, H. 2012. Flow and transport in regions with aquatic vegetation. *Annual Review of Fluid Mechanics*. 44: 123-142.

Nepf, H. and E. Vivoni. 2000. Flow and structure in depth-limited, vegetated flow.

Journal of Geophysical Research. 105: 28,547-28,557.

Oldham, C. and P. Lavery. 1999. Porewater nutrient fluxes in a shallow fetch-limited estuary. *Marine Ecology Progress Series* 183: 39-47.

Open University Team (Eds). (1989). Seawater: Its Composition, Properties and Behavior. (p. 130)

Ottosen, L. N. Risgaard-Peteren, and L. Nielsen. 1999. Direct and indirect measurements of nitrification and denitrification in the rhizosphere of aquatic macrophytes. *Aquatic Microbial Ecology*. 19: 81-91.

Paerl, H. and J. Pinckney. 1996. A mini0review of microbial consortia: Their roles in aquatic production and biogeochemical cycling. *Microbial Ecology*. 31: 225-247.
Payne, W. J. 1973. Reduction of nitrogenous oxides by microorganisms. *Bacteriological Reviews.* 37: 409-452.

Peckol, P. and S. Rivers. 1995. Physiological responses of the opportunistic macroalgae *Cladophora vagabunda* (L.) van den Hoek and *Gracilaria tikvahiae* (McLachlan) to environmental disturbances associated with eutrophication. *Journal of Experimental Marine Biology and Ecology*. 190: 1-16.

Peterson, C., R. Luettich, F. Micheli, and G. Skilleter. 2004. Attenuation of water flow inside seagrass canopies of differing structure. *Marine Ecology Progress Series*. 286: 81-92.
Phooprong, S., H. Ogawa, and K. Hayashizaki. 2007. Photosynthetic and respiratory responses of *Gracilaria salicornia* (C. Ag.) Dawson (Gracilariales, Rhodophyta) from Thailand and Japan. *Journal of Applied Phycology.* 19: 795-801.

Poulton, S. M. Krom, and R. Raiswell. 2004. A revised scheme for the reactivity of iron (oxyhydr)oxide minerals towards dissolved sulfide. *Geochimica et Cosmochimica Acta*. 68: 3703-3715.

Reay, W., D. Gallagher, and G. Simmons Jr. 1995. Sediment-water column oxygen and nutrient fluxes in nearshore environements of the lower Delmarva Peninsula, USA. *Marine Ecology Progress Series*. 118: 215-227.

Rozan, T. F. Taillefert, M. R. Trouwborst, B. Glazer, S. Ma, J. Herszage, L. Valdes, K. Price, and G. Luther III. 2002. Iron-sulfur-phosphorus cycling in the sediments of a shallow coastal bay: Implications for sediment nutrient release and benthic macroalgal blooms. *Limnology and Oceanography*. 47: 1346-1354.

Ruiz-Halpern, S., S. A. Macko, and J. W. Fourqurean. 2008. The effects of manipulation

of sedimentary iron and organic matter on sediment biogeochemistry and seagrasses in a subtropical carbonate environment. *Biogeochemistry*. 87: 113-126.

Rysgaard, S., N. Risgaard-Petersen, and N. Sloth. 1996. Nitrification, denitrification, and ammonification in sediments of two coastal lagoons in Southern France. *Hydrobiologia*. 329: 133-141.

Rysgaard, S., N. Risgaard-Petersen, N. Sloth, K. Jensen, and L. Nielsen. 1994. Oxygen regulation of nitrification and denitrification in sediments. *Limnology and Oceanography*. 39: 1643-1652.

Schaffelke, B., J. Smith, and C. Hewitt. 2006. Introduced macroalgae- a growing concern. *Journal of Applied Phycology*. 18: 529-541.

Seitzinger, S. 1988. Denitrification in freshwater and coastal marine ecosystems: ecological and geochemical significance. *Limnology and Oceanography*. 33: 702-724.

Sfriso, A., A. Marcomini, and B. Pavoni. 1987. Relationships between macroalgal biomass and nutrient concentrations in a hypertrophic area of the Venice Lagoon. *Marine Environmental Research*. 22: 297-312.

Slomp, C., E. Epping, W. Helder, and W. Van Raaphorst. 1996b. A key role for iron-bound phosphorus in authigenic apatite formation in North Atlantic continental platform sediments. *Journal of Marine Research*. 54: 1179-1205.

Slomp, C., S. Van der Gaast, and W. Van Raaphorst. 1996a. Phosphorus binding by poorly crystalline iron oxides in North Sea sediments. *Marine Chemistry*. 52: 55-73.

Smith, J. E., C.L. Hunter, and C.M. Smith. 2002. Distribution and reproductive characteristics of nonindigenous and invasive marine algae in the Hawaiian Islands. *Pacific Science*. 56: 299–315.

Smith, J., J. Runcie, and C. Smith. 2005. Characterization of a large-scale ephemeral bloom of the green alga *Cladophora sericea* on the coral reefs of West Maui, Hawai‘i. *Marine Ecology Progress Series*. 302: 77-91.

Smith, J., M. Shaw, R. Edwards, D. Obura, O. Pantos, E. Sala, S. Sandin, S. Smriga, M. Hatay, and F. Rohwer. 2006. Indirect effects of algae on coral: algae-mediated, microbe-induced coral mortality. *Ecology Letters*. 9: 835-845.

Sørensen, J. 1982. Reduction of ferric iron in anaerobic, marine sediment and interaction with reduction of nitrate and sulfate. *Applied and Environmental Microbiology*. 43: 319-324.

Sørensen, J. and B.B. Jørgensen. 1987. Early diagenesis in sediments from Danish coastal waters: Microbial activity and Mn-Fe-S geochemistry. *Geochimica et Cosmochimica Acta*. 51: 1583-1590.

Sprent, J., J. Sutherland, S. de Faria, M. Dilworth, H. Corby, J. Beckingm L. Materon and J. Drozd. 1987. Some aspects of the biology of nitrogen-fixing organisms (and discussion). *Philosophical Transactions of the Royal Society of London*. *Series B, Biological Sciences*. 317: 111-129.

Stainsen, J. and S. Sundby. 2001. Improved methods for generating and estimating turbulence in tanks suitable for fish larvae experiments. *Scientia Marina*. 65: 151-167.

Stookey, L.L. 1970. Ferrozine – A new spectrophotometric reagent for iron. *Analytical Chemistry*. 42: 779-781.

Straub, K. L., M. Benz, B. Schink and F. Widdel. 1996. Anaerobic, nitrate-dependent microbial oxidation of ferrous iron. *Microbiology.* 62: 1458-1460.

Sundback, K. V. Enoksson, W. Graneli, and K. Pettersson. 1991. Influence of sublittoral microphytobenthos on the oxygen and nutrient flux between sediment and water: a laboratory continuous-flow study. *Marine Ecology Progress Series*. 74: 263-279.

Sundback, K., A. Miles, S. Hulth, L. Pihl, P. Engstrom, E. Selander, and A. Svenson. 2003. Importance of benthic nutrient regeneration during initiation of macroalgal blooms in shallow bays. *Marine Ecology Progress Series*. 246: 115-126.

Sundback, K., B. Jonsson, P. Nilsson, and I. Lindstrom. 1990. Impact of accumulating drifting macroalgae on a shallow-water sediment system: an experimental study. *Marine Ecology Progress Series*. 58: 261-274.

Sundbäck, K., F. Linares, F. Larson, A. Wulff and A. Engelsen. 2004. Benthic nitrogen fluxes along a depth gradient in a microtidal fjord : The role of denitrification and microphytobenthos. *Limnology and Oceanography.* 49: 1095-1107.

Sundby, B., C. Gobeil, N. Silverberg and A. Mucci. 1992. The phosphorus cycle in coastal marine sediments. *Limnology and Oceanography.* 37: 1129–1145.

Sundby, B., L.G. Anderson, P.O.J. Hall, A. Iverfeldt, M.M. Rutgers van der Loeff, and S.F.G. Westerlund. 1986. The effect of oxygen on release and uptake of cobalt, manganese, iron and phosphate at the sediment-water interface. *Geochimica et Cosmochimica Acta*. 50: 1281-1288.

Tans, Peter and Ralph Keeling. Trends in Atmospheric Carbon Dioxide. NOAA. http://www.esrl.noaa.gov/gmd/ccgg/trends/mlo.html

Tebo, B.M., B.D. Clement, and G.J. Dick. 2007. Biotransformations of manganese. Editor(s): Hurst, C.J. Manual of Environmental Microbiology (3rd Edition). 1223-1238.

Thamdrup, B., H. Fossing, and B.B. Jørgensen. 1994. Manganese, iron and sulfur cycling in a coastal marine sediment, Aarhus Bay, Denmark. *Geochimica et Cosmochimica Acta*. 58: 5115-5129.

Thomas, F. and C. Cornelisen. 2003. Ammonium uptake by seagrass communities: effects of oscillatory versus unidirectional flow. *Marine Ecology Progress Series.* 247: 51-57.

Valiela, I., J. McClelland, J. Hauxwell, P. Behr, D. Hersh, and K. Foreman. 1997. Macroalgal blooms in shallow estuaries: controls and ecophysiological and ecosystem consequences. *Limnology and Oceanography*. 42: 1105-1118.

Viaroli, P., M. Bartoli, C. Bondavalli, R.R. Christian, G. Giordani, and M. Naldi. 1996. Macrophyte communities and their impact on benthic fluxes of oxygen, sulfide and nutrients in shallow eutrophic environments. *Hydrobiologia*. 329: 1050-119.

Viaroli, P., M. Bartoli, G. Giordani, M. Naldi, S. Orfanidis, and J. Zaldivar. 2008. Community shifts, alternative stable states, biogeochemical controls and feedbacks in eutrophic coastal lagoons: a brief overview. *Aquatic Conservation: Marine and Freshwater Ecosystems*. 18: S105-S117.

Wheeler, W. 1980. Effect of boundary layer transport on the fixation of carbon by the giant kelp *Macrocystis pyrifera*. *Marine Biology*. 56: 103-110.

Widdows, J. and M. Brinsley. 2002. Impact of biotic and abiotic processes on sediment dynamics and the consequences to the structure and functioning of the intertidal zone. *Journal of Sea Research*. 48: 143-156.

Wigley, T.M. 1983. The pre-industrial carbon dioxide level. *Climatic Change*. 5(4): 315-320.

Williams, S. and J. Smith. 2007. Distribution, taxonomy, and impacts of introduced seaweeds. *Annual Review of Ecology, Evolution, and Systematics*. 38: 327-359.

Yao, W. and F. Millero. 1996. Adsorption of phosphate on manganese dioxide in seawater. *Environmental Science and Technology*. 30: 536-541.

Young, C. 2011. Perturbation of nutrient inventories and phytoplankton community composition during storm events in a tropical coastal system: He‘eia Fishpond, O’ahu, Hawai‘i. M.S. Thesis.